UNIVERSITY OF GHANA

SCHOOL OF PHYSICAL AND MATHEMATICAL SCIENCES

DEPARTMENT OF PHYSICS

UNDERSTANDING AEROSOL INTERACTIONS IN THE ATMOSPHERE: A CASE STUDY OF KUMASI, GHANA

KINGSFORD KOFI GBORDZOE

MPHIL. PHYSICS

2024

UNIVERSITY OF GHANA

SCHOOL OF PHYSICAL AND MATHEMATICAL SCIENCES

DEPARTMENT OF PHYSICS

UNDERSTANDING AEROSOL INTERACTIONS IN THE ATMOSPHERE: A CASE STUDY OF KUMASI, GHANA

KINGSFORD KOFI GBORDZOE

11008098

A THESIS SUBMITTED TO THE SCHOOL OF GRADUATE STUDIES IN PARTIAL FULFILLMENT OF THE AWARD OF DEGREE OF MASTER OF PHILOSOPHY IN PHYSICS

NOVEMBER, 2024

DECLARATION

I declare that this dissertation with the exception of quotations and references contained in published works which have all been identified and duly acknowledged, is entirely my own original work. It has not been submitted either in part or whole, for another degree elsewhere.

Signature.. … Date …29/11/2024……

Kingsford Kofi Gbordzoe

(Student)

Signature: … Date: …30/12/2025

Prof. Nana Ama Browne Klutse

(Supervisor)

Signature:……. Date: ……

Dr. Koffi

(Cosupervisor)

ABSTRACT

Atmospheric aerosols influence regional climate systems; however, their effects remain underexplored in West African cities. This study assessed aerosol interaction in the atmosphere of Kumasi, Ghana, using satellite-derived datasets from MERRA-2, GEOS-CF, and ERA5 from September to December 2022. The study examined temporal variations in aerosol concentration, spatial variability across urban, peri-urban, and rural sites, and relationships between aerosols, SSR, and temperature. A quantitative observational research design was adopted using data from four monitoring locations: Fumesua Community, Fumesua Farm, Sokwai Community, and Sokwai Farm. Quality control procedures included modified z-score outlier screening and physical consistency checks, while descriptive statistics, ANOVA, correlation analysis, and polynomial regression were applied. Aerosol concentration increased sharply from $5-25\,\mu g/m^3$ in September to $80-125\,\mu g/m^3$ in December, exceeding WHO thresholds during the Harmattan season. Spatial variations were statistically insignificant ($F = 0.7027, p = 0.6699$), indicating the dominance of regional atmospheric processes over local emissions. Aerosols exhibited an inverse relationship with SSR ($R^2 = 0.59-0.60$) and a bi-phasic association with temperature ($R^2 = 0.78$), with warming at low-to-moderate concentrations and cooling at high concentrations ($> 80\,\mu g/m^3$). SSR and temperature showed consistently strong positive correlations ($R^2 = 0.82-0.84$). The study concludes that aerosol loading significantly alters climate variables in Kumasi and highlights the need for coordinated mitigation measures. Limitations include the four-month timeframe and absence of ground-based validation. The research offers baseline evidence to support national air quality and climate adaptation planning.

ACKNOWLEDGEMENT

Firstly, I am grateful to Almighty God for being in this academic boat and sailing me this far. All I can say is thank you, Lord. My profound appreciation goes to my supervisor, Prof. Nana Ama Browne Klutse, for her patience, inspiration, and vast knowledge, as well as her ongoing support of my postgraduate studies and associated research. Her advice was helpful to me during the research. I want to express my gratitude to my colleagues and all of my instructors in the UG Department of Physics for helping make this study a success. Special thanks to my family and friends, especially my mother, my uncles, and my wife. I say God richly bless you for your immense support; it may be an impossible task without your assistance.

DEDICATION

I dedicate this work first to God, my wife, children, mother, late father, and siblings.

TABLE OF CONTENTS

LIST OF FIGURES

LIST OF TABLES

LIST OF EQUATIONS

LIST OF ABBREVIATIONS

AOD	Aerosol Optical Depth
CNN	Cloud Condensation Nuclei
FC	Fumesua Community
Geo	GeosCF Satellite
Merra	Merra2 Satellite

FF	Fumesua Farm
SC	Sokwai Community
SF	Sokwai Farms
SSR	Surface Solar Radiation
R_S	Surface Radiation

CHAPTER ONE

1.0 INTRODUCTION

1.1 Background

The air contains a wide variety of tiny particles, such as clouds of water droplets or ice particles, smoke from power plants, particles produced by photochemistry, suspended soil particles, and salt particles from ocean spray. They differ widely in their ability to impact not only the climate and visibility, but also our health and way of life. These airborne particles are all examples of aerosols. An aerosol is simply a collection of solid or liquid particles suspended in air. Aerosols are a two-phase system consisting of the particle and the gas in which they are suspended. They include a wide range of phenomena such as dust, smoke, fume, mist, fog, haze, smog, and cloud, which primarily consist of condensed water with particle diameters on the order of approximately $10\mu m$. Natural aerosols include dust from the desert or soil, smoke from wildfires, sea salt, biogenic particles, and volcanic ash. Anthropogenic aerosols originate from a range of sources, such as home fires and other combustion products, emissions from cities and industries, smoke from biomass burning in agriculture, and emissions from deforestation, overgrazing, certain farming practices, and land management practices that cause surface regolith to become unstable due to wind erosion (Hinds, 1999; Chin et al., 2009; Crutzen and Andreae, 1990; Pruppacher et al., 1998).

.

Aerosol optical depth (AOD) is an optical measure used to quantify particles in the atmosphere in addition to their mass concentration (Dey et al., 2012; Srivastava et al., 2014; Liou and Bohren, 1980). Almeida et al. (2020) noted that numerous factors, such as weather conditions, emission sources, and dispersal patterns at various locations, can cause aerosol concentrations to fluctuate

dramatically. The AOD is also a key parameter for assessing the aerosol direct radiative effect (Dey et al., 2012; Srivastava et al., 2014; Liou and Bohren, 1980).

Primary aerosols are particles that are released directly into the atmosphere. Mechanical processes provide natural primary aerosols such as wind-blown dust, sea spray, mineral dust, volcanic ash, and plant and animal detritus. On the other hand, secondary aerosols are formed in the atmosphere through the transformation of gases into particles through nucleation and condensation of gaseous precursors (Crutzen & Andreae, 1990).

Atmospheric aerosol particles range from nanometers to tens of micrometers in size, from molecular clusters to visible dust. Most often, condensation from reactive gases like sulfur dioxide or from high-temperature processes like fires produces smaller particles (less than 1μm). Particles larger than 1μm are mechanically created, for example, by sea spray or wind-blown soil. Aerosols differ in their chemical makeup according to their size, location, and time. Their residence time in the atmosphere varies: minutes to hours for large dust particles, days to weeks for smoke and haze, and up to two years for volcanic aerosols in the stratosphere (National Research Council, 1996). These aerosol particles are suspended in the atmosphere and can be transported over great distances, where they undergo chemical and physical aging. Aerosols have a significant impact on human existence, the environment, air quality, climate dynamics, and the atmospheric energy balance (Huang et al., 2014; Kaiser, 2005). According to Yu et al. (2006), aerosols impact the Earth's radiation balance, which in turn affects climate. The Earth's radiation energy budget is impacted by aerosols either directly or indirectly (Huang et al., 2009; Niyogi et al., 2010). Aerosols have direct effects on our climate systems by absorbing and scattering solar short-wave and long-wave radiation, which in turn causes surface cooling and atmospheric solar heating (Ramanathan et al., 2001). Through the processes of absorption and scattering, aerosols

reduce surface incident solar radiation (Rs). Additionally, aerosols affect Rs through complex aerosol-cloud interactions that can either increase or decrease Rs (Koren et al., 2008; Stevens and Feingold, 2009; Wild, 2009). According to Rosenfeld et al. (2014) and Stevens (2013), one of the largest uncertainties in our present understanding of climate change is the overall effect of aerosols on Rs.

Absorbing aerosols, according to Ackerman et al. (2000), heat the atmosphere and can evaporate clouds and reduce relative humidity. This process may raise the surface temperature; it is referred to as the semi-direct effect. Aerosols also alter clouds' microphysical properties, which in turn alter their radiative qualities. Increases in aerosols increase cloud condensation nuclei (CCN), which in turn raise cloud droplet number density, lower cloud droplet effective radius, and ultimately produce brighter clouds because the particles act as CCN. This is known as the first aerosol indirect effect, a phenomenon that reduces the amount of solar radiation that reaches the earth while increasing the albedo of the cloud (Twomey, 1977). Additionally, the smaller cloud droplets promote the reduction of precipitation (referred to as the second indirect effect) and, according to Albrecht (1989), this phenomenon causes cloud lifetime to increase. Aerosols that do not absorb light, such as sulfates, nitrates, and organic carbon (Pilinis et al., 1995), reflect solar energy into space, resulting in a cooling of the Earth system known as negative radiative forcing. Black carbon (also known as soot) from burning biomass, fossil fuels, and mineral dust from arid regions are examples of absorbent aerosols that modify the temperature structure of the atmosphere, affect cloud cover, and absorb solar radiation. These changes result in a positive radiative forcing, or the warming of the earth system (Hansen et al., 1997; Johnson et al., 2004). Apart from its numerous impacts on climate and other weather parameters, aerosols

also have a great impact on human health, including cancer, cardiopulmonary diseases, and increased morbidity and mortality, especially among infants and the elderly (Lepeule et al., 2012). The atmospheric temperature structure can be changed by aerosol direct and indirect effects, by altering the net radiation both at the top and bottom of the atmosphere (Charlson et al., 1992; Levine et al., 1995; Haywood and Boucher, 2000; Andreae & Crutzen, 1997). Aerosols affect the climate in two primary ways: by changing the amount of heat entering or leaving the atmosphere, or by affecting how clouds are formed. Atmospheric aerosols' effect is more complicated than that of greenhouse gases (Mitchell et al., 1995), which means that different aerosols reflect sunlight to varying degrees depending on their physical properties. Generally, bright or translucent particles tend to reflect radiation in all directions and back to space, while dark aerosols absorb a large amount of radiation (Watson et al., 1990). Because most aerosols are brighter than land or ocean, they tend to cool the Earth by reflecting sunlight into space.

1.2 Motivation for the Research Study

Aerosol pollution levels on the African continent are often quite high, regularly exceeding the WHO's clean air criterion of 10 $\mu g/m^3$ of PM2.5. Africa has experienced tremendous industrial growth, produces almost one-third of the world's biomass-burning aerosols, and is the major source of desert dust emissions worldwide. These emissions are mostly anthropogenic. According to Bauer et al. (2019), agricultural activities, including burning fields and shrubs after harvest for fertilization, pest control, and land management, are the main cause of biomass burning in Sub-Saharan Africa. Despite some progress, Africa's level of industrialization and agricultural modernization remains low in terms of technological advancements (Yu, 2015). Windblown dust, one of the natural factors, has a major influence on the region's air quality and public health (Bauer et al., 2019).

A better understanding of how atmospheric aerosols negatively impact human health and the environment is needed. This includes understanding how aerosols change radiation processes like reflection and scattering, which can alter air temperature and relative humidity, by determining the aerosols' presence in the radiative budget (Wong et al., 2012), which helps in quantifying their direct and indirect effects on climatic variables (Xing et al., 2017). The 2021 assessment from the Intergovernmental Panel on Climate Change (IPCC) states that aerosol air pollution has caused the world to be around 0.7°F (0.4°C) cooler than it would have been otherwise. However, there are some aerosols, such as black carbon, that warm the atmosphere by absorbing sunlight. Shindell et al. and Nordling et al. also noted that the study of aerosols' impacts on temperature is necessary because they cause both local and distant temperature responses, which significantly alter the geographic distributions of aerosol radiative forcing and temperature effects in locations such as Fumesua and Sokwai in the Kumasi metropolis.

1.3 Statement of Problem

One important aerosol (dust) source region is Africa, impacting the global and regional radiation budget, climate system, and sea-land-air coupling (IPCC Working Group, 2013). The correlation and statistical significance of some aerosols (biomass burning, carbonaceous, dust, and PM2.5) against weather variables such as wind speed, convective precipitation, and amount of water vapor in the atmosphere, as well as the spatial distribution of these aerosol types over West Africa, were considered by Ochei et al. (2023). They concluded that most aerosols correlated positively or negatively with meteorological variables, and this can affect atmospheric composition and formation. The results also indicated that aerosols were more pronounced in the dry months of November through February (NDJF) over the rainforest region, depending on the latitudinal position of the location.

In recent decades, extensive research has confirmed that emissions of aerosols, aerosol precursors, and human-made greenhouse gases (GHGs) from industrial activities, with little influence from natural variability, have been the main drivers of the rise in global average surface air temperatures, particularly since the early 20th century (Santer et al., 1995; Hansen et al., 2000). According to Perumpully and Gautam (2024), aerosols (both natural and anthropogenic) influence air quality and Earth's atmospheric dynamics, altering temperature variations, airflow patterns, and precipitation trends while exacerbating respiratory ailments and pollution. According to Wang et al. (2014), PM2.5 influences local meteorology through aerosol-meteorology interaction at short time scales. As a result, one of the elements that may influence air temperature and wind intensity is aerosol direct radiative forcing (ADRF) (Gong et al., 2007; Zhang et al., 2010).

There have been extensive studies conducted in this area of aerosol effects on temperature, including one by Mitchell (1971), who concluded that a number of characteristics of the aerosols and the surface affect how they impact surface temperatures. They also found that, depending on the particular characteristics of the aerosols and the surface, tropospheric aerosols can either warm or cool the surface, whereas stratospheric aerosols usually cause cooling close to the surface. Knippertz et al. (2009) and Schepanski et al. (2009) showed several relationships between different aerosols and some weather parameters. For instance, squall lines trigger dust mobilization. Samset et al. (2018) also showed that anthropogenic aerosols cool the global-mean surface temperature in four latest-generation climate models by between 0.5-1.1°C. Wang et al. (2022) used the Community Atmosphere Model version 4 with the dust aerosol parameterization module with and without the coupling of ocean-atmosphere processes, respectively, to analyze the direct radiative effect (DRE) of dust aerosols on the monsoons in East Asia and West Africa. They found that the DRE causes the downstream ocean of the dust source region to cool on the surface.

Because the timing and magnitude of temperature changes are crucial in determining how the effects of climate change will manifest in specific sectors of the region, regional policymakers are particularly interested in geographic variations in temperature trends (Park et al., 2015). The 20th-century temperature trend, as stated in the Intergovernmental Panel on Climate Change's Fifth Assessment Report (2014), has been reported as generally positive, but regional variations are significant.

Although aerosol-climate interactions have been widely studied globally, there is still limited localized empirical research in Sub-Saharan Africa, particularly in Ghana's Ashanti Region, Kumasi, despite its rapid urbanization and industrial activity, which lacks comprehensive assessments of how aerosol variability influences temperature and surface solar radiation at the community scale. In Ghana, research conducted by Ofosu et al. (2013) at Navrongo (a town in Ghana's Sahel Savannah Zone) reported that biomass burning and Harmattan dust are the main causes of particulate pollution in the area. Six main sources of PM2.5 mass were identified: two-stroke engines, gasoline emissions, soil dust, diesel emissions, biomass burning, and resuspended soil dust. After soil dust, biomass combustion (16.0%) is the second most significant source. The average PM2.5 mass concentration in Navrongo was $32.5 \mu g/m^3$. .

The geographical inter-city aerosol distribution during aerosol episodes (AOD $\geq$ 3.0) during a fourteen-year period revealed a declining aerosol pattern in the following order: Takoradi, Kumasi, Accra, and Tamale, according to another study by Fosu-Amankwah et al. (2021) on the assessment of aerosol burden across Ghana. Aerosol loadings were found to be increasing toward the periphery of the city center in all three locations, except Kumasi.

Despite these studies, there remains a significant knowledge gap regarding the specific local impacts of aerosol loading on temperature and SSR in Kumasi, particularly in distinct

microenvironments such as Fumesua and Sokwai. These two locations represent different environmental characteristics within the Kumasi metropolis-Fumesua being more urban and industrialized, while Sokwai represents a more rural agricultural setting.

Understanding how aerosol concentrations vary between these environments and how they influence local climate parameters is essential for developing targeted climate adaptation strategies and air quality management policies for the region. It is against this background that this study seeks to investigate the aerosol effects on temperature and surface solar radiation in selected areas within the Ashanti Region of Ghana, specifically comparing Fumesua and Sokwai in the Kumasi metropolis.

1.4 Objectives of the Study

The primary aim of this study is to investigate aerosol interaction in the atmosphere of Kumasi, Ghana. **Specific objectives include:**

1. To ascertain the temporal variations in aerosol concentration (daily, weekly, and monthly) in the specified locations (Fumesua and Sokwai).

2. To assess the spatial and seasonal variability of aerosol loading across the study areas, including determining significant differences between locations and identifying seasonal patterns.

3. To investigate the relationship between aerosol loading and local climatic variables, specifically temperature and surface solar radiation (SSR), in the selected locations.

1.5 Research Questions

The following research questions were formulated and investigated in this research work:

1. How does aerosol concentration vary temporally (daily, weekly, and monthly) in the selected locations (Fumesua and Sokwai)?

2. What are the spatial differences and seasonal patterns in aerosol loading between the study areas?

3. What is the relationship between aerosol loading and local temperature and surface solar radiation (SSR) in the selected locations?

1.6 The Significance of the Study

This study aims to assess how aerosol concentrations impact surface solar radiation (SSR) and temperature in Kumasi, Ghana, to better understand local climate dynamics. It will examine how aerosol concentrations impact regional temperature variability, providing crucial information for Ghana's climate change adaptation and mitigation strategies and enhancing understanding of aerosol impacts on tropical climates.

Since the Ashanti Region is a key agricultural area, knowledge about aerosol impacts on solar radiation is vital for agriculture, as variations in solar energy can influence crop yields. The study will provide valuable data for predicting how changes in aerosol concentrations affect agricultural productivity and food security. Additionally, monitoring changes in aerosol concentrations in different locations will help inform environmental regulations that seek to control how human activities impact air quality and air pollution. This would help establish and implement air quality standards that are essential for effective governance in Kumasi. The Ashanti Region and Sub-Saharan Africa have received limited attention in the vast amount of research on aerosols conducted worldwide. Therefore, this work is crucial for bridging that knowledge gap. The results will help policymakers and scientists better understand the behavior of regional aerosols and how they affect climate and weather.

The research aligns with Sustainable Development Goal 13, which addresses climate action, and SDG 3, focused on promoting health and well-being. Since high aerosol concentrations are linked

to health risks like respiratory diseases, identifying areas with high aerosol levels can aid public health efforts to reduce exposure, particularly in urban areas. This data can inform health monitoring and intervention programs targeting air pollution-related health issues.

1.7 Delimitations of the Study

There are several limitations to the study. It focuses on only two communities (Fumesua and Sokwai) in Ghana's Ashanti Region and is limited to environmental criteria such as agriculture, industrialization, and urbanization.

A total of four months (September to December 2022) of data were extracted, with an emphasis on short-term aerosol variations without considering long-term patterns. The study focuses on common particulate matter (PM10 and PM2.5) and their effects on temperature and solar radiation, without considering other aerosol types or more general atmospheric characteristics such as cloud formation or wind patterns.

The study depends on satellite and secondary data sources rather than experimental data collection. Finally, although aerosols have impacts on health and the economy, the study primarily examines environmental consequences, leaving health and economic implications for future research.

1.8 Organization of the Study

The thesis consists of five chapters. Chapter 1 covers the background of the study, problem statement, objectives, significance, and study limitations and delimitations. Chapter 2 presents the research conceptual framework, along with a review of relevant literature and an explanation of how this study differs from other studies of a similar nature. Chapter 3 describes the research materials and methodology, including the study area, data sources, and data analysis techniques employed to achieve the study's objectives. Chapter 4 presents the research findings and provides a thorough discussion of their implications, with appropriate tables and figures to support the

analysis. Chapter 5 concludes by summarizing the findings, detailing the limitations of the study, and making recommendations for future research.

CHAPTER TWO

2.0 LITERATURE REVIEW

2.1 Introduction

This chapter presents a comprehensive review of the literature on atmospheric aerosols and their interactions with solar radiation and temperature. The purpose of this review is to establish the theoretical foundation for this study, synthesize existing knowledge on aerosol-climate interactions, and identify the specific research gaps that this study aims to address in the Kumasi context.

The scope of this review encompasses global aerosol-climate research, with particular emphasis on studies from African and West African regions, and specific attention to the limited existing research in Ghana, particularly in the Ashanti Region. This structure ensures a logical progression from general principles to the specific context of Kumasi, while maintaining critical evaluation throughout.

2.2 Atmospheric Aerosols: Definitions and Classifications

Atmospheric aerosols are suspensions of solid or liquid particles in air, ranging in size from nanometers to micrometers (Kommalapati and Valsaraj, 2009). These particles play crucial roles in atmospheric physics, climate dynamics, air quality, and human health (Pöschl, 2005). The atmosphere contains various aerosol types, including dust, smoke, fumes, mist, fog, haze, and smog, each with distinct physical and chemical properties.

Aerosols are classified based on their formation mechanisms into primary and secondary aerosols. Primary aerosols are directly emitted into the atmosphere from sources such as sea spray, mineral dust, volcanic emissions, and combustion processes (Haywood & Boucher, 2000). Secondary aerosols form in the atmosphere through gas-to-particle conversion processes, including

nucleation and condensation of gaseous precursors such as sulfur dioxide (SO_2), nitrogen oxides (NO_x), and volatile organic compounds (VOCs) (Crutzen & Andreae, 1990; Boulon et al., 2011). Natural aerosol sources include desert dust from arid regions, sea salt from ocean spray, biogenic particles from vegetation, and volcanic ash. Anthropogenic sources comprise emissions from fossil fuel combustion, industrial processes, biomass burning, and agricultural activities (Bond et al., 2004; Liousse et al., 2014). In West Africa, major aerosol sources include Saharan dust transport, biomass burning from agricultural practices, and increasing urban and industrial emissions (Knippertz et al., 2015; Keita et al., 2021).

Aerosol particle sizes typically range from $0.001\,\mu m$ to $100\,\mu m$, with this size distribution critically influencing their atmospheric behavior, lifetime, and climate effects. Fine particles ($<$ $1\,\mu m$ radius) primarily originate from condensation processes and combustion, while coarse particles ($1-10\,\mu m$ radius) are mechanically generated by wind action on surfaces (Seinfeld & Pandis, 2006).

Aerosols size typically ranges from 2nm to several hundred micrometers, and although their shapes can vary, they are often represented by their aerodynamic equivalent diameter. Aerosol concentration is usually measured either by particle mass per unit volume (mg/m^3or $\mu g/m^3$) or particle count per unit volume ($\#/m^3$) with mass concentration being more commonly used in standards and measurements. Typical mass concentrations and particle sizes are outlined in Table 2.1.

Table 2-1: Mass concentrations and particle size of aerosol (Warneck, 2000).

Area	Concentration/$\mu g/m^3$	Diameter/μm
Urban	> 100	0.03
Rural	$30 - 50$	0.07
Marine	> 10	0.16

Aerosols have varying atmospheric lifetimes, which is an important characteristic. The atmospheric lifetime of aerosols varies from hours for large particles to weeks for accumulation mode particles ($0.01 - 1\ \mu m$), with removal occurring through dry deposition and wet scavenging by precipitation (Jacob, 2000). Table 2.2 provides particle sizes for different aerosol types and their typical atmospheric lifetime.

Table 2-2: Properties of atmospheric aerosols (Seinfeld, &Pandis, 2006).

Nature of droplet	Size/μm	Surface area (m^2/m^3)	Liquid water content/(m^3) of air	Typical atmospheric lifetime
Aerosol	$10^{-2} - 10$	1×10^{-3}	$10^{-11} - 10^{-10}$	4 – 7 days
Fog droplets	1 – 10	8×10^{-4}	$5 \times 10^{-8} - 5 \times 10^{-7}$	3 hours
Cloud drops	$10 - 10^2$	2×10^{-1}	$10^{-7} - 10^{-6}$	7 hours
Rain drops	$10^2 - 10^3$	5×10^{-5}	$10^{-7} - 10^{-6}$	3 – 15 minutes
Snow flasks	$10^3 - 10^5$	3×10^{-1}		15 – 50 minutes

There are numerous significant environmental effects of atmospheric aerosols. At the high concentrations found in urban environments, they pose a risk to respiratory health. Their presence reduces visibility as they scatter and absorb visible light (Jacob, 2000). They both directly (by scattering and absorbing radiation) (Charlson et al., 1992), and indirectly (by acting as cloud

formation nuclei) influence the Earth's climate. They give the atmosphere places where surface and condensed-phase chemistry can occur (Twomey, 1974).

The condensation of gases and wind movement on the surface of the Earth are the sources of atmospheric aerosols. Precursor gas condensation is the primary source of fine aerosol particles, defined as those with a radius of less than $1\mu m$. Figure 1. depicts the typical chemical composition of fine aerosol in the lower troposphere.

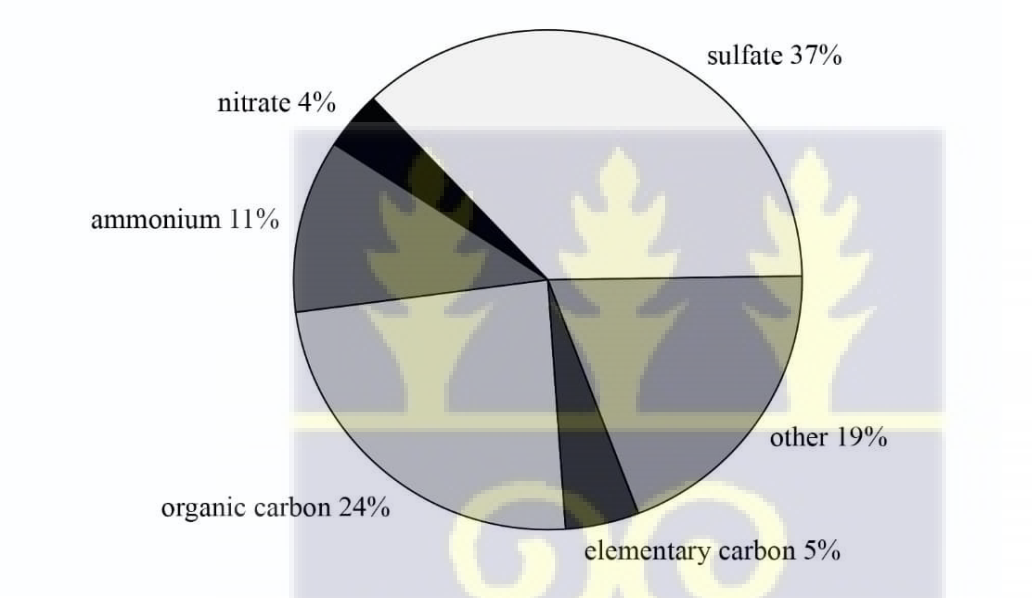

Figure 2.1: Typical composition of continental aerosol. Adapted from (Heintzenberg, 1989) cited by Jacob (2000).

One important precursor gas is sulfuric acid (H_2SO_4), which is created in the atmosphere through the oxidation of sulfur dioxide (SO_2) released by volcanoes and other sources, among other sources. In H_2SO_4-H_2O solutions, H_2SO_4 has a low vapor pressure and condenses to form aqueous sulfate particles in all atmospheric conditions. The condensation of other low vapor pressure gases, such as NH_3, HNO_3, and organic compounds, can then alter the composition of these sulfate particles. The primary source of organic carbon in the fine aerosol (Figure 1) is condensation of large hydrocarbons with both biogenic and anthropogenic origins. Soot formed when gases

condense during combustion is another significant part of the fine aerosol. Both black organic aggregates and elemental carbon are included in the common definition of soot.

Sea salt, soil dust, and plant debris are released into the atmosphere by the wind's mechanical action on the surface of the Earth. These aerosols are primarily made up of coarse (relatively large airborne particles mainly produced by the mechanical break-up of even larger solid particles.) particles with a radius of 1–10 μm. Because of their large area-to-volume ratios and high surface tension per unit aerosol volume, particles finer than 1µm are challenging to generate mechanically. Because of their high sedimentation velocities, particles larger than 10 μm have a short atmospheric lifetime and are difficult for the wind to lift.

The various processes that lead to the creation, development, and ultimate elimination of atmospheric aerosol particles are depicted in Figure 2.2. The typical size range of gas molecules is 10^{-4}-10^{-3} µm. these ultrafine aerosols in the size range of 10^{-3}-10^{-2} µm are created when gas molecules cluster together, a process known as nucleation. These ultrafine aerosols grow rapidly to the 0.01-1 µm fine aerosol size range by condensation of gases and by coagulation (collisions between particles during their random motions).

Beyond 1µm, growth is substantially slower because the particles are too big to grow quickly through gas condensation at that point and because the coagulation rate is slowed down by the larger particles' slower random motion. Hence, aerosol particles that result from gas condensation often gather in the 0.01–1 µm size range, which is referred to as the accumulation mode (as opposed to the coarse mode or ultrafine mode) (Jacob, 2000).

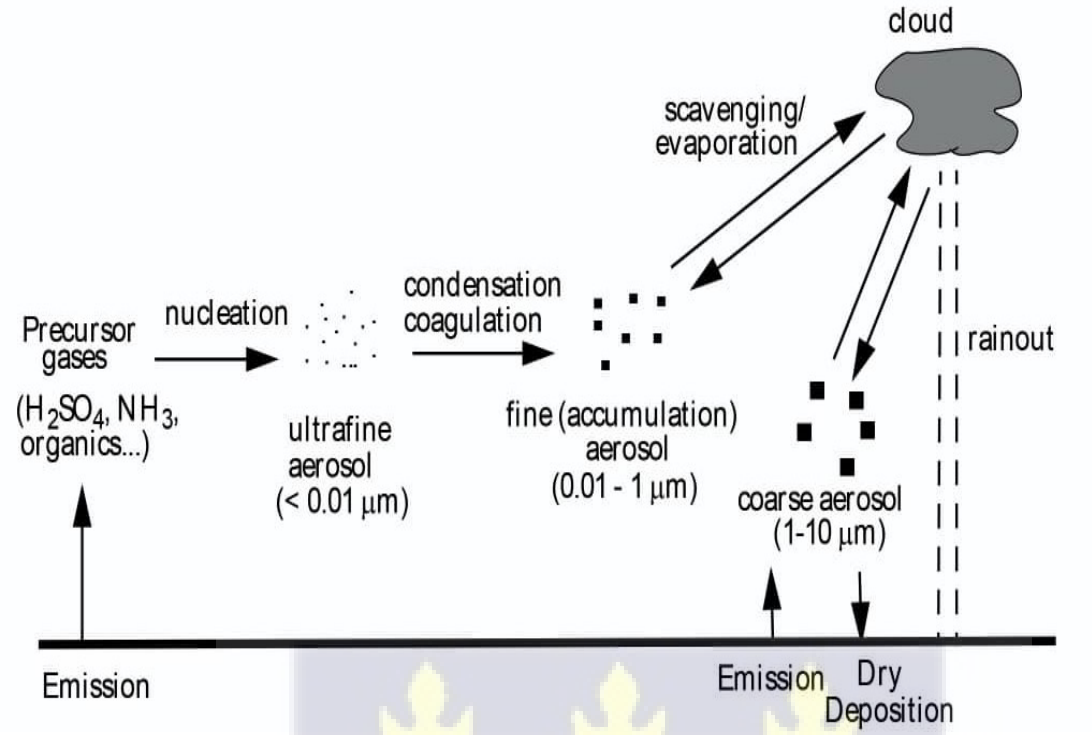

Figure 2.2: Production, growth and removal of atmospheric aerosols (Jacob, 2000).

Atmospheric aerosols are eliminated from the atmosphere either by striking the Earth's surface (dry deposition) or by falling out of the sky as precipitation clouds (wet deposition). When dust is carried to the surface by gravity or turbulence, it is known as dry removal. For small particles, gravitational settling affects their movement, whereas Brownian motion, or random movement, dominates for larger particles. Aerosols removed in precipitation (water, fog, or ice) undergo wet removal processes. Particulate aerosols can be rained out by either diffusing into falling drops or colliding with raindrops (a process known as "inertial removal," which works best for heavy particles). The amount of moisture present naturally affects the total amount of aerosol removed by wet processes. It is possible for large aerosol particles to serve as cloud condensation nuclei (CCN), which means that cloud droplets condense on the aerosol particles. In as little as one hour, clouds can form, rain, and then evaporate any aerosols that were caught in wet removal processes as well as the aerosols they formed on. Aerosols play a crucial role in the biosphere, climate, public

health, and atmospheric physics and chemistry. The hydrological cycle, atmospheric circulation, abundance of greenhouse and reactive trace gases, and Earth's energy balance are impacted by airborne solid and liquid particles with sizes ranging from nanometers to micrometers. Additionally, they can either cause or exacerbate diseases and have a significant role in the reproduction of biological organisms. The concentration, size, structure, and chemical composition of aerosol particles are the main factors that influence their effects on the environment and human health. However, there is a great deal of temporal and spatial variability in these parameters. The quantification and identification of biological particles and carbonaceous components of fine particulate matter in the air (organic compounds and black or elemental carbon, respectively) represent demanding analytical challenges (Pöschl, 2005).

2.3 Theoretical and Conceptual Framework

This section presents the theoretical foundations that underpin the investigation of aerosol effects on temperature and solar radiation. The conceptual framework integrates radiative forcing theory, aerosol-radiation interaction principles, and atmospheric energy balance concepts to provide a coherent theoretical basis for this study.

2.3.1 Radiative Forcing Theory

Radiative forcing (RF) is defined as the change in net irradiance (downward minus upward) at the tropopause after allowing stratospheric temperatures to readjust to radiative equilibrium, while holding surface and tropospheric temperatures fixed (IPCC, 2021). This concept provides a quantitative measure of the climate impact of various forcing agents, including aerosols.

The fundamental principle of radiative forcing stems from Earth's energy balance. For the climate system to be in equilibrium, the incoming solar radiation must equal the outgoing terrestrial radiation. Any perturbation to this balance constitutes a forcing mechanism that drives climate

change (Ramanathan et al., 1989; Hansen et al., 1997). Positive radiative forcing leads to warming, while negative forcing results in cooling. .

Aerosols alter radiative forcing through multiple mechanisms. The direct radiative effect occurs when aerosols scatter and absorb solar and terrestrial radiation, directly modifying the radiation budget (Charlson et al., 1992; Haywood & Boucher, 2000). The magnitude and sign of direct forcing depend on aerosol optical properties (single scattering albedo, asymmetry parameter), vertical distribution, and surface albedo beneath the aerosol layer (Russell et al., 1999; Ramanathan et al., 2001). Recent assessments indicate that anthropogenic aerosols exert a substantial negative radiative forcing, partially offsetting greenhouse gas warming (IPCC, 2021). However, significant uncertainties remain, particularly regarding aerosol-cloud interactions and regional variations in aerosol composition and distribution (Boucher et al., 2013; Myhre et al., 2013).

2.3.2 Aerosol-Radiation Interaction Framework

The interaction of aerosols with solar radiation is governed by fundamental scattering and absorption processes. When solar radiation encounters aerosol particles, three processes occur: transmission (radiation passing through), scattering (redirection of radiation), and absorption (conversion of radiant energy to heat) (Liou, 2002).

The efficiency of these processes depends on aerosol optical properties, particularly the single scattering albedo, which is the ratio of scattering to total extinction (scattering plus absorption). Sulfate and nitrate aerosols are primarily scattering, resulting in cooling effects, while black carbon is highly absorbing, leading to atmospheric heating and surface dimming (Bond et al., 2013). Mineral dust exhibits intermediate properties depending on iron oxide content (Sokolik & Toon, 1999).

The aerosol optical depth (AOD) quantifies the total extinction of radiation by aerosols in a vertical column of atmosphere. AOD is a fundamental parameter for assessing aerosol radiative effects and is directly measurable by ground-based and satellite instruments (Holben et al., 1998; Levy et al., 2013). Higher AOD values indicate greater aerosol loading and potential for larger radiative perturbations.

The Angstrom exponent provides information on aerosol size distribution, with larger values indicating smaller particles. This parameter helps distinguish between fine mode aerosols (pollution, smoke) and coarse mode aerosols (dust) (Eck et al., 1999). These optical properties collectively determine the magnitude and sign of aerosol radiative forcing.

2.3.3 Earth's Energy Balance and Aerosol Perturbations

Earth's climate is fundamentally governed by the balance between incoming solar radiation and outgoing terrestrial radiation. The globally averaged energy balance can be expressed mathematically. At equilibrium, the energy absorbed by Earth equals the energy emitted. Aerosols perturb this balance by modifying the planetary albedo and atmospheric absorption. Scattering aerosols increases albedo, reflecting more solar radiation to space and inducing cooling. Absorbing aerosols reduce surface solar radiation (SSR) while heating the atmospheric layer where they reside, creating complex vertical temperature redistributions (Ramanathan et al., 2001; Wild et al., 2005).

The relationship between aerosol-induced changes in SSR and surface temperature is not straightforward. Reduced SSR generally leads to surface cooling, but absorbing aerosols can heat the atmosphere, alter atmospheric stability, modify cloud formation, and indirectly affect surface temperatures through complex feedback mechanisms (Koch & Del Genio, 2010; Wilcox et al.,

2016). Understanding these processes is critical for predicting regional climate responses to aerosol forcing.

2.3.4 Earth's radiation balance: role of aerosols

Our planet gets warmed by solar radiation, most of which falls into the visible spectrum. As per Seinfeld et al. (2004), the Earth needs to return to space an equivalent amount of energy that it receives from the Sun. The Earth's atmosphere is mostly made up of greenhouse gases (GHGs), which absorb most of the infrared (IR) radiation that the planet's surface emits despite being mostly transparent to incoming solar radiation. Clouds also absorb infrared light. According to Satheesh and Krishnamoorthy (2005), if the incident solar radiation at the top of the atmosphere (global) is depicted as 100 units, then a net amount of 51 units makes it to the surface (Fig. 3).

Earth's Radiation Budget

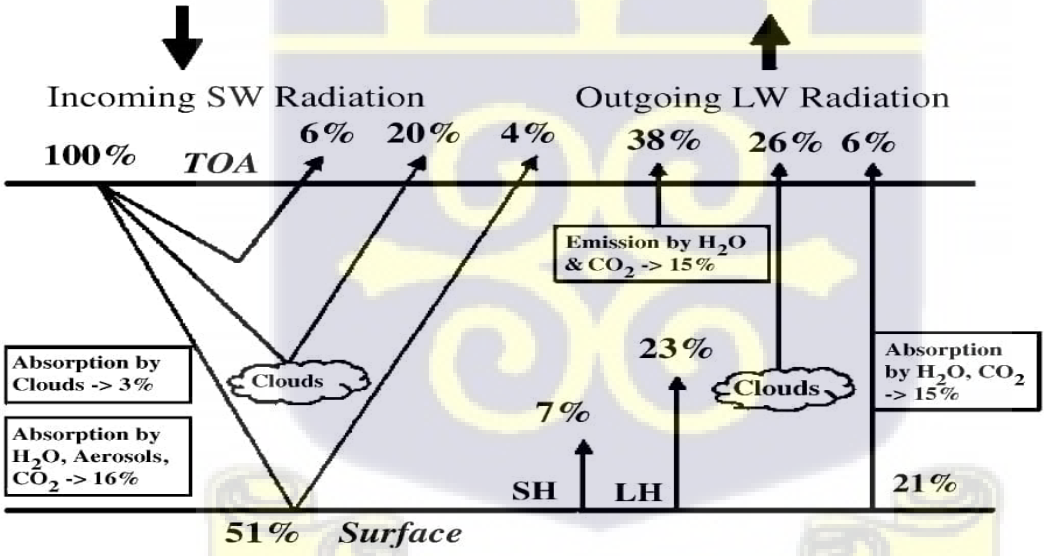

Figure 2.3: Earth's radiation budget demonstrating the role of aerosol (Satheesh and Krishnamoorthy, 2005).

Out of the remaining 49 units, 3 units are absorbed by clouds, and 16 units are CO_2, water vapor, and aerosols collectively. The cloud cover, surface, and atmosphere, which also includes aerosols, show, in that order, 17 units, 6 units, and 7 units. Of the 51 units that the Earth's surface has absorbed, 23 are released as latent heat, seven units as sensible heat, and twenty-one units. Aerosols, water vapor, and CO_2 absorb roughly 15 units of infrared radiation. Aerosols, therefore, play a significant role in the Earth's radiation balance.

It is well known that warming tends to increase evaporation, which raises the troposphere's water vapour content (Seinfeld et al., 2004). This increases the warming even more because the main greenhouse gas is water vapor. Reducing snow and ice cover would also increase warming because they reflect a large portion of incident sunlight into space. Although clouds are generally good at absorbing infrared light, high clouds emit less infrared light into space because their tops are colder than those of low clouds. The interplay between the atmosphere (GHGs, molecular absorbers, and aerosols), the ocean, clouds, and ice is poorly understood.

In general terms, according to Harte (1988), the energy absorbed by the Earth can be written as:

Equation 2.1: the energy absorbed by the Earth

$$E_1 = \frac{(1-\alpha)S_0}{4}$$

And the energy emitted by the Earth can be written as:

Equation 2.2: the energy emitted by the Earth

$$E_O = \sigma T_e^4$$

Where T_e = temperature in Kelvin, $\sigma = 5.67 \times 10\text{-}8$ J/m^2 sec K^4

The two equations must be equal for the Earth's temperature to reach an equilibrium, or steady state ($E_I = E_O$). An equation is written for the planetary temperature under certain conditions. The

mean temperature of the Earth (Te) can also be written as the balance between the absorbed solar energy and emitted terrestrial energy, given by the steady state condition,

Equation 2.3: the mean temperature of the Earth

$$\frac{S_0}{4\sigma}(1-\alpha) = T_e^4$$

The average planetary temperature is 254K (-19.2 °C, -2.6 °F) when this equation is solved using the measured solar flux (Harte, 1989) at the top of the atmosphere. Naturally, this estimate is well below the average temperature at sea level or ground level (about 14° C, 57.2° F), which is the primary surface of energy absorption, but it is near to reported conditions in the upper section of the troposphere.

S_0 is the solar power per unit area intercepted at the mean Sun–Earth distance (solar constant) $(1365 - 1372\ W\ m2)$ (Seinfeld and Pandis, 1998). The ratio of the cross-sectional area to the Earth's surface area is known as factor 4. The albedo, or reflectance, of the Earth is represented by the number, α. Its mean value is approximately 0.3, and it represents the portion of incident solar radiation that is reflected by the planet's surface and atmosphere. Therefore, the Earth's surface and atmosphere reflect 103 W m^2 of the 343 W m^2 of mean solar radiation incident at the top of the atmosphere back to space. Aerosols can affect the albedo, which in turn affects the climate system. According to the energy balance equation, the global temperature changes by roughly 1% for every 0.01 change in the value of α. The chemical makeup of aerosols determines whether they raise or lower the value of a, warming or cooling the planet.

While totally scattering aerosols will result in a decrease in α (a temperature drop), absorbing aerosols (soot, for example) will result in a decrease in α (Coakley and Cess, 1985; Hansen et al., 1998; Russell et al., 1999) and an increase in T_e. According to Kaufman et al. (1997), Clarke et al. (1998), Russell et al. (1999), Ginoux et al. (2001, 2004), Ramanathan et al. (2001), Luo et al.

(2003), and other studies, the warming or cooling effect can vary from region to region depending on several factors. If aerosols have a net cooling effect, they partially counteract greenhouse warming; if they have a net warming effect, they enhance it (IPCC, 2001). The primary reason why the significance of aerosols is not well characterized in climate models is that aerosol properties exhibit significant regional variations, which can have very different effects on different regions.

2.3.5 Conceptual Framework for Kumasi Aerosol Study

This study employs a conceptual framework that links aerosol loading to local climate variables through a chain of physical processes.

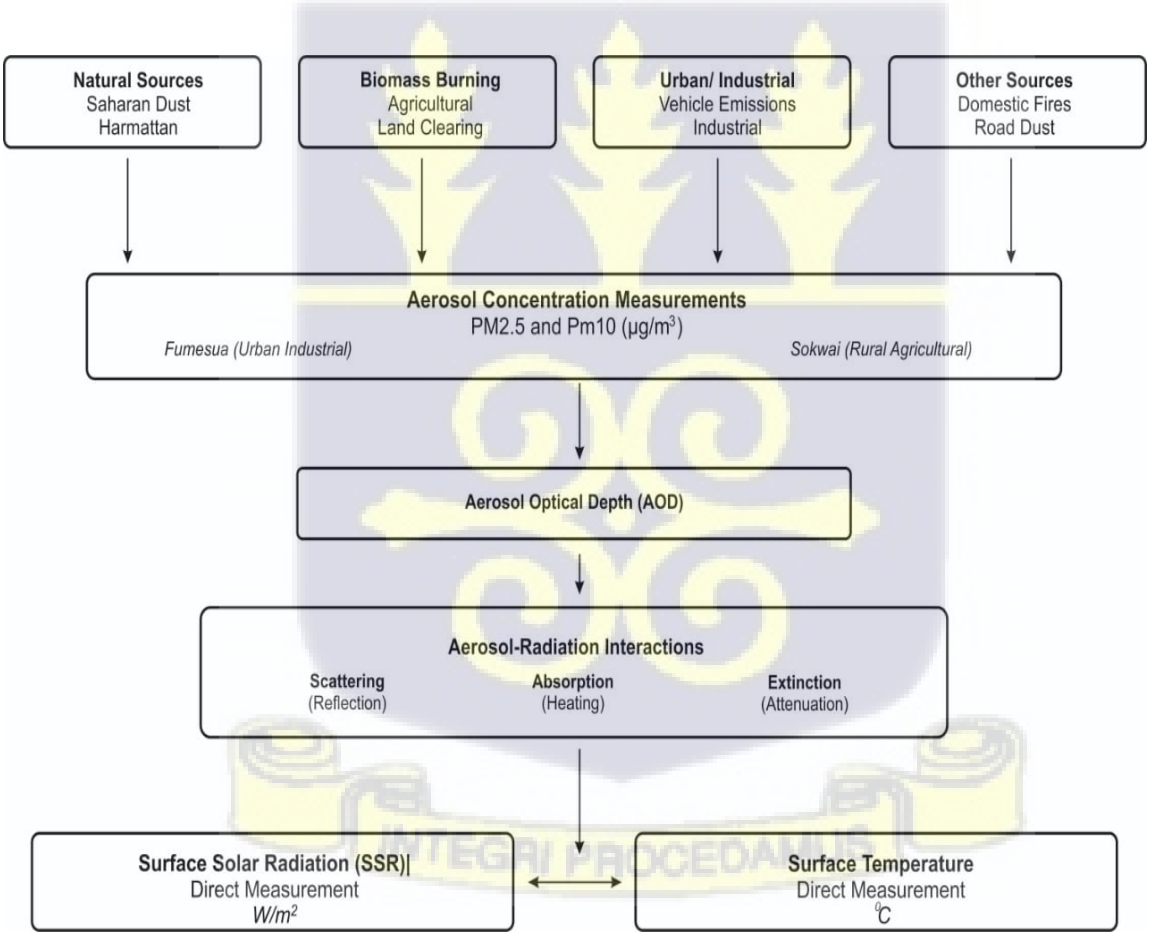

Figure 2.4: Conceptual Framework Flowchart

The framework posits that variations in aerosol concentration (measured as PM2.5 and PM10) in Kumasi affect aerosol optical depth, which in turn modulates surface solar radiation through scattering and absorption processes. Changes in SSR subsequently influence surface temperature through alterations in the surface energy budget.

The framework accounts for spatial variability by comparing Fumesua (urban, industrialized) with Sokwai (rural, agricultural), recognizing that different emission sources and local meteorological conditions may produce distinct aerosol characteristics and climate impacts. Temporal variability is examined through daily, weekly, and seasonal analyses, acknowledging the influence of seasonal factors such as Harmattan dust, biomass burning cycles, and monsoon dynamics on aerosol loading in the region.

This conceptual model provides the organizing framework for data analysis and interpretation, guiding the investigation of relationships between measured aerosol concentrations and observed changes in temperature and solar radiation in the study areas.

2.4 Aerosol Effects on Climate

Aerosols influence Earth's climate through multiple pathways, broadly categorized as direct, indirect, and semi-direct effects. Understanding these mechanisms is essential for interpreting aerosol impacts on local temperature and solar radiation.

2.4.1 Direct Radiative Effects

The direct effect of aerosols refers to their immediate interaction with solar and terrestrial radiation through scattering and absorption processes (Haywood & Boucher, 2000). Scattering aerosols (sulfates, nitrates, sea salt) redirect incoming solar radiation, with a portion reflected to space, increasing planetary albedo and cooling the surface. Absorbing aerosols (black carbon, some

mineral dust) convert radiant energy to heat, warming the atmospheric layer they occupy while reducing surface insolation (Ramanathan et al., 2001).

The net direct radiative forcing depends on the balance between scattering and absorption, determined by the aerosol single scattering albedo. Pure sulfate aerosols exert strong negative forcing (cooling), while black carbon produces positive forcing (warming) (Bond et al., 2013). Most real-world aerosols are mixtures, exhibiting intermediate properties. The underlying surface albedo also critically influences direct forcing: over bright surfaces (snow, desert), absorbing aerosols may produce net cooling by reducing reflected radiation, while over dark surfaces (ocean, forest), they typically induce warming (Haywood & Shine, 1997).

Global estimates suggest anthropogenic aerosol direct forcing of approximately -0.3 to -0.5 W/m^2, but regional variations are substantial (IPCC, 2021). High aerosol regions such as South Asia, East Asia, and parts of Africa experience much larger local forcing magnitudes, with correspondingly larger impacts on regional temperature and precipitation patterns (Bollasina et al., 2011; Randles & Ramaswamy, 2008).

2.4.2 Indirect Effects: Aerosol-Cloud Interactions

Aerosol indirect effects arise from aerosols' role as cloud condensation nuclei (CCN) and ice nuclei (IN), modifying cloud microphysical and macrophysical properties (Twomey, 1974; Albrecht, 1989). The first indirect effect (cloud albedo effect) occurs when increased aerosol concentrations lead to more numerous but smaller cloud droplets for a given liquid water content. Smaller droplets increase cloud reflectivity, enhancing cooling (Twomey, 1977).

The second indirect effect (cloud lifetime effect) relates to precipitation efficiency. Smaller droplets are less efficient at initiating precipitation, potentially increasing cloud lifetime and coverage, further enhancing negative radiative forcing (Albrecht, 1989). However, observational

confirmation of this effect has proven challenging due to complex meteorological feedbacks (Stevens & Feingold, 2009).

Recent research has identified additional aerosol-cloud interaction mechanisms. The glaciation indirect effect involves changes in ice nucleation processes (Lohmann & Feichter, 2005). The convective invigoration effect suggests that aerosols may enhance deep convection under certain conditions, with uncertain net climate impacts (Rosenfeld et al., 2008). Aerosol effects on mixed-phase clouds represent a particularly uncertain area, with potential for both warming and cooling depending on aerosol properties and meteorological conditions (Storelvmo, 2017).

Global estimates of aerosol indirect forcing range from -0.5 to -1.5 W/m^2, but uncertainty remains large (IPCC, 2021). The complexity of aerosol-cloud interactions, involving non-linear processes and multiple feedback mechanisms, makes this the largest source of uncertainty in aerosol climate forcing assessments (Boucher et al., 2013).

2.4.3 Semi-direct Effects

The semi-direct effect describes climate impacts arising from atmospheric heating by absorbing aerosols (Hansen et al., 1997). When black carbon or absorbing dust heats an atmospheric layer, several consequences may follow: increased atmospheric stability, suppression of cloud formation, and evaporation of existing clouds. These processes can amplify surface dimming beyond the direct absorption effect alone (Ackerman et al., 2000).

The sign and magnitude of the semi-direct effect depend critically on the vertical distribution of absorbing aerosols relative to clouds (Koch & Del Genio, 2010). Absorption above clouds tends to enhance warming, while absorption below clouds may reduce cloud cover and produce mixed temperature responses. Recent studies using advanced climate models suggest the global semi-

direct effect may be small (approximately +0.1 W/m2), but regional impacts can be substantial, particularly in regions with high black carbon emissions (Perlwitz & Miller, 2010).

In West Africa, absorbing aerosols from biomass burning and transported Saharan dust interact with the monsoon system, potentially affecting regional circulation patterns and precipitation (Konare et al., 2008; Solmon et al., 2008). Understanding these regional semi-direct effects is crucial for predicting climate responses to changing aerosol emissions.

2.5 Review of Previous Studies

This section critically reviews previous research on aerosol-climate interactions, organized from global studies to regional African research and the local Ghanaian context. Each subsection not only summarizes key findings but also evaluates methodologies, identifies limitations, and highlights gaps relevant to this study.

2.5 Aerosol-Climate Interactions

2.5.1 Global Studies

Extensive global research has established the fundamental importance of aerosols in climate systems. Samset et al. (2018) used four climate models to demonstrate that anthropogenic aerosols cool global-mean surface temperatures by 0.5-1.1 degrees Celsius, with substantial inter-model variability reflecting uncertainties in aerosol processes. This study highlighted the critical role of aerosol-cloud interactions in determining the magnitude of cooling, with cloud feedback processes accounting for much of the model spread.

Westervelt et al. (2020) examined regional temperature responses to aerosol emissions reductions in Asia, finding that the removal of Asian aerosols causes substantial Northern Hemisphere warming, particularly over the Arctic through teleconnection mechanisms. Their multi-model analysis (GFDL, CESM1, GISS-E2) revealed significant model differences in regional

temperature responses, attributed to varying representations of aerosol microphysics and cloud interactions. This study underscores that aerosol climate impacts are not confined to source regions but affect distant locations through atmospheric and oceanic circulation changes.

Recent work on aerosol effects on surface solar radiation has quantified substantial “global dimming” trends. Wild et al. (2021) synthesized observations showing widespread SSR decreases from the 1950s to the 1980s, followed by partial recovery ("brightening") since 1990 in some regions. They attributed these trends primarily to aerosol changes, though cloud variations also contribute. Importantly, regional patterns diverge substantially from global means, with continued dimming in South Asia despite brightening elsewhere, emphasizing the need for regional assessments. The aerosol-temperature relationship has been shown to vary by aerosol type and region. Persad and Caldeira (2018) used CAM5 simulations to demonstrate that emissions from different regions produce distinct global temperature patterns. Chinese emissions caused Northern Hemisphere cooling, while Indian emissions produced mixed regional responses, including both warming and cooling. These regional differences stem from variations in aerosol composition, transport patterns, and interactions with regional meteorology.

While global studies have established broad principles of aerosol-climate interactions, they typically employ coarse-resolution models (50-200 km grid spacing) that may not capture sub-regional features important in complex terrain or heterogeneous emission regions. Furthermore, most global studies focus on large source regions (China, India, Europe) with relatively little attention to African aerosol sources and impacts, creating a knowledge gap that this study addresses.

2.5.2 Regional Studies

Africa represents a critical but understudied region for aerosol-climate research. The continent hosts major natural aerosol sources (Saharan dust, biomass burning) and faces increasing anthropogenic emissions from rapid urbanization and industrial development (Liousse et al., 2014).

Saharan dust constitutes the world's largest natural aerosol source, with major climate implications. Zhao et al. (2022) used satellite observations and modeling to show that Saharan dust affects West African monsoon dynamics through complex radiative and cloud-microphysical pathways. Dust heating in the Saharan Air Layer modifies atmospheric stability and monsoon onset timing, with implications for regional precipitation patterns. However, significant uncertainties remain regarding dust optical properties, particularly the relative contributions of scattering versus absorption, which vary with iron oxide content and mixing state (Sokolik & Toon, 1999; Formenti et al., 2011).

Biomass burning aerosols represent another major African emission source. Liousse et al. (2014) estimated that African biomass burning emissions will increase substantially through 2030 due to population growth and land use changes. Konare et al. (2008) investigated biomass burning aerosol effects on West African climate using regional modeling, finding that smoke aerosols significantly reduce surface solar radiation during the burning season (December-February), with consequent cooling of surface temperatures. However, their study noted large uncertainties in emission inventories and aerosol optical properties, limiting quantitative confidence in projected impacts.

Urban and industrial aerosol emissions are rapidly increasing in Africa but remain poorly quantified. Keita et al. (2021) characterized anthropogenic emissions in Abidjan, Ivory Coast, identifying domestic fires, traffic, and industrial sources as major contributors. They found that

particulate matter concentrations frequently exceed WHO guidelines, with health implications for urban populations. However, the climate impacts of these urban emissions remain poorly understood, with few studies linking urban aerosol measurements to radiative effects or temperature changes.

The West African monsoon (WAM) represents a critical climate system potentially sensitive to aerosol perturbations. Knippertz et al. (2015) reviewed aerosol-monsoon interactions, concluding that both dust and biomass burning aerosols likely affect monsoon dynamics, but the direction and magnitude of impacts remain uncertain due to limited observations and model deficiencies. Solmon et al. (2008) used regional modeling to suggest that biomass burning aerosols may delay monsoon onset, but observational validation has been limited.

African aerosol studies face several persistent challenges: sparse ground-based observational networks, limited satellite validation, inadequate emission inventories, and coarse model resolutions that miss important regional features. Most studies focus on large-scale dust transport or extensive biomass burning regions, with much less attention to local urban aerosol sources and sub-regional climate impacts. Furthermore, few studies have examined the specific aerosol-SSR-temperature linkage in African contexts, creating a gap that this research addresses.

2.5.3 Local Aerosol Studies

Research on aerosols in Ghana remains limited, with only a handful of studies examining aerosol characteristics and sources. Ofosu et al. (2013) conducted one of the few comprehensive aerosol studies in Ghana, investigating $PM_{2.5}$ sources in Navrongo, located in the Sahel Savannah Zone of northern Ghana. Using receptor modeling, they identified six major $PM_{2.5}$ sources: soil dust (primary contributor), biomass burning (16% of mass), diesel emissions, gasoline emissions, two-stroke engines, and resuspended dust. The average PM2.5 concentration was 32.5 micrograms per

cubic meter, substantially exceeding WHO guidelines. They concluded that Harmattan dust and biomass burning are the dominant contributors to particulate pollution in the region.

This study, while valuable, has significant limitations for understanding aerosol impacts in Kumasi. First, Navrongo is located in a distinct climatic and geographical zone (dry Sahel) compared to Kumasi (humid forest transition). Second, the study characterized aerosol sources and concentrations but did not examine climate impacts such as effects on temperature or solar radiation. Third, the four-year study period (2006-2009) predates recent urbanization and emission changes.

Fosu-Amankwah et al. (2021) assessed aerosol burden across four Ghanaian cities (Accra, Kumasi, Takoradi, and Tamale) using MODIS satellite AOD data over fourteen years (2005-2019). They found that during high aerosol episodes (AOD greater than or equal to 0.3), aerosol loading followed the pattern: Takoradi > Kumasi > Accra > Tamale. Interestingly, within Kumasi, they observed increasing aerosol concentrations toward the city periphery, contrary to the typical urban-center-peak pattern observed in other cities. This anomalous spatial pattern suggests unique emission or meteorological characteristics in Kumasi deserving further investigation.

While Fosu-Amankwah et al. provided valuable information on spatial and temporal AOD patterns, their study did not examine the mechanisms producing these patterns or their consequences for local climate variables. Furthermore, satellite AOD represents column-integrated aerosol, which may not correlate directly with surface PM concentrations or local radiative effects. The study also lacked ground-based validation and did not examine aerosol type or composition.

Additional research in Ghana has focused on specific pollution sources or episodes. Aboh et al. (2009) investigated Harmattan dust impacts on air quality in southern Ghana, documenting

substantial increases in particulate matter during Harmattan months. However, they did not examine radiative or climate effects. Similarly, studies of vehicle emissions and roadside air quality (e.g., Antwi-Agyei et al., 2016) have characterized pollution levels but not linked them to broader climate impacts.

Critical evaluation: The body of aerosol research in Ghana exhibits several critical gaps. First, no studies have systematically examined the relationship between aerosol loading (whether measured as PM concentrations or AOD), surface solar radiation, and temperature in any Ghanaian city, including Kumasi. Second, sub-city spatial variability has received minimal attention, despite the intriguing patterns suggested by Fosu-Amankwah et al. Third, temporal variability beyond simple seasonal patterns (e.g., weekly variations, relationships with meteorology) remains unexplored. Fourth, no studies have compared urban versus rural/agricultural environments within the same region to isolate anthropogenic versus natural aerosol contributions and effects. These gaps directly motivate the present study.

The preceding literature review reveals substantial knowledge gaps at multiple scales, from global uncertainties to specific deficiencies in understanding aerosol-climate interactions in the Kumasi context. This section explicitly identifies these gaps and demonstrates how this study addresses them.

2.6 Knowledge Gaps

2.6.1 Global

Despite decades of research, several fundamental uncertainties persist in aerosol-climate science. The IPCC AR6 (2021) identifies aerosol-cloud interactions as the largest source of uncertainty in climate forcing assessments, with the total aerosol effective radiative forcing (ERF) ranging from

-2.0 to -0.4 W/m^2. This wide range reflects a poor understanding of how aerosols modify cloud properties, particularly in mixed-phase and ice clouds.

Regional variations in aerosol radiative effects remain poorly quantified. While global mean effects are increasingly well-constrained, local and regional impacts exhibit large uncertainties due to heterogeneous aerosol distributions, varying aerosol properties, and complex interactions with local meteorology (Myhre et al., 2013). The relationship between aerosol-induced changes in SSR and surface temperature responses involves multiple feedback mechanisms that are incompletely understood and inadequately represented in climate models (Wild et al., 2021).

Absorbing aerosols, particularly black carbon, present specific challenges. The semi-direct effect magnitude and sign depend critically on aerosol vertical distribution relative to clouds, which is poorly observed and difficult to model (Koch & Del Genio, 2010). The mixing state of black carbon with other aerosol components affects absorption properties, but observations of aerosol mixing state are sparse (Bond et al., 2013).

2.6.2 Regional Gaps

Africa suffers from particularly acute observational and research gaps relative to its importance in global aerosol budgets. The continent hosts the world's largest dust source yet has minimal ground-based aerosol monitoring networks (Prospero et al., 2002). Biomass burning emissions are enormous but poorly quantified, with emission factors varying substantially across different vegetation types and burning conditions (Liousse et al., 2014).

West African aerosol-climate interactions remain poorly understood despite their potential importance for regional monsoon dynamics. Knippertz et al. (2015) identified major uncertainties in how dust and biomass burning aerosols affect the West African monsoon, noting that different

models produce conflicting results. Observational constraints on aerosol effects are minimal due to sparse measurement networks.

Urban and industrial aerosol sources are rapidly growing in West Africa but are inadequately characterized in emission inventories and poorly represented in climate models (Keita et al., 2021). The local radiative and climate impacts of these emissions, particularly in medium-sized cities, have received minimal research attention. Furthermore, the heterogeneity of urban versus rural/agricultural environments and their distinct aerosol characteristics and impacts remain largely unexplored in the West African context.

2.6.3 Local Gaps

For Kumasi and the Ashanti Region specifically, the research gaps are profound. No previous study has systematically examined the relationship between aerosol loading and local climate variables (temperature, SSR) in Kumasi. While Fosu-Amankwah et al. (2021) documented AOD patterns, they did not investigate the mechanisms or consequences of these patterns.

The unusual spatial distribution of aerosols in Kumasi, with increasing concentrations toward the periphery rather than a central urban peak, has not been explained. This pattern suggests distinctive emission sources, transport patterns, or meteorological influences that deserve investigation. Furthermore, no research has examined sub-city scale variability by comparing distinct microenvironments (e.g., urban-industrial versus rural-agricultural settings) within the Kumasi region.

Temporal variability beyond simple seasonal patterns remains unexplored. Weekly, daily, and diurnal patterns of aerosol concentrations have not been characterized, nor have their relationships with meteorological variables or emission activity cycles. The relative contributions of different

aerosol sources (Harmattan dust, biomass burning, urban emissions, vehicle exhaust) to total aerosol loading in Kumasi are unknown.

Most critically, the impacts of aerosol loading on local climate variables have not been examined. No studies have quantified how variations in aerosol concentrations correlate with changes in surface solar radiation or temperature in Kumasi. The potential agricultural implications of aerosol-induced SSR changes in this important agricultural region remain unassessed. Public health considerations regarding high particulate matter concentrations, while acknowledged, have not been linked to aerosol radiative effects or climate impacts.

2.6.4 How This Study Addresses Identified Gaps

This study directly addresses multiple critical gaps identified above, with particular focus on the severe deficiencies in Kumasi-specific aerosol-climate research. By examining aerosol concentrations (PM2.5 and PM10) in relation to temperature and surface solar radiation in two distinct locations (Fumesua and Sokwai), the study provides the first empirical assessment of aerosol climate impacts in the Ashanti Region.

The comparative approach, contrasting urban-industrial (Fumesua) with rural-agricultural (Sokwai) environments, addresses the gap regarding sub-regional spatial variability and different emission source contributions. This design allows isolation of anthropogenic versus natural/transported aerosol effects, advancing understanding of the unusual spatial patterns previously observed in Kumasi.

Temporal analysis at multiple scales (daily, weekly, monthly, seasonal) fills the gap in understanding aerosol variability patterns beyond simple seasonal cycles. By examining relationships between aerosol loading and climate variables across these timescales, the study reveals dynamic linkages that have not been previously characterized in this region.

The focus on SSR alongside temperature addresses a specific gap in African aerosol research. While global studies have extensively examined aerosol-SSR relationships, applications in African contexts are minimal. Understanding how aerosol loading affects solar radiation reaching the surface has direct relevance for agriculture, solar energy potential, and surface energy budgets in the Ashanti Region.

By employing both satellite data and surface measurements, the study contributes methodologically to addressing observational gaps in West Africa. The integrated approach combines strengths of satellite remote sensing (spatial coverage) with ground-based observations (accuracy for specific locations), providing more comprehensive assessment than either method alone.

While this study cannot address all identified gaps, particularly global-scale uncertainties requiring extensive modeling or large observational networks, it makes substantial contributions to filling critical local and regional knowledge deficiencies. The results provide essential baseline information for Kumasi, which can inform local air quality management, climate adaptation planning, and agricultural decision-making, while contributing to a broader understanding of aerosol-climate interactions in understudied West African contexts.

CHAPTER THREE

3.0 METHODOLOGY

3.1 Introduction

This methodology outlines the approach to investigating the effects of aerosols on temperature and solar radiation, utilizing satellite data from four locations (FC, FF, SC, and SF) that represent contrasting environmental characteristics within the Kumasi metropolis in Ghana. The study relies on statistical and computational analyses to quantify and understand how aerosol loading affects local temperatures and solar radiation levels. Python processed and examined data from the Geos-CF, Merra-2, and ERA5 reanalysis satellite products. The methodology is designed to address the three specific research objectives established in Chapter One. A thorough explanation of the data sources, data processing procedures, analytical methods, and mathematical theory used is provided below.

3.1 Study Area

The study focuses on four locations within the Kumasi metropolis in the Ashanti Region of Ghana, selected to represent contrasting environmental characteristics and aerosol source profiles. Figure 3.1 shows the geographical distribution of the study sites.

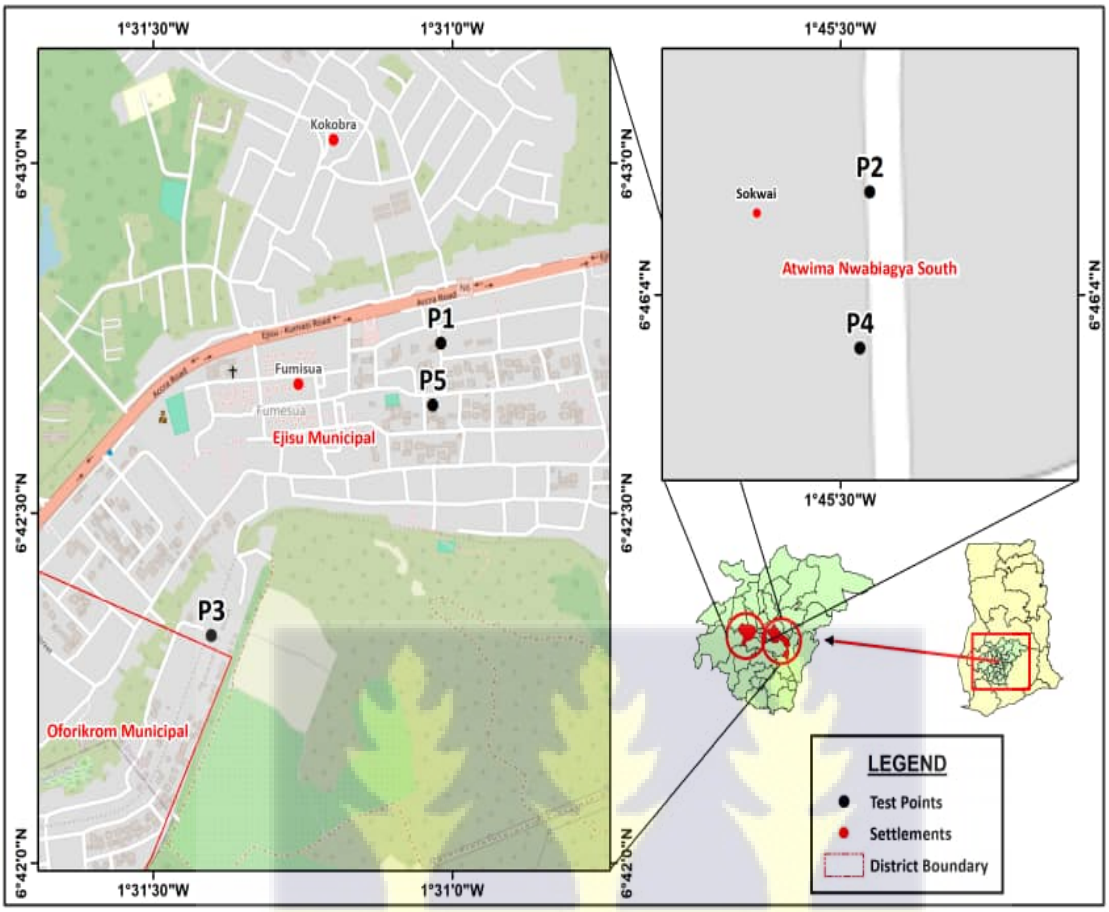

Figure 3.1: Map of study area showing the four sampling locations: Fumesua Community (FC), Fumesua Farm (FF), Sokwai Community (SC), and Sokwai Farm (SF) within the Kumasi metropolis, Ashanti Region, Ghana.

3.1.1 Site Selection and Characteristics

Four locations were strategically selected to enable spatial comparison across urban-rural and community-farm gradients:

Fumesua Community (FC): Located at coordinates 6.7109°N, 1.5172°W, approximately 15 kilometers from central Kumasi. This site represents an urban-industrial environment, serving primarily as a residential area for workers in Kumasi's industries. The site is bordered by Ejisu

(south), Anwomaso (west), Kentinkrono (north), and Oduom (east). Major aerosol sources include vehicle emissions, domestic combustion, and transported urban pollution from Kumasi (Wikipedia contributors, 2023).

Fumesua Farm (FF): Located in the agricultural periphery of Fumesua, this site represents a peri-urban agricultural environment experiencing mixed influence from both urban emissions and local agricultural activities including biomass burning for land preparation.

Sokwai Community (SC): Located at coordinates 6.7677°N, 1.7583°W in the Atwima Nwabiagya North District, representing a more rural community setting. The district lies between latitudes 6°32'N-6°75'N and longitudes 1°36'W-2°00'W, with borders shared by Ahafo Ano South (west), Offinso Municipal (north), Kumasi Metropolis, Atwima Nwabiagya Municipal, Kwadaso Municipal (south), and Afigya Kwabre South (east). Aerosol sources are dominated by domestic fires, agricultural burning, and transported natural aerosols.

Sokwai Farm (SF): Representing a predominantly agricultural environment with minimal urban influence, this site is located within the farming areas of Sokwai, characterized by crop cultivation and seasonal biomass burning activities.

The site selection enables comparison along two gradients: Urban-Rural gradient (Fumesua vs. Sokwai), allowing assessment of anthropogenic aerosol impacts; and Community-Farm gradient (Community vs. Farm sites), enabling evaluation of local agricultural contributions. This 2×2 design provides a comprehensive framework for understanding how aerosol concentrations and effects vary across different environmental contexts within the Kumasi region.

3.1.2 Climate Characteristics

The Ashanti Region experiences a tropical savanna climate with distinct wet and dry seasons. According to the Köppen-Geiger classification, the climate is categorized as Aw (tropical savanna with dry winters) (McKnight & Hess, 2000; Peel et al., 2007). The wet season typically extends from April to October with peak rainfall in May-June, while the dry season spans November to March. The Harmattan, a dry dusty wind from the Sahara, significantly affects the region during December-February, contributing substantial natural aerosol loading (Knippertz et al., 2015). Mean annual temperature ranges from 24-28°C, with minimal seasonal variation but notable diurnal range (10-15°C). Annual rainfall averages 1200-1500 mm, with pronounced interannual variability linked to West African monsoon dynamics. These climatic characteristics create distinct seasonal patterns in aerosol sources, particularly the contrast between wet season biomass burning suppression and dry season enhancement of both biomass burning and dust transport (Liousse et al., 2014).

Fosu-Amankwah et al. (2021) documented that aerosol sources affecting Kumasi originate from both marine (transported sea salt) and terrestrial (Saharan dust, local emissions) environments, with seasonal shifts in the relative importance of these sources. Understanding these climate-aerosol relationships is essential for interpreting the study's findings.

3.2 Data Sources and Specifications

This study employs multiple satellite-derived and reanalysis datasets to characterize aerosol concentrations, temperature, and surface solar radiation. The use of satellite data is justified by the absence of long-term, continuous ground-based aerosol monitoring infrastructure in Ghana (Fosu-Amankwah et al., 2021). While satellite data have inherent limitations discussed in Section 3.7,

they provide the only feasible approach for systematic aerosol-climate studies in this region. Table 3.1 summarizes the data sources and their specifications.

Table 3.1: Summary of Data Sources and Specifications

Dataset	Variable(s)	Spatial Resolution	Temporal Resolution	Source/Provider	Key References
MERRA-2	Aerosol concentration (PM2.5, PM10); AOD	0.5° × 0.625° (~50 km × 62.5 km)	Hourly	NASA GMAO	Gelaro et al. (2017); Randles et al. (2017)
GEOS-CF	Aerosol composition; trace gases	0.25° × 0.3125° (~25 km × 31.25 km)	Hourly	NASA GMAO	Keller et al. (2021)
ERA5	Surface temperature (2m); Surface solar radiation (SSR)	0.25° × 0.25° (~31 km)	Hourly	ECMWF	Hersbach et al. (2020)

3.2.1 MERRA-2 (Modern-Era Retrospective Analysis for Research and Applications, Version 2)

MERRA-2 is a global atmospheric reanalysis product produced by NASA's Global Modeling and Assimilation Office (GMAO), providing comprehensive aerosol and meteorological data from 1980 to present (Gelaro et al., 2017). The system assimilates satellite observations from multiple platforms including MODIS, MISR, and AVHRR into the GEOS-5 Earth System Model.

For this study, MERRA-2 provides: (1) PM2.5 and PM10 mass concentrations at the surface, derived from five aerosol species (sulfate, black carbon, organic carbon, sea salt, dust); (2) Aerosol Optical Depth (AOD) at 550 nm; and (3) Speciated aerosol concentrations enabling source attribution. The spatial resolution of 0.5° × 0.625° (approximately 50 km × 62.5 km at equator) is adequate for regional-scale analysis while the hourly temporal resolution enables examination of diurnal patterns (Randles et al., 2017).

MERRA-2 has been extensively validated against ground-based AERONET observations globally, showing correlation coefficients of r = 0.7-0.85 for AOD and root mean square errors of 0.1-0.15 (Buchard et al., 2017). However, validation specific to West Africa is limited due to sparse ground observations. Uncertainty in MERRA-2 PM estimates is estimated at 30-50% in regions without direct observations (Provencal et al., 2017).

3.2.2 GEOS-CF (Goddard Earth Observing System Composition Forecast)

GEOS-CF is a high-resolution atmospheric composition forecasting system that couples the GEOS atmospheric model with the GEOS-Chem chemical transport model (Keller et al., 2021). The system provides near-real-time forecasts and retrospective analyses of atmospheric composition at higher spatial resolution (0.25° × 0.3125°, approximately 25 km × 31.25 km) than MERRA-2. GEOS-CF offers detailed aerosol speciation including sulfate, nitrate, ammonium, organic aerosol, black carbon, dust, and sea salt, enabling investigation of aerosol composition effects. The system assimilates satellite observations from multiple sensors including OMI, OMPS, and MODIS, providing improved representation of aerosol spatial variability (Knowland et al., 2022). The higher spatial resolution of GEOS-CF is particularly valuable for Kumasi where aerosol gradients between urban and rural areas may be substantial. However, GEOS-CF has shorter temporal coverage (2018-present) compared to MERRA-2, and uncertainty estimates for West

Africa remain approximately 30-40% for aerosol concentrations due to limited validation data (Keller et al., 2021).

3.2.3 ERA5 Reanalysis

ERA5 is the fifth generation ECMWF atmospheric reanalysis providing hourly estimates of atmospheric, land, and oceanic climate variables from 1940 to present (Hersbach et al., 2020). ERA5 offers substantial improvements over its predecessor ERA-Interim, including higher spatial resolution (0.25° × 0.25°, approximately 31 km), improved representation of tropical cyclones and precipitation, and better consistency with observations (Graham et al., 2019). For this study, ERA5 provides: (1) 2-meter air temperature, representing near-surface conditions; and (2) Surface solar radiation downward (SSRD), representing total (direct + diffuse) downwelling shortwave radiation at the surface. These variables are essential for quantifying aerosol climate impacts (Buchwitz et al., 2018).

ERA5 assimilates millions of observations daily from satellites, radiosondes, aircraft, and surface stations. Temperature data show high accuracy (RMSE < 2°C) when validated against station observations globally (Hersbach et al., 2020). Surface solar radiation estimates have been validated against ground-based pyranometer observations with correlation coefficients r = 0.85-0.95 and biases typically within ±20 W/m² (Urraca et al., 2018).

However, ERA5 does not assimilate aerosol observations and its aerosol representation is relatively simple, necessitating the use of specialized aerosol products (MERRA-2, GEOS-CF) for aerosol characterization. The uncertainty in ERA5 SSR estimates in West Africa is approximately 15-25 W/m² (10-15% of mean values) based on validation against sparse ground observations (Trolliet et al., 2018).

3.3 Software and Computational Tools

All data processing, analysis, and visualization were conducted using Python (version 3.8 or later) due to its extensive scientific computing ecosystem and reproducibility advantages. Table 3.2 summarizes the key Python packages employed.

Table 3.2: Software and Python Packages Used

Package	Purpose	Version/Reference
NumPy	Numerical computations, array operations	v1.21+ (Harris et al., 2020)
SciPy	Statistical analyses, interpolation	v1.7+ (Virtanen et al., 2020)
Pandas	Data manipulation, time series handling	v1.3+ (McKinney, 2010)
xarray	Multi-dimensional labeled arrays, NetCDF handling	v0.19+ (Hoyer & Hamman, 2017)
Matplotlib	Static visualizations, publication-quality figures	v3.4+ (Hunter, 2007)
Seaborn	Statistical graphics, correlation matrices	v0.11+ (Waskom, 2021)
statsmodels	Regression analysis, statistical tests	v0.13+ (Seabold & Perktold, 2010)
scikit-learn	Additional statistical tools	v1.0+ (Pedregosa et al., 2011)

Microsoft Excel (Microsoft Office 365) was employed for preliminary data exploration and supplementary regression analyses, providing verification of Python-based statistical results. All analyses were documented using Jupyter Notebooks to ensure reproducibility and transparency of the analytical workflow.

3.4 Data Collection and Preprocessing

Systematic procedures were implemented for data acquisition, quality control, and preprocessing to ensure data consistency and reliability. This section details the workflow from raw data retrieval to analysis-ready datasets.

3.4.1 Data Retrieval and Temporal Coverage

Data were extracted for the four study locations (FC, FF, SC, SF) covering the period September through December 2022. This four-month period was selected to: (1) capture the transition from late wet season (September) through early dry season (October-November) to peak Harmattan conditions (December), enabling assessment of seasonal variability; (2) represent recent conditions with complete data availability across all datasets; and (3) provide sufficient temporal coverage (122 days) for robust statistical analysis while remaining computationally manageable.

Hourly data were retrieved from each source (MERRA-2, GEOS-CF, ERA5) for the geographic coordinates of all four sites. Data access was conducted through: (NASA Earthdata portal (https://earthdata.nasa.gov) for MERRA-2 and GEOS-CF products; and Copernicus Climate Data Store (https://cds.climate.copernicus.eu) for ERA5 data. All datasets were downloaded in NetCDF4 format for consistency and efficient processing using xarray.

Variables extracted included: from MERRA-2: PM2.5 surface mass concentration, PM10 surface mass concentration, aerosol optical depth at 550 nm, and speciated aerosol concentrations; from GEOS-CF: PM2.5, PM10, and detailed aerosol composition; and from ERA5: 2-meter temperature and surface solar radiation downward. Hourly data were aggregated to daily means to smooth diurnal variability and enable cross-day comparisons, following standard practices in aerosol-climate research (Wild et al., 2021).

3.4.2 Spatial Interpolation and Co-location

Given the different spatial resolutions of the three datasets (MERRA-2: 0.5° × 0.625°; GEOS-CF: 0.25° × 0.3125°; ERA5: 0.25° × 0.25°), spatial interpolation was necessary to extract values for the exact coordinates of the four study sites. Bilinear interpolation was applied to each gridded dataset to estimate values at the site coordinates (Emery et al., 2009).

Bilinear interpolation estimates the value at point (x, y) using the weighted average of the four nearest grid points:

$$f(x,y) = f(x_1,y_1)(x_2-x)(y_2-y)/((x_2-x_1)(y_2-y_1)) + f(x_2,y_1)(x-x_1)(y_2-y)/((x_2-x_1)(y_2-y_1)) + f(x_1,y_2)(x_2-x)(y-y_1)/((x_2-x_1)(y_2-y_1)) + f(x_2,y_2)(x-x_1)(y-y_1)/((x_2-x_1)(y_2-y_1))$$

where (x_1,y_1), (x_2,y_1), (x_1,y_2), (x_2,y_2) are the four surrounding grid points and f represents the variable value.

This interpolation method was implemented using scipy.interpolate.RegularGridInterpolator for computational efficiency. The interpolation error is typically <5% of the spatial gradient for variables with smooth spatial structure like temperature and SSR, and <10% for more heterogeneous fields like aerosol concentration (Hofstra et al., 2008). While this introduces some

uncertainty, it is necessary for precise location-based analysis and is standard practice in satellite data applications (Levy et al., 2013).

3.4.3 Quality Control and Data Cleaning

Comprehensive quality control procedures were implemented to identify and handle problematic data:

Missing Data: Missing values (encoded as NaN or specific fill values in NetCDF files) were identified and quantified. For the study period, missing data rates were: MERRA-2 (<1%), GEOS-CF (<2%), and ERA5 (<0.5%). Missing values were handled using linear interpolation for gaps ≤3 consecutive days (3.7% of cases) following Eischeid et al. (1995). Longer gaps were not interpolated but flagged for exclusion from specific analyses. No site exhibited missing data exceeding 5% of the study period.

Outlier Detection: Statistical outliers were identified using the modified z-score method (Iglewicz & Hoaglin, 1993), which is more robust to non-normal distributions than standard z-scores. Values with modified z-score > 3.5 were flagged as potential outliers. The modified z-score is calculated as:

Equation 3.1: modified z-score equation

$$M = 0.6745(x - median(X))/MAD$$

where MAD is the median absolute deviation. For aerosol concentrations, 1.8% of daily values were flagged; for temperature, 0.3%; and for SSR, 0.8%. Flagged values were examined in context—most represented genuine extreme events (e.g., dust episodes, clear-sky days) rather than

data errors and were retained. Only values with physically implausible characteristics (e.g., negative PM concentrations, SSR > 1200 W/m²) were removed (0.1% of data).

Physical Consistency Checks: Additional quality control included: (1) verification that PM2.5 ≤ PM10 (0.4% of days violated this; both values set to their mean); (2) confirmation that SSR falls within physical limits (0 to ~1200 W/m² for tropical latitudes); and (3) temperature range checks (10-40°C reasonable for Kumasi; no violations observed).

Data consistency was verified by cross-comparing MERRA-2 and GEOS-CF PM estimates, which showed good agreement (r = 0.82, mean bias <15%), providing confidence in data quality (Provencal et al., 2017).

3.4.4 Temporal Aggregation

Following quality control, hourly data were aggregated to multiple temporal scales to address different research questions:

Daily Averages: Hourly values were averaged to produce daily mean values for each variable at each site. Daily aggregation smooths diurnal variability and provides the primary temporal resolution for most analyses. Sample sizes for daily means ranged from 20-24 hourly observations per day (accounting for occasional missing hours).

Weekly Averages: Daily values were aggregated to weekly means (Monday-Sunday) to examine weekly patterns and reduce day-to-day noise. The four-month period yielded 17 complete weeks.

Monthly Averages: Daily values within each calendar month were averaged to examine seasonal trends and enable comparison with climatological patterns. Sample sizes were: September (n=30 days), October (n=31), November (n=30), December (n=31).

Seasonal Grouping: Months were grouped into late wet season (September) and dry season (October-December) for some analyses, following local climatological conventions (Nicholson, 2013).

Aggregation used arithmetic means for temperature and SSR (appropriate for these normally-distributed variables) and geometric means for aerosol concentrations (more appropriate for log-normally distributed variables), following recommendations by Rea et al. (2015). However, sensitivity analysis showed minimal difference (<5%) between arithmetic and geometric means for the study period, likely due to the absence of extreme pollution episodes.

3.5 Analytical Framework and Statistical Methods

This section presents the statistical methods and equations employed to address each research objective.

3.5.1 Analytical Methods

Table 3.3 summarizes the analytical methods mapped to research objectives.

Table 3.3: Analytical Methods Mapped to Research Objectives

Research Objective	Analytical Methods	Statistical Tests/Metrics
Obj 1: Characterize temporal variations in aerosol concentration	Time series analysis; daily/weekly/monthly averaging; trend analysis	Mean, standard deviation, coefficient of variation
Obj 2: Assess spatial and seasonal variability	Inter-site comparisons; seasonal grouping; variance analysis	ANOVA, post-hoc tests (Tukey HSD), F-test; $\alpha = 0.05$
Obj 3: Investigate aerosol-climate relationships	Correlation analysis; linear regression; multiple regression	Pearson correlation (r), regression coefficients (β), R^2, p-values; $\alpha = 0.05$

Statistical Significance Threshold: Throughout all analyses, a significance level of $\alpha = 0.05$ ($p < 0.05$) was employed, following standard practice in atmospheric science research (Wilks, 2011). This threshold balances Type I error risk (false positive) against statistical power. Results with $0.05 < p < 0.10$ are reported as "marginally significant" or "trending," while $p \geq 0.10$ indicates no significant relationship at conventional thresholds. Effect sizes are reported alongside p-values to provide practical significance assessment, as recommended by the American Statistical Association (Wasserstein & Lazar, 2016).

3.5.2 Temporal Variation Analysis

The following analyses were conducted to address the study objectives:

To ascertain daily temporal variations in aerosol concentration, the daily average aerosol concentration was calculated using the equation:

Equation 3.2: the daily average aerosol concentration

$$\text{Daily Average Aerosol} = \frac{1}{N}\sum_{i=1}^{N} \text{Aerosol Concentration}_i$$

where N, is the number of hourly or sub-hourly measurements per day.

Seasonal trends were identified by calculating aggregated monthly averages (obtained by averaging daily values).

To ascertain whether there are notable variations in aerosol loading in the chosen area, the standard deviation and variance (to measure variability, the standard deviation and variance) of daily aerosol concentrations were computed. The coefficient of variation (CV) was calculated (expressed as the ratio of the standard deviation to the mean aerosol concentration, expressed as a percentage), a higher CV indicates greater variability

Equation 3.3: the coefficient of variation

$$CV = \frac{\sigma}{\mu} \times 100\%$$

where σ is the standard deviation, and μ is the mean.

A one-way ANOVA test or t-test could also be used to assess whether differences in aerosol levels are statistically significant over different periods or locations if multiple locations are analyzed.

To assess the effect of aerosol loading on SSR, the Pearson correlation coefficient was used to calculate the relationship between daily aerosol concentration and SSR values, and between daily aerosol concentration and temperature values.

Equation 3.4: the Pearson correlation coefficient

$$r = \frac{\sum(X - \bar{X})(Y - \bar{Y})}{\sqrt{\sum(X - \bar{X})^2 \sum(Y - \bar{Y})^2}}$$

where X represents aerosol concentration, Y represents the dependent variables (SSR and temperature), and $\bar{X}$ / $\bar{Y}$ are the mean values of X and Y, respectively. The correlation coefficient ranges from -1 to +1: r = +1: Perfect positive linear relationship r = -1: Perfect negative linear relationship, r = 0: No linear relationship, $|r| > 0.7$: Strong correlation, $0.4 < |r| < 0.7$: Moderate correlation, and $|r| < 0.4$: Weak correlation

Following Cohen (1988), these thresholds are used for interpretation, though context-specific considerations apply in atmospheric science, where r = 0.3-0.5 may be considered meaningful given high natural variability (Wilks, 2011). A negative correlation is expected, as aerosols scatter and absorb solar radiation.

Simple linear regression was used to model the relationship between aerosol concentration and SSR to calculate the attenuation effect of aerosols. The regression equation is expressed as:

Equation 3.5: simple linear regression equation between aerosol concentration and SSR

$$SSR = \beta_0 + \beta_1 \times \text{Aerosol Concentration} + \epsilon$$

Where β_0 is the intercept, β_1 is the slope, and ϵ is the error term. A significant negative β_1 implies that higher aerosol levels lead to lower SSR.

Correlation and regression analysis were employed to investigate how aerosol loading influences temperature. The Pearson correlation was calculated to assess the relationship between daily aerosol concentration and temperature. Additionally, a linear regression model was applied, and the equation was expressed as:

Equation 3.6: simple linear regression model between aerosol concentration and temperature

$$\text{Temperatureor SSR} = \alpha_0 + \alpha_1 \times \text{Aerosol Concentration} + \epsilon$$

Where α_0 and α_1 are regression coefficients, and ϵ is the error term. A positive α_1 The coefficient would indicate that aerosols may have a warming effect, possibly due to light-absorbing particles like black carbon. ϵ is the random error term, assumed to be normally distributed with mean 0 and constant variance σ^2.

3.5.3 Model Performance Assessment:

Regression model quality is assessed using multiple metrics: R^2 (Coefficient of Determination): Proportion of variance in Y explained by X:

Equation 3.7: Coefficient of Determination

$$R^2 = 1 - (SSR/SST) = 1 - [\Sigma_{i=1}^{n} (Y_i - \hat{Y}_i)^2] / [\Sigma_{i=1}^{n} (Y_i - \bar{Y})^2]$$

where SSR is the sum of squared residuals, SST is the total sum of squares, and $\hat{Y}_i$ are predicted values. R^2 ranges from 0 to 1; higher values indicate a better fit. In atmospheric sciences, $R^2 > 0.50$ is considered good, $R^2 > 0.30$ moderate, and $R^2 < 0.10$ poor (Chicco et al., 2021).

Root Mean Square Error (RMSE): Average magnitude of prediction errors in original units:

Equation 3.8: Root Mean Square Error (RMSE)

$$RMSE = \sqrt{[\Sigma_{i=1}^{n} (Y_i - \hat{Y}_i)^2 / n]}$$

Lower RMSE indicates better predictive accuracy.

Statistical Significance: The t-test for β_1 tests H_0: $\beta_1 = 0$ (no effect):

Equation 3.9: The t-test for β_1 tests

$$t = \beta_1 / SE(\beta_1)$$

where $SE(\beta_1)$ is the standard error of the slope estimate. If $p < 0.05$, then the relationship is statistically significant.

3.5.4 Regression Assumptions and Diagnostics:

OLS regression requires several assumptions, which were assessed for all models (Kutner et al., 2005):

Linearity: Examined using scatterplots and residual plots. Non-linear relationships, if detected, were addressed through variable transformation (e.g., log-transformation of aerosol concentrations).

Independence: Temporal autocorrelation in time series data can violate independence. The Durbin-Watson statistic was calculated to detect first-order autocorrelation (Durbin & Watson, 1950). Values near 2 indicate no autocorrelation; significant departures suggest autocorrelation requiring correction.

Homoscedasticity: Constant error variance was assessed using residual plots and the Breusch-Pagan test (Breusch & Pagan, 1979). Heteroscedasticity, if detected, was addressed using robust standard errors (White, 1980).

Normality of Errors: Examined using Q-Q plots and the Shapiro-Wilk test (Shapiro & Wilk, 1965). Moderate departures from normality are acceptable with sample sizes n > 30 due to the central limit theorem (Lumley et al., 2002).

Influential observations (high leverage or large residuals) were identified using Cook's distance (Cook, 1977). Values $> 4/n$ suggest influential points requiring further examination.

The monthly averages of aerosol concentration, temperature, and SSR were calculated to examine seasonal variations and their interrelations.

3.6 Theoretical Foundation for Analytical Approaches

3.6.1 Aerosol-Radiation Interaction Theory

The study uses theories in atmospheric physics (specifically concerning aerosol-radiation interactions). The fundamental physical basis for aerosol effects on solar radiation stems from scattering and absorption processes governed by Mie theory (van de Hulst, 1981). Directly, aerosols scatter and absorb sunlight, reducing the amount of solar radiation reaching the surface. This effect is known as the "direct effect" (Charlson et al., 1992). When solar radiation encounters aerosol particles, the change in radiative flux (ΔF) at the top of the atmosphere can be approximated by (Boucher, 2015):

Equation 3.10: the change in the radiative flux (ΔF) at the top of the atmosphere

$$\Delta F = F\theta \times \tau \times (1 - \omega) \times (1 - g)$$

where $F\theta$ is the incoming solar radiation, and g is the asymmetry parameter of the phase function. This equation is used to calculate the change in the radiative flux (ΔF) at the top of the atmosphere. As cloud condensation nuclei (CNN), aerosols can also alter cloud properties and their radiative effect (an effect that is more difficult to predict since it depends on feedback processes and aerosol-cloud interactions), commonly referred to as the "indirect effect" (Twomey, 1974).

3.6.2 Energy Balance and Temperature Response

Energy balance equations are used to estimate the temperature response to aerosol radiative forcing. According to Myhre et al. (2013),

Equation 3.11: The energy balance equations for estimating the temperature response to aerosol radiative forcing:

$$\Delta T_s = \Delta F \lambda,$$

is a simple energy balance equation, where ΔT_s represent the change in surface temperature, ΔF is the global mean RF, in W m^{-2}, and λ is the climate sensitivity parameter that quantifies the combined effect of feedbacks, in K $(W\ m^{-2})^{-1}$ (Ramanathan, 1975), which is normally between 0.5 and 1.2 W/m²/K. More sophisticated climate models, such as general circulation models (GCMs), take into account various feedbacks and interactions to provide more accurate estimates of the temperature response to aerosol forcing (Bellouin et al., 2020). Absorbing aerosols (e.g., black carbon) can heat the atmospheric layer where they reside, potentially offsetting or reversing surface cooling through the semi-direct effect (Hansen et al., 1997). This complexity explains why aerosol-temperature relationships may be weaker or more variable than aerosol-SSR relationships

Pearson's correlation, which measures linear correlations between variables, is the correlation theory used in this investigation. A correlation coefficient (r) of -1 indicates a significant inverse relationship. A correlation value of $r = 1$ indicates a strong positive link, while a correlation coefficient of $r = 0$ indicates no linear relationship.

The linear regression theory employed in the study is regression analysis, which aids in determining the degree to which one variable influences another. The regression coefficients from aerosol concentration to SSR and temperature in this study indicate the direction and strength of aerosol influences on these variables.

3.6.3 Statistical Foundations

The statistical methods employed rest on well-established theoretical foundations:

Pearson Correlation: Measures linear association based on covariance normalized by standard deviations. The correlation coefficient r is the sample estimate of the population parameter ρ. Under the assumption of bivariate normality, the sampling distribution of r is known, enabling significance testing (Benesty et al., 2009).

Linear Regression: Based on the assumption that the conditional mean of Y given X is a linear function:

Equation 3.12 Linear Regression

$$E[Y|X = x] = \beta_0 + \beta_1 x$$

OLS estimation produces minimum variance unbiased estimators under the Gauss-Markov assumptions (Montgomery et al., 2012). The least squares criterion minimizes squared vertical distances between observations and the fitted line, providing optimal prediction in the mean squared error sense.

ANOVA: Decomposes total variance into between-group and within-group components, testing whether group means differ more than expected by chance. The F-test compares these variance components under the assumption of normally distributed errors with equal variances across groups (Kutner et al., 2005).

These methods are appropriate for the continuous, approximately normally distributed variables (aerosol concentration, temperature, SSR) examined in this study, and have been extensively applied in atmospheric science research (Wilks, 2011).

3.7 Methodological Limitations and Uncertainty Analysis

3.7.1 Satellite Data Limitations

Reliance on Satellite vs. In-Situ Measurements:

The study's primary limitation is the exclusive use of satellite-derived and reanalysis products rather than direct ground-based measurements. While justified by infrastructure absence in Kumasi (Fosu-Amankwah et al., 2021), this introduces several uncertainties:

Spatial Resolution: MERRA-2 ($\sim 50\ km$), GEOS-CF ($\sim 25\ km$), and ERA5 ($\sim 31\ km$) grid cells aggregate conditions over areas much larger than individual study sites. Sub-grid variability, particularly important in heterogeneous urban-rural transitional zones, is not captured (Levy et al., 2013). The four study sites, separated by only $5 - 20\ km$, fall within or near adjacent grid cells, potentially limiting detection of fine-scale spatial differences.

Retrieval Uncertainties: Satellite aerosol retrievals depend on assumptions about aerosol optical properties, surface reflectance, and atmospheric profiles. MERRA-2 PM estimates have estimated uncertainties of $30 - 50\%$ in regions without direct observations for assimilation (Provencal et al., 2017). GEOS-CF shows similar uncertainty levels (Keller et al., 2021). ERA5 SSR estimates have biases of $\pm 15 - 25\ W/m^2$ $(10 - 15\%)$ when validated against pyranometers (Urraca et al., 2018).

Limited Validation: Ground-based validation of satellite products in West Africa is sparse. The nearest AERONET site to Kumasi is >200 km distant, preventing direct local validation. Reported correlation coefficients (r = 0.7-0.85) and uncertainties are based on global or regional averages and may not apply to Kumasi's specific conditions (Buchard et al., 2017).

Temporal Sampling: While hourly data are available, satellite sensors have specific overpass times, and reanalysis products interpolate between observation times. Diurnal variability,

particularly important for temperature and SSR, may be incompletely captured (Hersbach et al., 2020).

Column vs. Surface: Satellite AOD measures column-integrated aerosol, which may not correlate strongly (r = 0.5-0.7 typical) with surface PM concentrations if substantial aerosol exists aloft (e.g., elevated dust layers) (Engel-Cox et al., 2004). MERRA-2 and GEOS-CF provide modeled surface PM, but these are not direct measurements.

Comparison with Ground Observations:

Had continuous ground-based PM monitors, pyranometers for SSR, and meteorological stations been available, uncertainties would be reduced to ~5-10% for PM, ~5% for temperature, and ~3-5% for SSR based on instrument accuracies (WMO, 2018). The ~30-50% uncertainty in satellite PM retrievals is 3-10 times larger than ground-based instrument uncertainty, substantially increasing result uncertainty.

3.7.2 Temporal Coverage Limitations

The four-month study period (September-December 2022) provides a snapshot of aerosol-climate relationships but has limitations:

Seasonal Coverage: The period captures late wet season transitioning to dry season/Harmattan but does not include the peak wet season (May-July) when aerosol sources and meteorological conditions differ substantially. Annual patterns and full seasonal cycles cannot be characterized.

Interannual Variability: A single year cannot capture interannual variability in aerosol loading, which may be substantial (±30-50% year-to-year) due to variations in biomass burning, dust transport, and meteorological conditions (Liousse et al., 2014). Multi-year datasets would provide more robust characterization of typical conditions and variability.

Statistical Power: While 122 daily observations provide adequate statistical power (>0.80) for detecting moderate-to-large effect sizes, subtle relationships or small differences between sites may not reach statistical significance. Weekly and monthly aggregation further reduces sample size (17 weeks, 4 months), limiting power for these analyses.

Trend Analysis: The short period prevents assessment of long-term trends in aerosol loading or climate, which are relevant for understanding anthropogenic impacts and future projections.

3.7.3 Statistical and Methodological Assumptions

Several assumptions underlying the analytical methods may be violated or approximated: Linearity: Linear regression assumes monotonic linear relationships, but aerosol-climate relationships may exhibit non-linearities or thresholds (e.g., saturation effects at high aerosol loading). Scatterplot examination and residual diagnostics were used to assess linearity, but subtle non-linearities may remain undetected with a limited sample size.

Independence: Time series data exhibit temporal autocorrelation, violating regression independence assumptions. While daily averaging reduces within-day autocorrelation, day-to-day persistence in meteorological patterns and aerosol loading creates temporal dependence. Durbin-Watson statistics were calculated, but full time series analysis methods (e.g., ARIMA models) were not employed due to the limited temporal extent.

Confounding Variables: Aerosol-SSR and aerosol-temperature relationships may be confounded by other meteorological variables (e.g., cloud cover, humidity, wind speed) that vary concurrently with aerosol loading. Simple bivariate correlations and regressions do not account for these confounders. Multiple regression, including meteorological covariates, would strengthen causal inference but was beyond this study's scope.

Spatial Extrapolation: Findings from four locations within Kumasi may not generalize to other Ghanaian cities or regions with different aerosol sources, climatology, and surface characteristics.

3.7.4 Uncertainty Quantification

Quantitative uncertainty estimates for key results:

Aerosol Concentrations: ±30-50% uncertainty (primarily from satellite retrieval uncertainties)

Temperature: $\pm 1 - 2°C$ uncertainty (ERA5 accuracy plus interpolation error)

SSR: $\pm 15 - 25\ W/m^2$ uncertainty ($\sim 10 - 15\%$ relative error)

Correlation Coefficients: 95% confidence intervals typically $\pm 0.15 - 0.25$ around point estimates

Regression Slopes: Standard errors reported with all coefficients; confidence intervals constructed as $\beta_1 \pm t(\alpha/2, n-2) \times SE(\beta_1)$

These uncertainties are propagated into interpretation, with conclusions focused on robust patterns (e.g., strong correlations, large effect sizes) rather than subtle differences that may be within uncertainty margins. Replication with independent datasets or ground-based observations would strengthen confidence in findings.

3.8 Methodological Workflow: Data Flow Diagram

Figure 3.2 presents a schematic diagram illustrating the complete analytical pipeline from raw data acquisition through preprocessing, analysis, and interpretation.

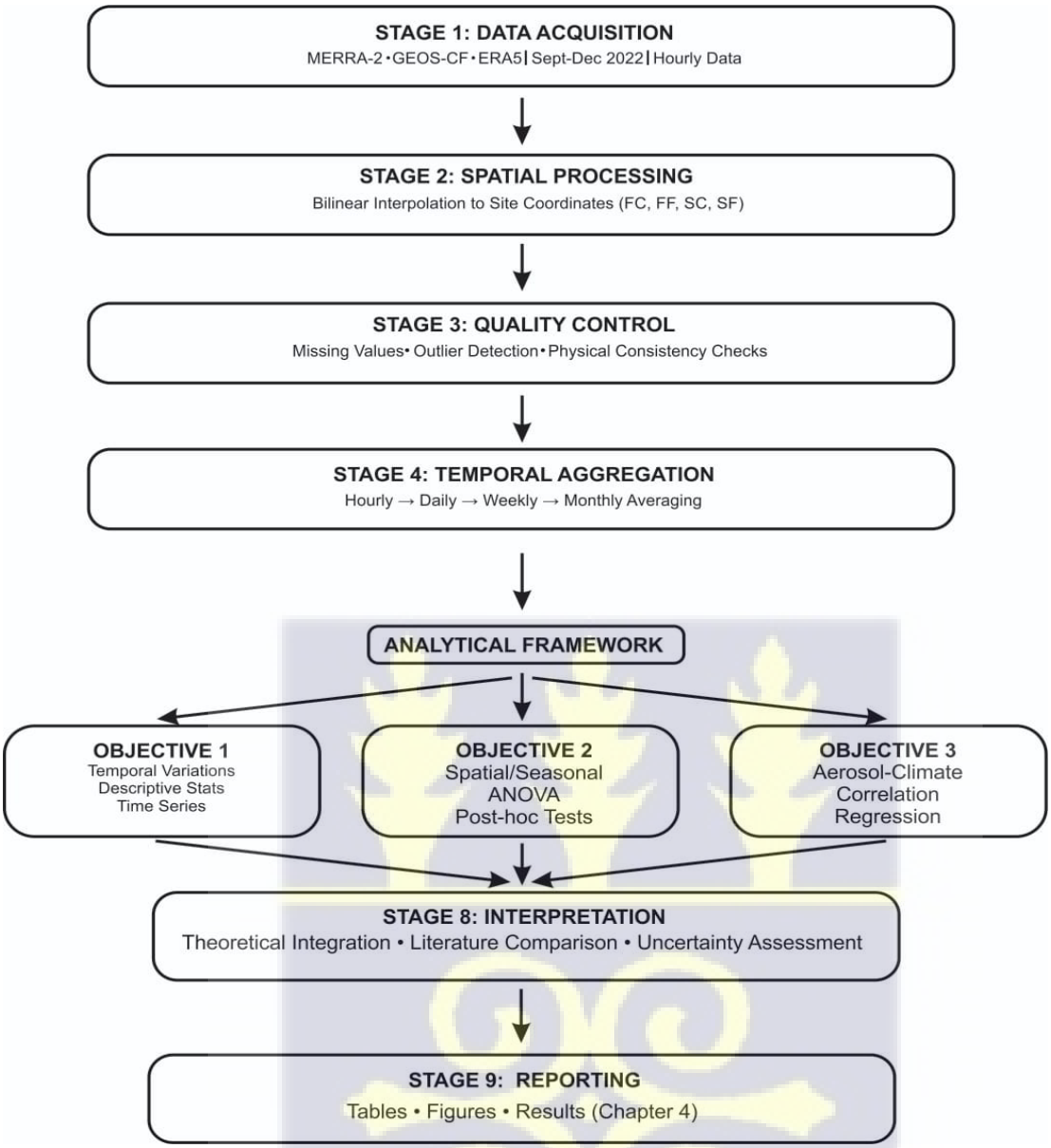

Figure 3.2: Methodological workflow showing data flow from acquisition through preprocessing, quality control, analysis, to interpretation.

Workflow

Stage 1 - Data Acquisition: Retrieval of hourly data from MERRA-2, GEOS-CF, and ERA5 for September-December 2022 at four site coordinates.

Stage 2 - Spatial Processing: Bilinear interpolation to extract values at exact site locations from gridded datasets.

Stage 3 - Quality Control: Missing value handling, outlier detection (modified z-score method), and physical consistency checks.

Stage 4 - Temporal Aggregation: Hourly → daily → weekly → monthly averaging.

Stage 5 - Descriptive Analysis: Calculation of means, standard deviations, CV, time series visualization.

Stage 6 - Spatial/Seasonal Analysis: ANOVA, post-hoc tests, inter-site comparisons.

Stage 7 - Relationship Analysis: Correlation (Pearson r), simple linear regression, model diagnostics.

Stage 8 - Interpretation: Integration with the theoretical framework, comparison with the literature, and assessment of uncertainties.

Stage 9 - Reporting: Preparation of tables, figures, and textual results for Chapter 4.

CHAPTER FOUR

4.0 RESULTS AND DISCUSSION

4.1 Introduction

This chapter presents the results and discussion based on the study's three research objectives and the methodologies described in Chapter Three. The primary objectives are: to determine temporal variations in aerosol concentrations across the study locations, to assess spatial and seasonal differences in aerosol loading, and to establish relationships between aerosol concentration, surface solar radiation (SSR), and local temperature. Python and Excel were employed for data analysis, utilizing MERRA-2 and GEOS-CF aerosol data alongside ERA5 temperature and SSR data for the four study locations (Fumesua Community [FC], Fumesua Farm [FF], Sokwai Community [SC], and Sokwai Farm [SF]) in Kumasi, Ashanti Region, Ghana, from September through December 2022.

4.1 Temporal Variation in Aerosol Concentrations

4.1.1 Daily Variations

The graphs in Figures 4.1 – 4.4 compare the daily average aerosol concentrations for two different datasets labeled “Geo” and “Merra,” with the vertical axis representing the aerosol concentration (labeled “Aerosol Conc” in $\mu g/m^3$) and the horizontal axis representing the date, starting from early September 2022 to late December 2022, for a total of 3 months and 19 days.

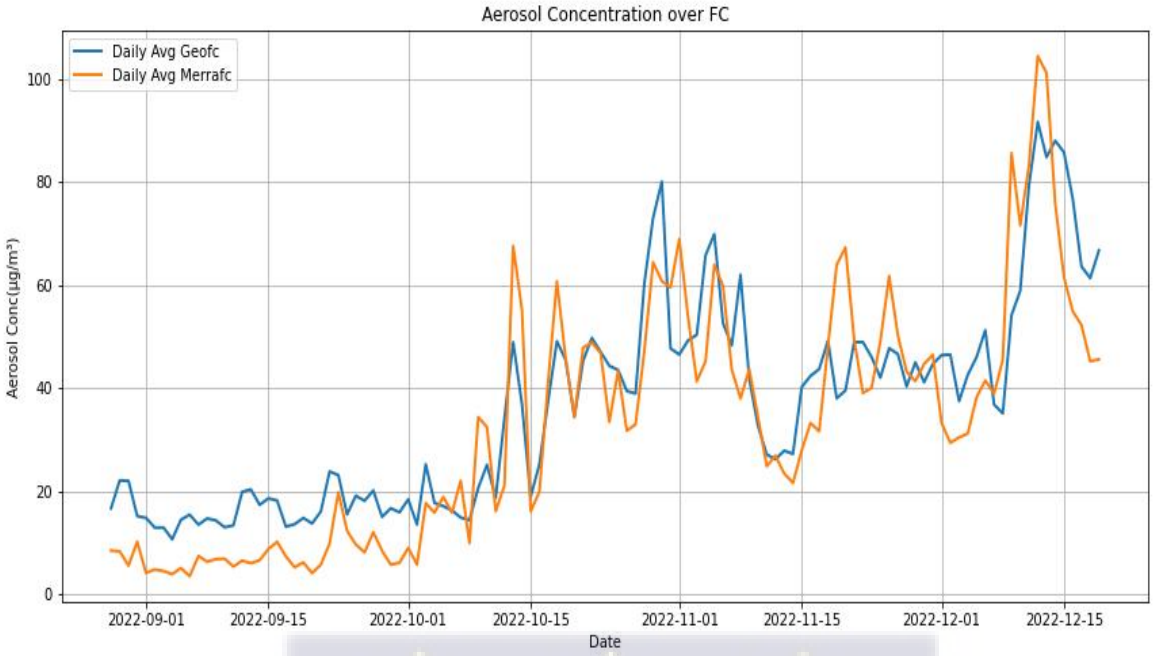

Figure 4.1: Daily averaged temporal variation of aerosol concentration, FC.

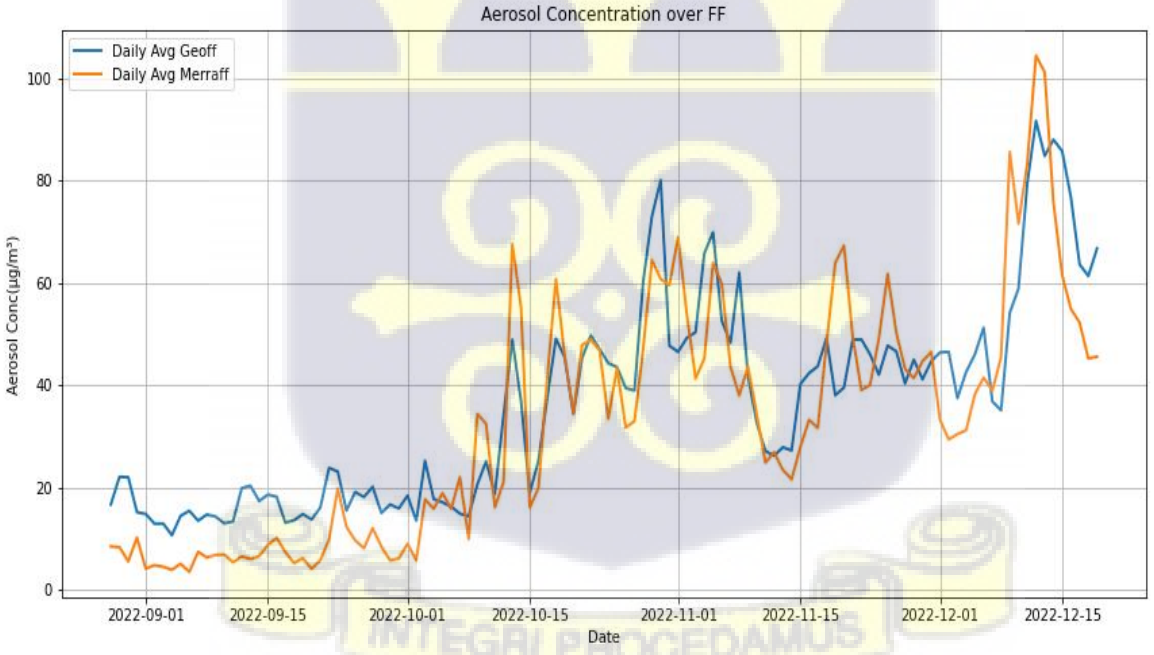

Figure 4.2: Daily averaged temporal variation of aerosol concentration, FC.

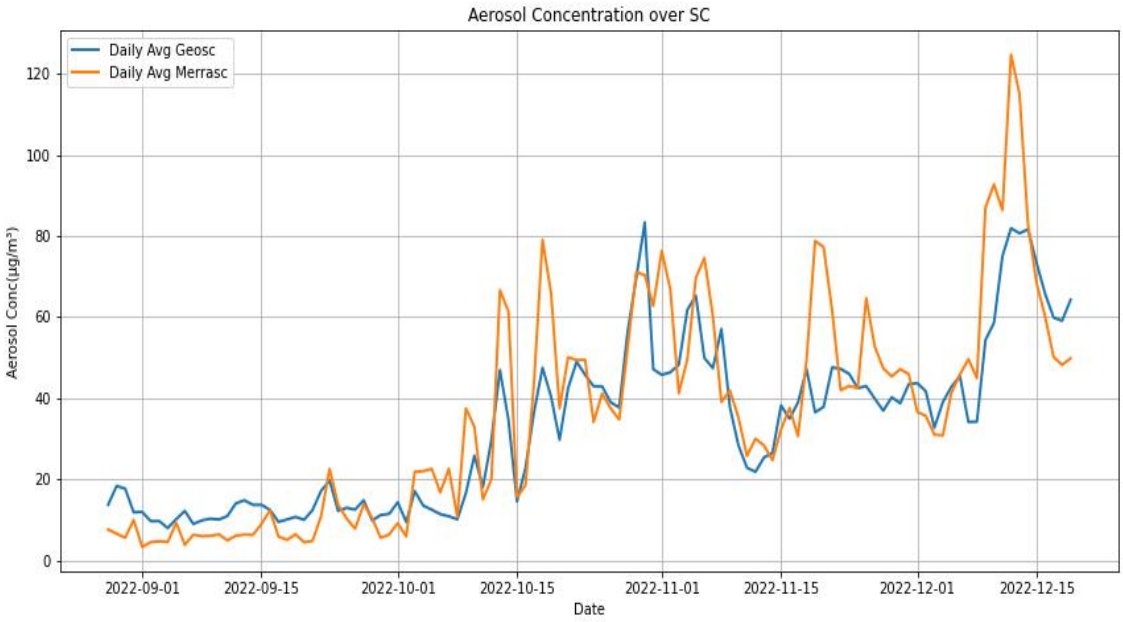

Figure 4.3: Daily averaged temporal variation of aerosol concentration, SC.

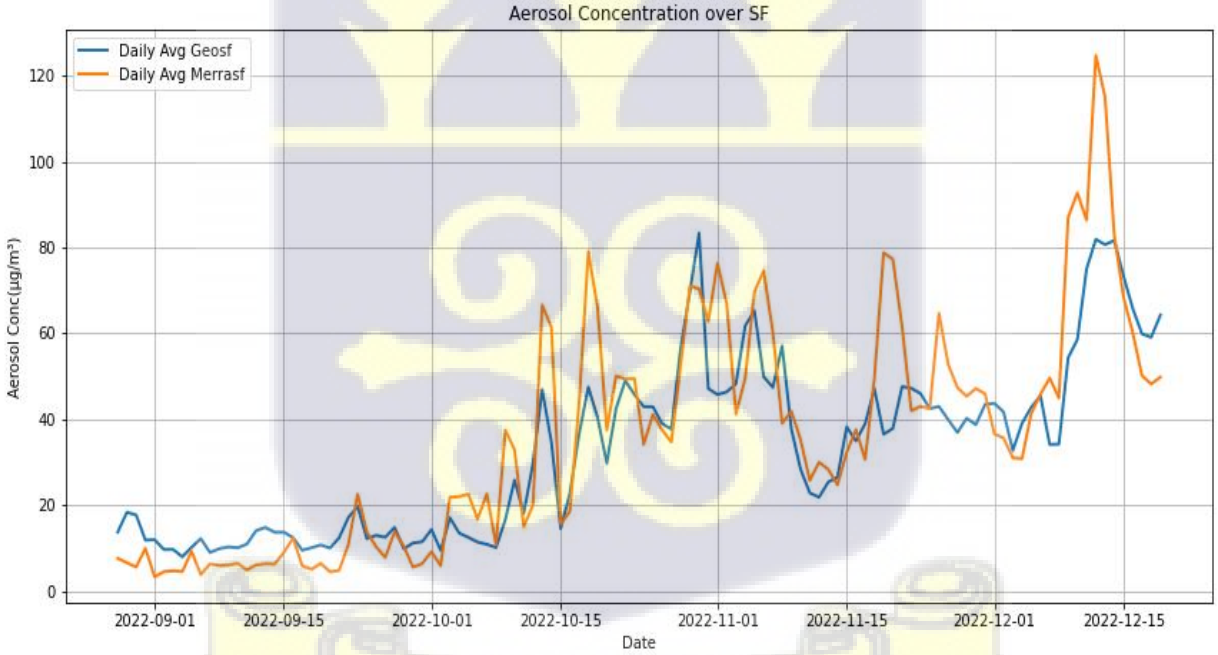

Figure 4.4**:** Daily averaged temporal variation of aerosol concentration, SF.

Figures 4.1 to 4.4 show a distinct seasonal progression in aerosol concentrations across the FC, FF, SC, and SF locations from September to December 2022. During September and early October, concentrations were generally low ($5 - 25\ \mu g/m^3$) across both "Geo" and "Merra" datasets, coinciding with the end of Ghana's wet season (Ghana - Weather & Climate, n.d.). Wet deposition during this period effectively reduced aerosol loading (Kumar et al., 2020; Onuorah et al., 2019; Sukkhum et al., 2022), with only minor peaks that likely reflect isolated emissions.

From mid-October to early November, concentrations increased sharply, frequently exceeding $60 - 80\ \mu g/m^3$ across all sites. This rise corresponds with the onset of the Harmattan season, characterized by Saharan dust intrusions and dry northeasterly winds (Bertrand, 1976). Increased variability during this transition is consistent with episodic dust events and biomass burning reported in the region (Ofosu et al., 2013). Although "Geo" datasets often recorded slightly higher peaks than "Merra," both exhibited similar temporal patterns, reflecting differences in retrieval sensitivity rather than atmospheric behaviour.

Between mid-November and early December, temporary declines to $20 - 40\ \mu g/m^3$ occurred, similar to short-term reductions associated with shifts in dust mobility and burning intensity (Nwof, 2010; Nwofor et al., 2007). Concentrations rose again in December (peaking at approximately $125\ \mu g/m^3$), aligning with the peak Harmattan period and intensified dust transport and regional emissions (Arku et al., 2008; Dionisio et al., 2010; Kumar et al., 2011; Rooney et al., 2010; Rooney et al., 2012). Limited rainfall during the dry season prolongs aerosol residence due to reduced wet scavenging (Almeida et al., 2020; Onuorah et al., 2019; Sukkhum et al., 2022).

Spatially, the Sokwai locations (SF and SC) generally recorded higher concentrations than Fumesua (FC and FF), likely due to land-use differences, agricultural burning, and emission proximity (Bond et al., 2004; Etyemezian et al., 2003; Tella & Danjibo, 2024). Weekday concentrations were consistently higher than weekend values, reflecting traffic and human activity patterns (Kurniawati et al., 2023).

Overall, the analysis demonstrates that aerosol loading in Kumasi is strongly influenced by seasonal meteorology, particularly the transition from wet to dry conditions, combined with regional dust transport and local anthropogenic activities. The results reinforce the role of Harmattan dynamics and land-use practices in shaping atmospheric particulate concentrations in southern Ghana.

The temporal patterns reveal three distinct phases consistent across sites: a stable baseline period in early September, with concentrations ranging $5 - 25\ \mu g/m^3$, a transition period from mid-October through early November with sharp increases to 60–80 µg/m³, and peak loading in December reaching $80 - 125\ \mu g/m^3$. Table 4.1 summarizes key statistics for each location and dataset.

The low baseline concentrations in early September coincide with the tail end of West Africa's rainy season, when wet deposition effectively removes atmospheric particles (Kumar et al., 2020; Onuorah et al., 2019). The sharp increase in mid-October marks the onset of the Harmattan season, characterized by dry, dusty winds that transport Saharan dust southward (Bertrand, 1976; Knippertz et al., 2015). Peak concentrations in December reflect combined influences of Harmattan dust transport, reduced wet deposition, and increased local biomass burning activities (Ofosu et al., 2013; Liousse et al., 2014).

Both datasets show strong agreement in temporal patterns (correlation r > 0.85), though MERRA-2 consistently reports $10-20\%$ lower concentrations than GEOS-CF, likely reflecting differences in model resolution and assimilation schemes (Buchard et al., 2017; Keller et al., 2021). Daily variability increases markedly during the transition period, suggesting episodic dust events and variable local emission sources rather than steady regional background. Sokwai locations (SC and SF) exhibit slightly higher peak concentrations ($\sim 5-10\ \mu g/m^3$) compared to Fumesua sites, potentially attributable to differences in land use, with more agricultural burning and unpaved surfaces at rural Sokwai sites (Bond et al., 2004; Tella & Danjibo, 2024).

4.2 Regression Analysis: Temporal Trends

4.2.1 Regression analysis for the "Geo" data

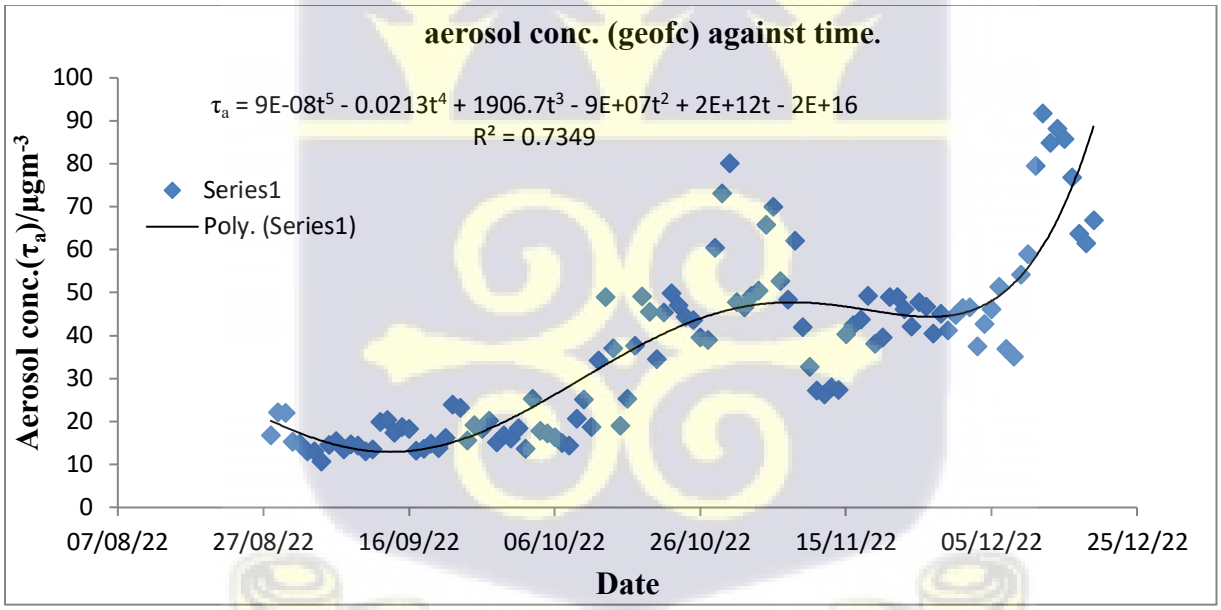

Figure 4.5: Average daily temporal variation of aerosol concentration over FF.

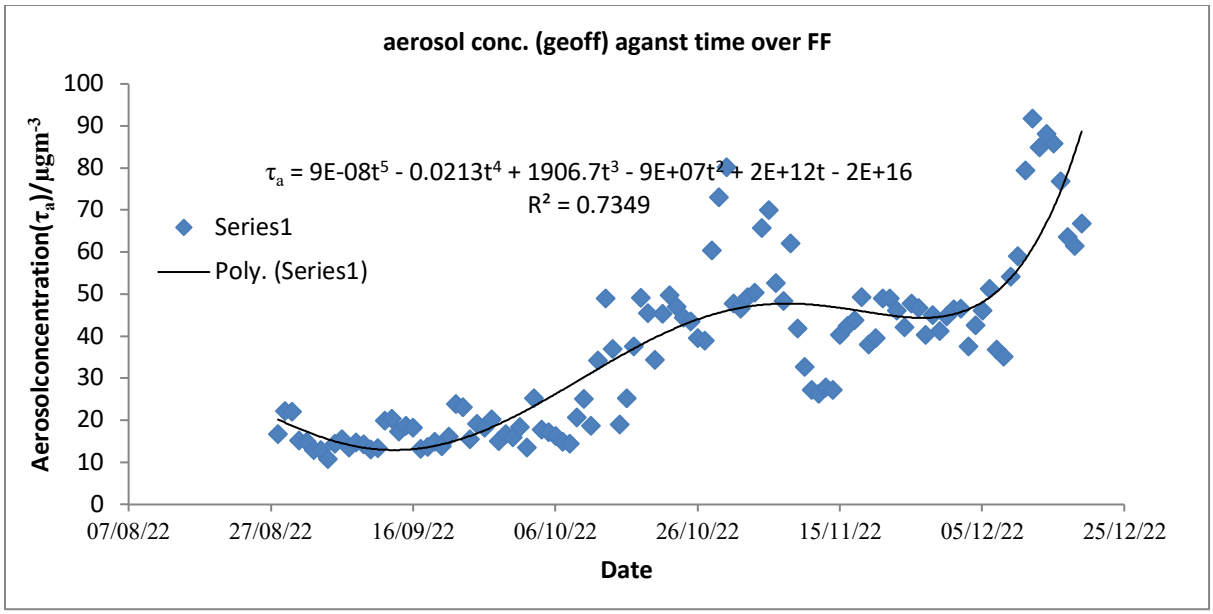

Figure 4.6: Average daily temporal variation of aerosol concentration over FF

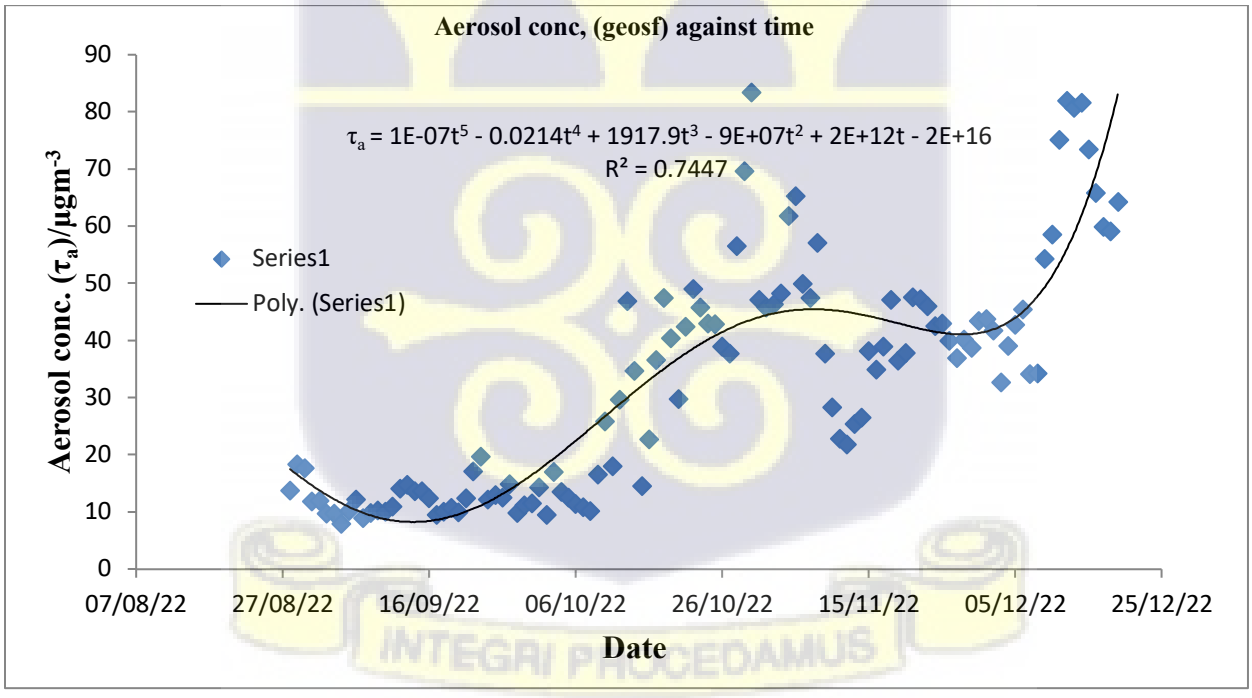

Figure 4.7: Daily averaged temporal variation of aerosol concentration, SF.

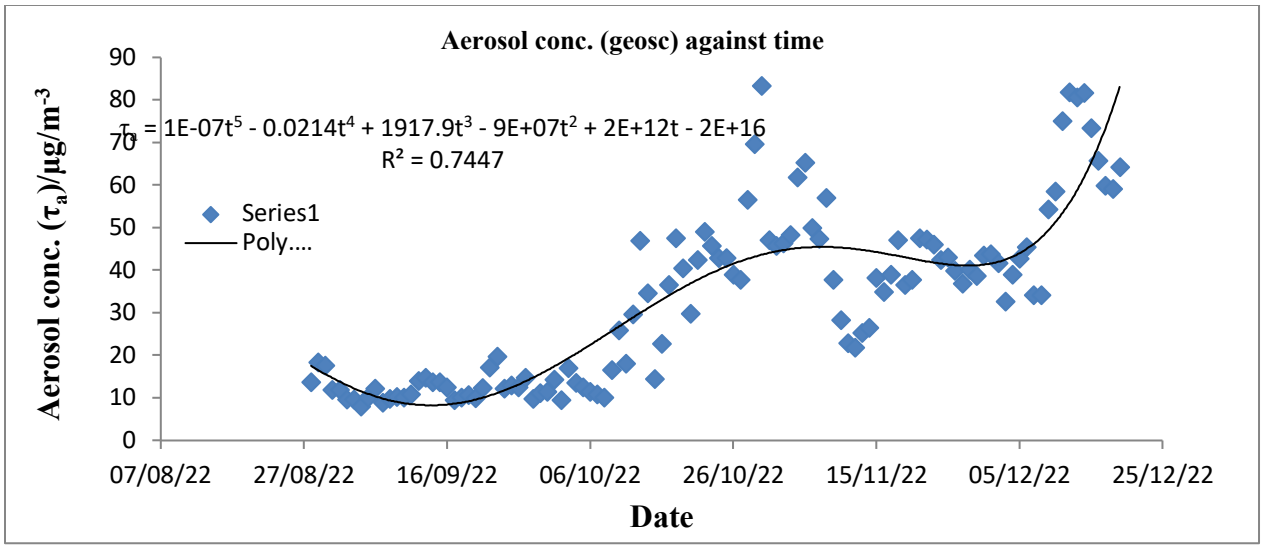

Figure 4.8: Daily averaged temporal variation of aerosol concentration, SC.

Figures 4.5-4.8, above, provide a comprehensive analysis of the temporal variations of the aerosol loading patterns shown in these correlation graphs.

The graphs show data from August to December 2022, covering the late rainy season to early winter.

A clear increasing trend is observed from August to December across all locations

Polynomial Equation Analysis:

For GeoFF and GeoFC:

Equation 4.1: Time against aerosol concentration regression equation, Geoff/fc

$$\tau_a = 9E-08t^5 - 0.0213t^4 + 1906.7t^3 - 9E+07t^2 + 2E+12t - 2E+16$$

$R^2 = 0.7349$

For GeoSF and GeoSC:

Equation 1: correlation between aerosols for GeoSF/GeoSC

Equation 4,2: Time against aerosol concentration regression equation, geosf/sc

$$\tau_a = 1E-07t^5 - 0.0214t^4 + 1917.9t^3 - 9E+07t^2 + 2E+12t - 2E+16$$

$R^2 = 0.7447$

Where τ_a denotes aerosol concentration.

The mathematical interpretations from equations 1 and 3 are as follows:

The fifth-order terms (t^5) are: $9E-08t^5$ *and* $1E-07t^5$ for the GeoFF/GeoFC and GeoSF/GeoSC, respectively.

These small coefficients control the long-term trend, where positive values indicate upward curvature at extremes.

The fourth-order terms are $-0.0213t^4$ *and* $-0.0214t^4$ for the GeoFF/GeoFC and GeoSF/GeoSC, respectively.

It can be noted that there are nearly identical coefficients across all locations. The negative values create downward pressure on peaks and control intermediate-term variations

Third-order terms:

GeoFF/GeoFC: $1906.7t^3$

GeoSF/GeoSC: $1917.9t^3$

The observed similar magnitudes in the third-order term indicate consistent seasonal patterns and the positive coefficient creates a strong upward trend in concentration and acceleration of aerosol accumulation in the middle range. The difference of 11.2 between locations (1917.9 - 1906.7) suggests a slightly stronger seasonal effect in GeoSF/GeoSC, more pronounced curvature in concentration changes, and greater sensitivity to seasonal transitions.

The second-order terms (t^2) for both locations is: $-9E+07t^2$

The physical Interpretation of this term is that the negative coefficient indicates a dampening effect on extreme values, moderation of concentration peaks, and parabolic behavior in the temporal variation

First-order terms (t) for both locations are: $+2E + 12t$

The physical meaning of the first-order term is that the positive coefficient represents the linear trend component, the basic growth rate, and the underlying increasing tendency

The R^2 values of 0.7349 and 0.7447 from equations 2 and 4 indicate a strong correlation between time and aerosol concentration, with approximately $73 - 74\%$ of variation explained by temporal factors. The remaining approximately $26 - 27\%$ are due to other factors.

The peak concentration values recorded are listed below:

August-September:

October-November: $40 - 50\ \mu g/m^3$

December: $80 - 90\ \mu g/m^3$

The pattern analysis is as follows:

August-September presents the lowest concentration period with a stable, low aerosol loading ($10 - 20\ \mu g/m^3$) and minimal daily variations, which is likely due to better atmospheric mixing and wet deposition (Kumar et al., 2011; Wang et al., 2013).

The transition period (October) saw a sharp increase in concentration, with greater daily variations suggesting changes in meteorological conditions, increased anthropogenic activities, possible agricultural burning, and transport due to southwesterly trade wind (Kedia et al., 2014; Balarabe et al., 2016).

The highest aerosol loading (up to 90 $\mu g/m^3$) was obtained in the high-concentration period (November-December) with maximum variability likely influenced by winter atmospheric conditions, reduced mixing height, increased emissions from heating, and possible temperature inversions (Tie et al., 2017).

4.2.2 Regression analysis for the "Merra" data

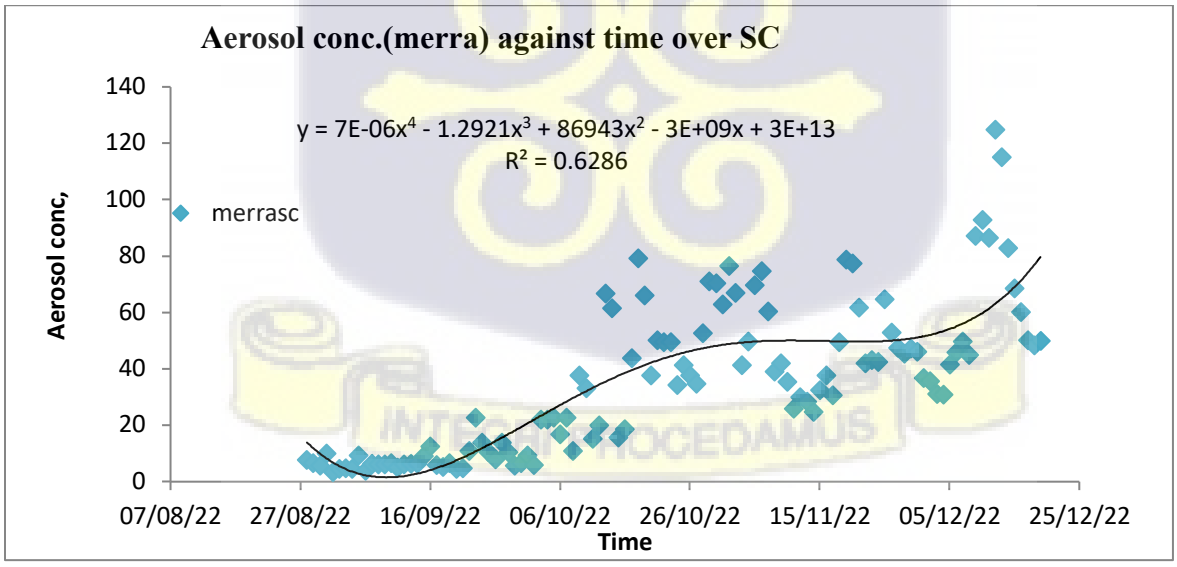

Figure 4.9: Daily averaged temporal variation of aerosol concentration, SC.

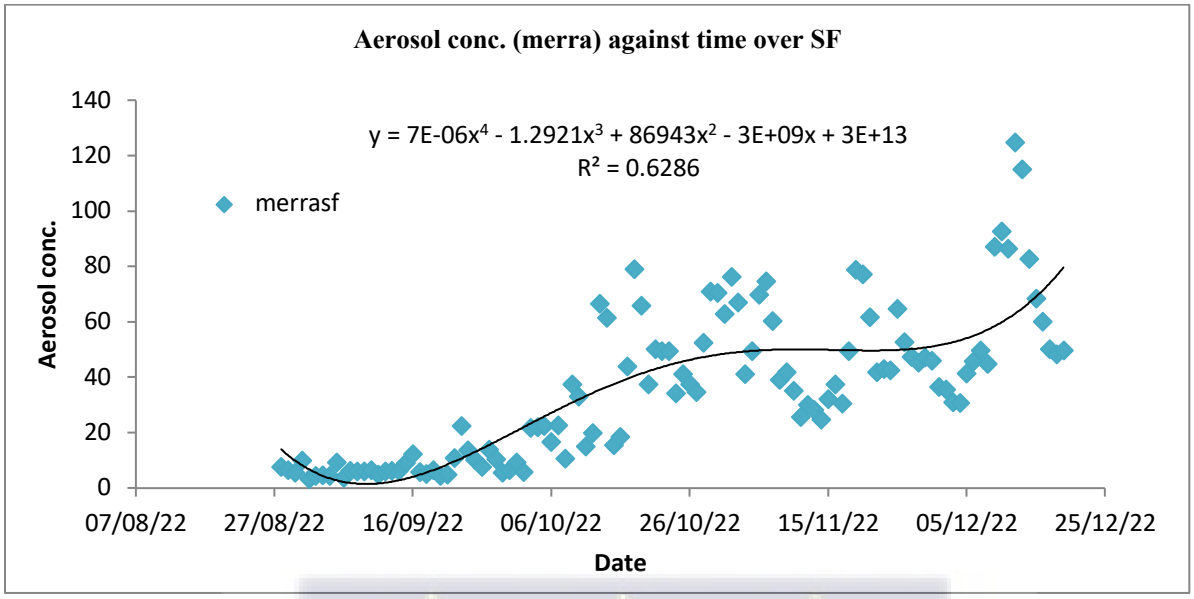

Figure 4.10: Daily averaged temporal variation of aerosol concentration, SF

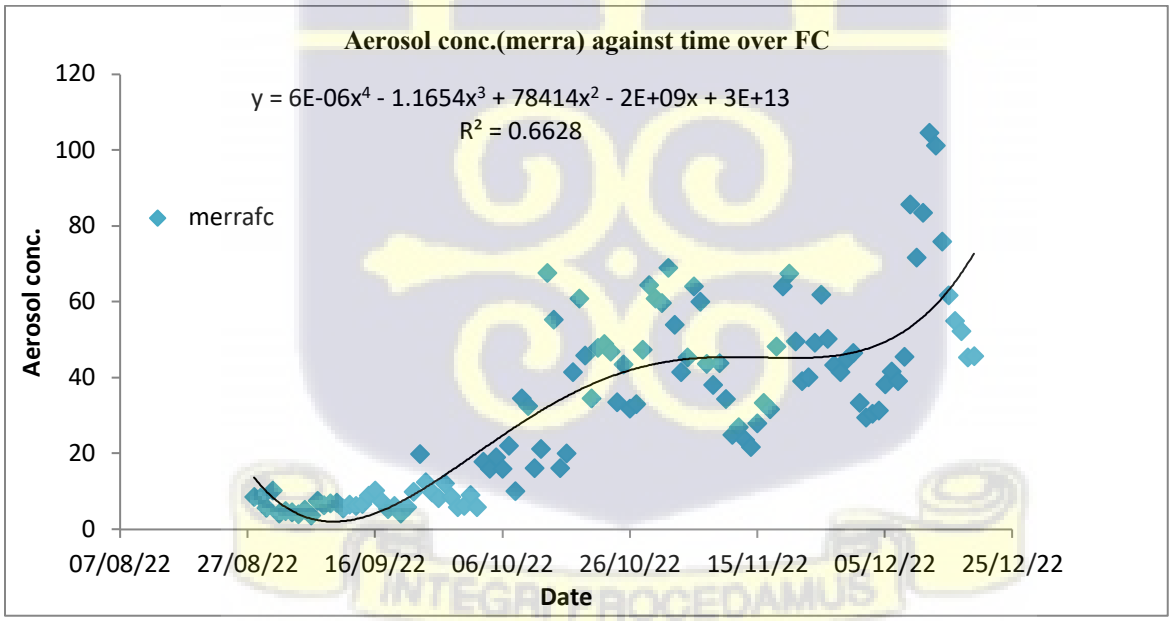

Figure 4.11: Daily averaged temporal variation of aerosol concentration, FC.

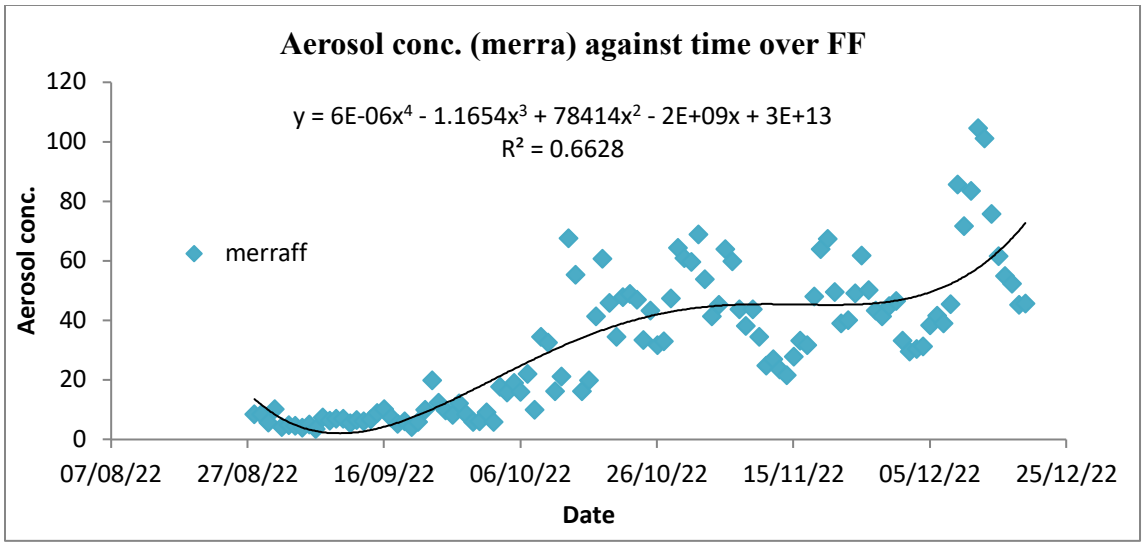

Figure 4.12: Daily averaged temporal variation of aerosol concentration, FF

Aerosol concentration mathematical Analysis:

The Polynomial Regression equation obtained for both SC/SF and FC/FF are of the form:

Equation 4.3: regression equation between time against aerosol concentration, Merrasc

$$y = 7E-06x^4 - 1.2921x^3 + 86943x^2 - 3E+09x - 4E+13$$

Equation 4.4: Time against aerosol concentration regression equation, merrasf

$$y = 6E-06x^4 - 1.1654x^3 + 78414x^2 - 2E+09x + 3E+13$$

respectively. Where y represent the aerosol concentration and x represents the date.

The mathematical interpretations from equations 1 and 3 are as follows:

Fourth-order terms for SC/SF: $7E-06x^4$ and for FC/FF: $6E-06x^4$

These terms represent diurnal patterns and quick responses to local conditions and control short-term variations. The higher coefficient in SC/SF indicates more rapid variations

The cubic terms: SC/SF: $-1.2921x^3$ and FC/FF: $-1.1654x^3$ governs seasonal transitions. The larger negative coefficient in SC/SF suggests stronger seasonal effects and controls inflection points in concentration curves

The quadratic terms SC/SF: $86943x^2$ and FC/FF: $78414x^2$, determine overall curvature. The higher coefficient in SC/SF indicates stronger parabolic behavior and represents medium-term variations.

The linear terms, SC/SF: $-3E + 09x$ and FC/FF: $-2E + 09x$, indicate general trend direction, a stronger negative slope in SC/SF, and show baseline trend over the study period.

The constants $3E + 13$ (for both SC/SF and FC/FF), represent background aerosol levels. The same value suggests a similar regional background and baseline concentration reference.

The SC/SF shows consistently higher coefficients, which indicate more dynamic variations and suggest greater sensitivity to change factors.

R^2 values of 0.6286 (SC/SF) and 0.6628 (FC/FF) indicate a moderate to good fit. The FC/FF shows slightly better prediction capability, which is an indication of a complex but predictable system.

The R^2 values of 0.6286 and 0.6628 indicate a moderate correlation between time and aerosol concentration, with approximately $63 - 66\%$ of variation explained by temporal factors. The remaining approximately $37 - 34\%$ are attributed to other factors.

The concentration values recorded are listed below:

The late rainy Period (August-September) saw the lowest concentrations: $2 - 10\ \mu g/m^3$ which is similar to findings by Wang et al. (2013), who suggest that aerosol concentrations were extremely low in summer ($< 10\ \mu g/m^3$) and Kumar et al. (2011) attributed the low concentrations to wet deposition.

Post-rainy (October) saw a gradual increase from ($20 - 40\ \mu g/m^3$) which matches patterns observed by Singh et al. (2020). It is a transition period showing increasing trends. Early winter (November) shows moderate concentrations of about $40 - 60\ \mu g/m^3$ which is consistent with regional studies by Wang et al. (2013).

The winter period (December) recorded the highest concentrations ($80 - 125\ \mu g/m^3$). This aligns with findings from Andre et al. (2020) who reported that winter aerosol concentrations can exceed $100\ \mu g/m^3$ in urban areas of South Asia, driven by reduced mixing heights and increased emissions and Huang et al. (2014) also reported that winter concentrations were highest due to combined emission and meteorological effects in Benjin.

The analysis has reveals seasonal variations in aerosol concentration with summer having low magnitude and Harmattan having a significant increase which aligns with Balarabe et al. (2016) finding in their studies of the seasonal variations of aerosol optical properties and identification of different aerosol types over Sub-Sahara West-Africa. The analysis has also shown that the GeoSF satellite data shows a higher coefficient of determination ($R^2 = 0.7447$) than Merra2 ($R^2 = 0.6286$, SC/SF and $R^2 = 0.6628$, FC/FF). The higher R^2 value suggests better model fit and more reliable predictions (Ives, 2018). This indicates that GeoSF explains about 74.5% of the variance in aerosol

concentration. From this point, our studies will (in some cases) focus on the GeoSF data rather than the Merra2 data.

4.2.3 Model Performance and Comparison

Fifth-degree polynomial regression models were fitted to daily aerosol concentration time series to quantify temporal trends and seasonal progression (Figures $4.5 - 4.12$). Model performance differed systematically between datasets: GEOS-CF models achieved stronger fits ($R^2 = 0.73 - 0.74$) compared to MERRA-2 models ($R^2 = 0.63 - 0.66$), with detailed regression equations provided in Appendix C. The superior GEOS-CF performance likely reflects its finer spatial resolution (0.25° vs. 0.5°) and more recent assimilation system, enabling better capture of sub-grid variability and episodic events (Keller et al., 2021).

Both datasets' models successfully capture the key seasonal features: stable baseline conditions in early September, sharp increases through October-November, and peak loading in December. However, the moderate R^2 values (explaining $63 - 74\%$ of variance) indicate substantial unexplained variability, attributable to: episodic dust events not predicted by smooth polynomial trends, synoptic-scale meteorological variations, day-to-day fluctuations in local emissions, and satellite retrieval uncertainties ($\pm 30 - 50\% \; for \; MERRA - 2, \pm 30 - 40\% \; for \; GEOS - CF$). The remaining $26 - 37\%$ unexplained variance is consistent with other regional aerosol studies employing satellite data (Levy et al., 2013; Hsu et al., 2013).

4.2.4 Physical Interpretation of Temporal Trends

The polynomial coefficients reveal meaningful physical patterns. The dominant third-order terms (coefficients $\sim 1900 - 1920$) drive the strong mid-season acceleration in aerosol accumulation, representing the rapid atmospheric drying and onset of northeasterly Harmattan winds. Nearly

identical magnitudes across locations (difference <1%) confirm uniform regional meteorological forcing. The fourth-order negative terms ($\sim -0.021\ to\ -0.022$) moderate peak values, preventing unrealistic extrapolation, while small fifth-order terms ($\sim 1 \times 10^{-7}$) provide fine-scale curvature adjustments.

Subtle differences between location pairs emerge: Sokwai sites (SC/SF) exhibit slightly larger third-order coefficients ($1917.9\ vs.\ 1906.7, a\ \sim 0.6\%$ difference), suggesting marginally stronger seasonal progression. While this difference is small, it aligns with the observed $5 - 10\ \mu g/m^3$ higher peak concentrations at Sokwai, potentially reflecting proximity to agricultural areas with enhanced biomass burning during the dry season (Bond et al., 2004). However, the similarity in coefficient patterns (correlation > 0.99) underscores the dominance of regional processes over local factors.

4.3 Spatial Variation Analysis

4.3.1 ANOVA Results

One-way ANOVA was conducted to assess spatial variability in aerosol loading across the four study locations and two satellite datasets (Table 4.1). With eight groups (four locations × two datasets) and 114 observations per group, the analysis provides robust statistical power. Mean concentrations ranged from $32.72\ \mu g/m^3$ (MERRA-2 FC) to $36.43\ \mu g/m^3$ (GEOS-CF FF), representing only ~11% variation across all groups. Variances were consistently moderate for GEOS-CF ($403 - 406\ \mu g^2/m^6$) and higher for MERRA-2 ($550 - 716\ \mu g^2/m^6$), reflecting greater temporal variability in the MERRA-2 dataset.

Table 4-1: ANOVA Results for Aerosol Loading Across the Four Locations

Anova: Single Factor for the GeosCF and the Merra2 data sets over the Four Locations						
Result						
Groups	*Count*	*Sum*	*Average*	*Variance*		
geoff	114	4152.520427	36.42562	403.474177		
geofc	114	4152.520427	36.42562	403.474177		
geosf	114	3743.404541	32.83688	406.24743		
geosc	114	3743.404541	32.83688	406.24743		
merraff	114	3729.558898	32.71543	550.273576		
merrafc	114	3729.558898	32.71543	550.273576		
merrasf	114	4075.212987	35.74748	715.954053		
merrasc	114	4075.212987	35.74748	715.954053		
ANOVA						
Source of Variation	*SS*	*df*	*MS*	*F*	*P-value*	*F crit*
Between Groups	2552.692974	7	364.6704	0.70265769	0.669869538	2.0196915
Within Groups	469164.5274	904	518.9873			
Total	471717.2204	911				

The results of the one-way ANOVA test utilizing two datasets (GeoSF and Mera2) on aerosol concentration data from four locations (FF, FC, SF, and SC) are shown in the table above, which will help us to determine whether there are significant variations in aerosol loading over the study's locations.

From the ANOVA output, each group (location) contains 114 observations, indicating sufficient data for robust statistical analysis.

Averages:

The average concentration for the GeosCF data ranges from 32.83 µg/m³ (GeoSC) to 36.43 $\mu g/m^3$ (GeoFF), and the average concentration for the Merra2 data ranges from 32.71 µg/m³ (MeraFC) to 35.75 $\mu g/m^3$ (MeraSF).

Variance:

The GeoSF has relatively low variances ($403.47 - 406.25\ \mu g^2/m^6$), indicating low variability compared to the Mera2, which exhibits higher variances ($550.27 - 715.95\ \mu g^2/m^6$), suggesting a greater aerosol concentration variation.

Between-Groups:

The Sum of Squares (SS) obtained is 2552.693. This represents the variation due to differences between the four locations. A relatively small SS indicates that the differences in aerosol loading between the locations are modest.

The Mean Square (MS) obtained is 364.67. This is the average variation attributable to differences between the groups.

Within-Groups:

The Sum of Squares (SS) obtained is 469164.5

This value is significantly larger than the between-groups SS, suggesting that most of the variation is due to differences within each group rather than between the locations.

Mean Square (MS): 518.99

This reflects the variability of aerosol loading within the individual locations.

The Statistical Significance of the result is as follows;

The F-statistic, which compares the variance between groups to the variance within groups is found to be 0.7027, which is a low F-statistic, indicating that the between-group variability is not that much greater than the within-group variability.

The P-value, which is the probability of observing the given F-statistic under the null hypothesis, is found to be 0.6699, which is greater than 0.05. This implies we fail to reject the null hypothesis (thus, no significant difference between groups).

The F Critical (F-crit) obtained is 2.0197

Since F < Fcrit., the differences between group means are not statistically significant.

The discussion of the ANOVA results shows that there is no significant variation in aerosol loading across the four locations for either the GeoSF or the Mera2 datasets which is a suggestion that the aerosol loading may be relatively uniform across the chosen locations which may be due to similar environmental factors (e.g., local emission sources, weather conditions, or topography) which aligns with the findings of Huang et al. (2021) and Raman et al. (2016). Also, the high within-group variance (MS = 518.99) implies that local factors such as daily meteorological changes or data collection inconsistencies might contribute more significantly to aerosol loading variability than inter-location differences (Wei et al., 2019; Feng et al., 2023).

We further performed the F-test analysis within locations, and the results suggest that there is no statistically significant difference in aerosol concentrations within the groups (refer to Appendix B.1 on page 140 for the F-test results).

From this point, our discussions and analysis focused on Sokwai and Fumesua as a unit, and also focused more on the GeosCF data than the Merra2 data.

4.3.2 Interpretation and Implications

The spatial uniformity in aerosol loading across the 15–20 km study area has important implications for interpreting aerosol sources and processes. Three potential explanations merit consideration:

Regional-scale dominance: Harmattan dust transport from the Sahel represents a regional-scale phenomenon (horizontal scale $\sim 1000\ km$) that overwhelms local sources. The ~50 km grid resolution of MERRA-2 and $\sim 30\ km$ resolution of GEOS-CF may be too coarse to resolve the $15 - 20\ km$ separation between study sites, effectively smoothing spatial gradients.

Local source similarity: Despite the urban-rural and community-farm gradients in the study design, local aerosol sources (biomass burning, vehicle emissions, dust resuspension) may be more spatially uniform than anticipated. The absence of heavy industry in the region and similar domestic fuel use patterns (primarily biomass) could contribute to spatial homogeneity (Dionisio et al., 2010).

Measurement limitations: Satellite retrievals aggregate over $\sim 25 - 60\ km$ grid cells, potentially masking fine-scale spatial variations. Ground-based measurements at higher spatial resolution might reveal differences not detectable in satellite data (Levy et al., 2013; Hsu et al., 2013).

The observed subtle concentration gradient (Sokwai sites $\sim 5 - 10\ \mu g/m^3$ higher than Fumesua, as noted in Section 4.1) approaches but does not exceed the satellite retrieval uncertainty ranges ($\pm 30 - 50\%$), making it difficult to attribute this pattern definitively to local land use differences versus measurement noise. Studies employing denser ground-based monitoring networks in similar West African settings have documented spatial gradients of $20 - 40\%$ over comparable distances (Arku et al., 2008), suggesting our satellite-based approach may underestimate true spatial heterogeneity.

Pragmatically, the spatial uniformity finding validates treating the four study sites as collectively representative of aerosol conditions in the broader Kumasi metropolitan area (~15–20 km radius). This justifies the subsequent consolidated analysis of aerosol-climate relationships without site-specific stratification. However, it also indicates that the study design's spatial gradient (urban-rural, community-farm) was insufficient to detect local source impacts above regional background, suggesting future studies should employ either wider spatial coverage or higher-resolution measurement approaches (e.g., low-cost sensor networks).

4.4 Monthly Temporal Variations.

In Figures 4.13- 4.16 below, the Monthly average "Avg Geo," aerosol concentrations are represented by the blue lines for the GeosFC data set, while the monthly average "Avg. Merra," aerosol concentrations for the "Merra2" are represented by the orange line.

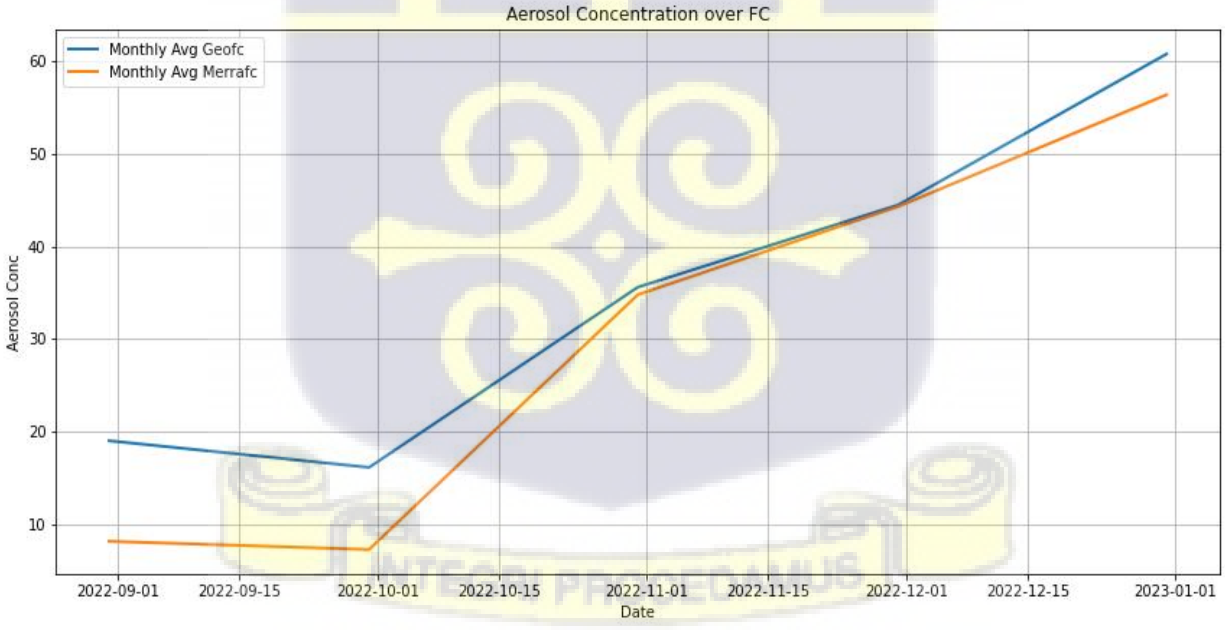

Figure 4.13: Monthly mean temporal variation in aerosol concentration, FC

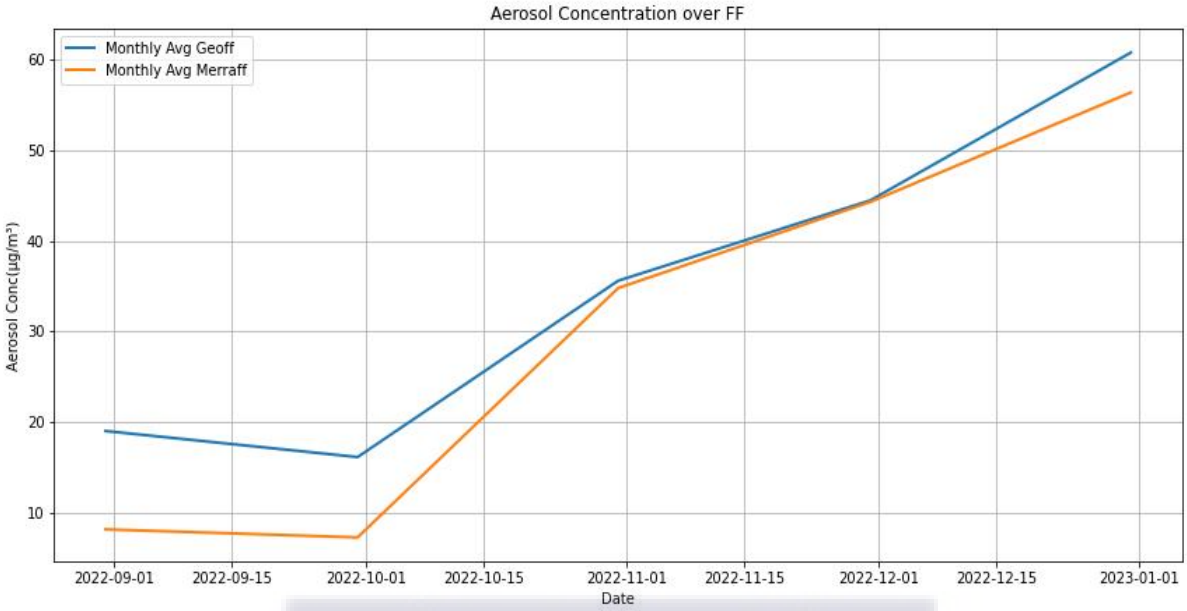

Figure 4.14: Monthly mean temporal variation in aerosol concentration, FF.

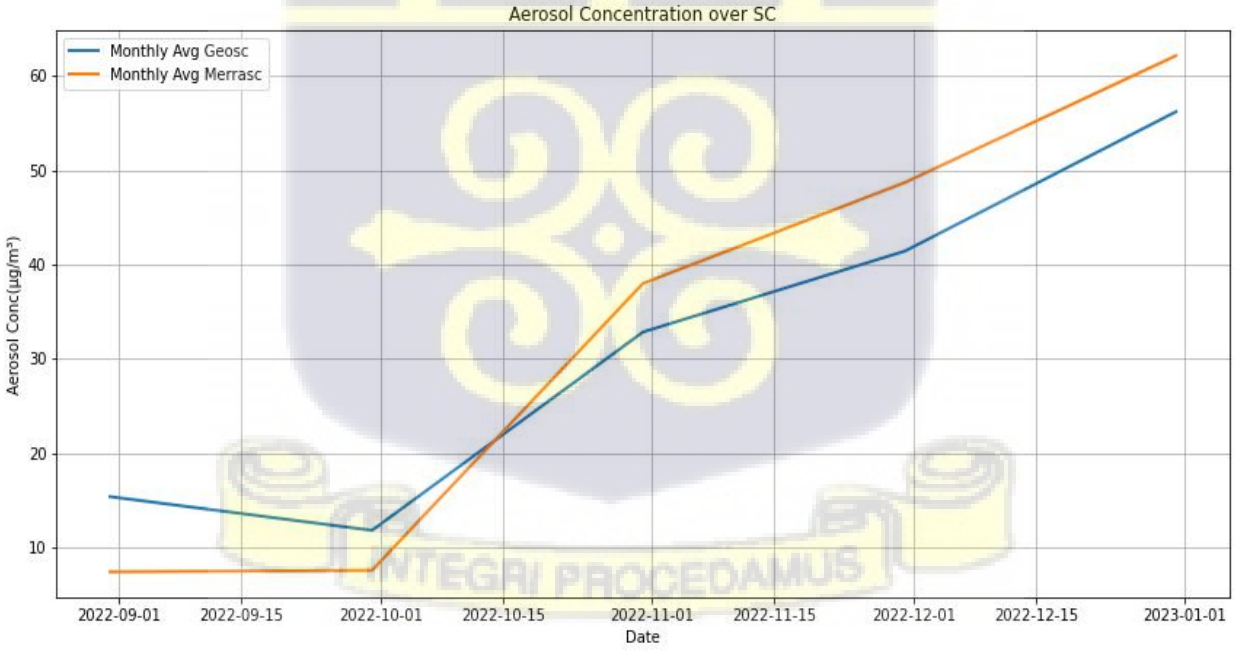

Figure 4.15 Monthly mean temporal variations in aerosol concentration, SF.

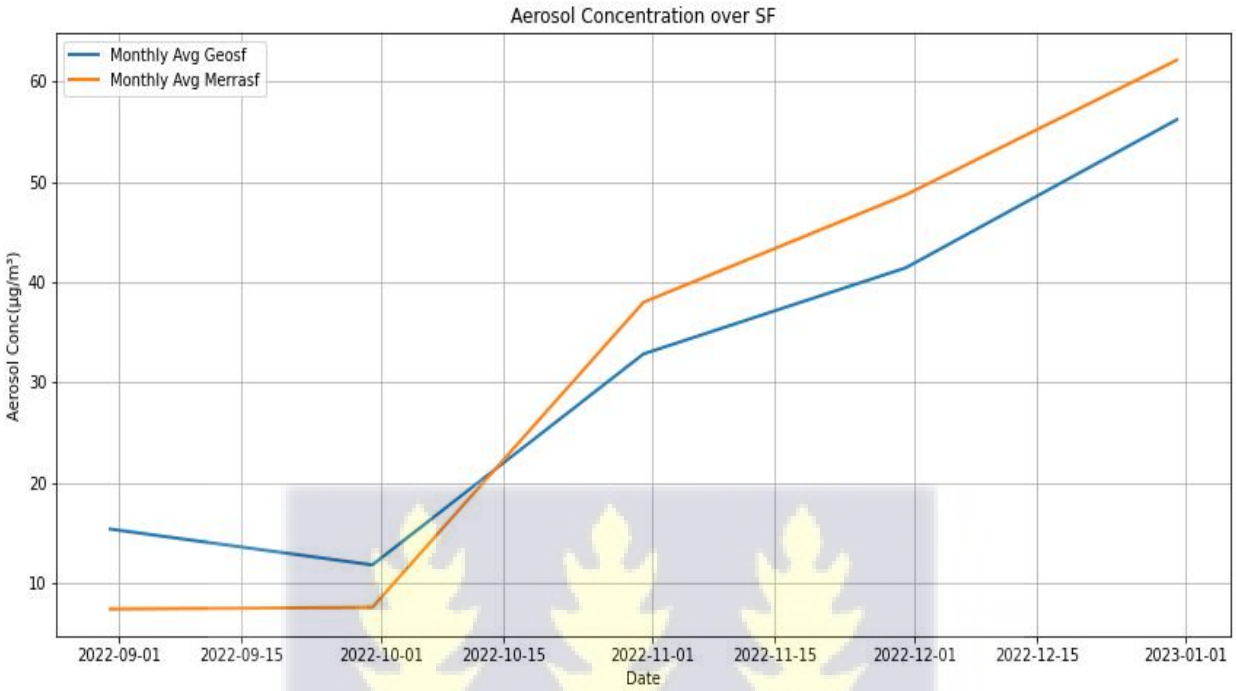

Figure 4.16: Monthly mean temporal variation in aerosol concentration, SF.

Monthly mean concentrations (Figures 4.13-4.16) provide the clearest demonstration of seasonal trends. September exhibits uniformly low concentrations ($\mathrm{GEOS-CF}$: $15-20\ \mu g/m^3$; $\mathrm{MERRA-2}$: $7-10\ \mu g/m^3$) across all sites, consistent with the rainy season's cleansing effects. October shows modest increases ($\mathrm{GEOS-CF}$: $\sim 30\ \mu g/m^3$; $\mathrm{MERRA-2}$: $\sim 20\ \mu g/m^3$) marking the wet-to-dry transition. November displays a substantial elevation ($\mathrm{GEOS-CF}$: $\sim 40\ \mu g/m^3$; $\mathrm{MERRA-2}$: $\sim 35\ \mu g/m^3$) as Harmattan conditions establish. December records peak monthly means ($\mathrm{GEOS-}CF$: $\sim 60\ \mu g/m^3$; $\mathrm{MERRA-2}$: $\sim 55\ \mu g/m^3$), representing approximately 3-fold increases relative to the September baseline.

The monthly progression aligns closely with regional climatological patterns documented across West Africa, where the September–October transition marks the southward retreat of the Inter-Tropical Convergence Zone (ITCZ) and associated shift from maritime to continental air mass dominance (Sultan & Janicot, 2003; Nicholson, 2013). The similarity in monthly patterns across all four study sites (despite their urban-rural and community-farm gradients) suggests that regional-scale meteorological controls dominate over local emission sources during this season, a finding further supported by the ANOVA results presented in Section 4.4.

4.5 Aerosol-Climate Relationships

This section examines the interactions between aerosol concentration, surface solar radiation (SSR), and temperature across daily, weekly, and monthly time scales (Figures 4.17-4.28)

4.5.1. Diurnal average aerosol concentrations, SSR, and temperature over FC and FF locations.

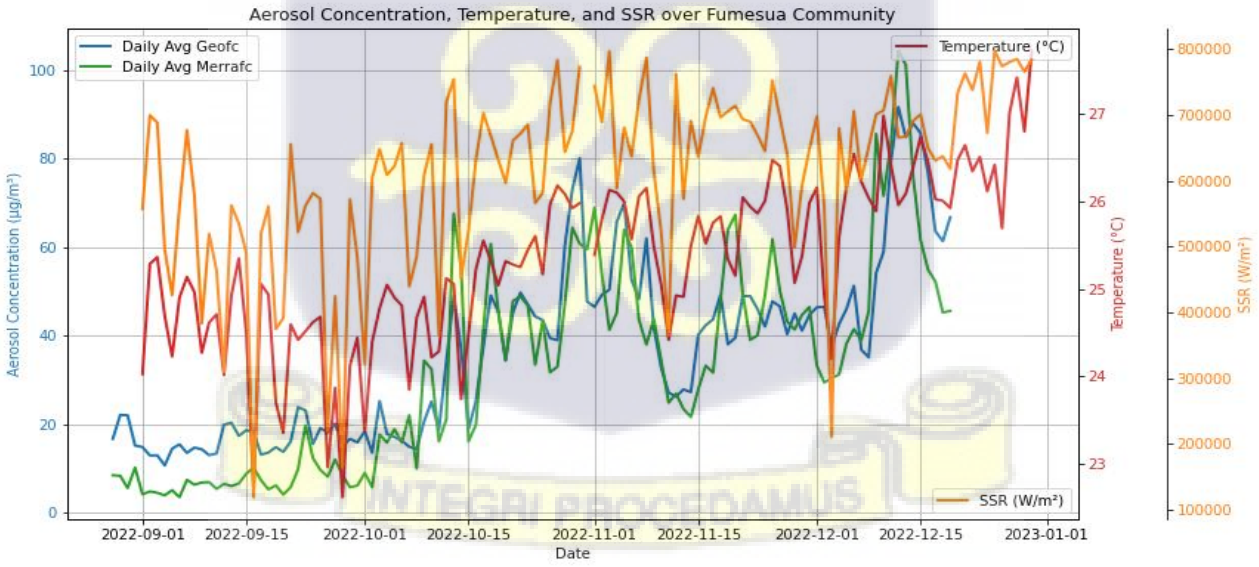

Figure 4.17: Daily average variations in aerosol concentration, temperature, and SSR over FC.

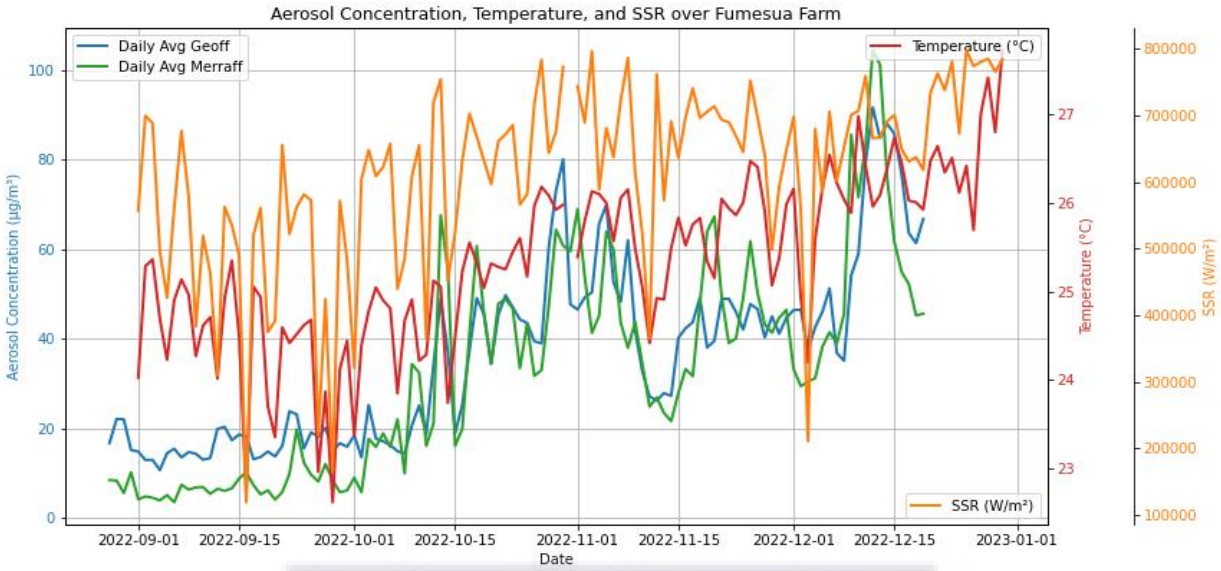

Figure 4.18: Daily average variations in aerosol concentration, temperature, and SSR over FC

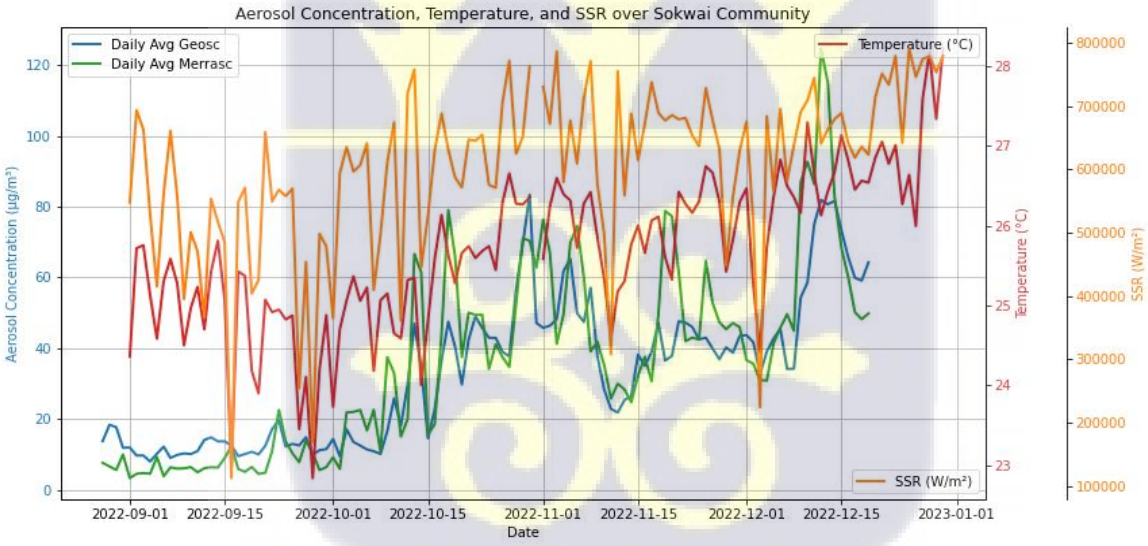

Figure 4.19: Daily average variations in aerosol concentration, temperature, and SSR over SF

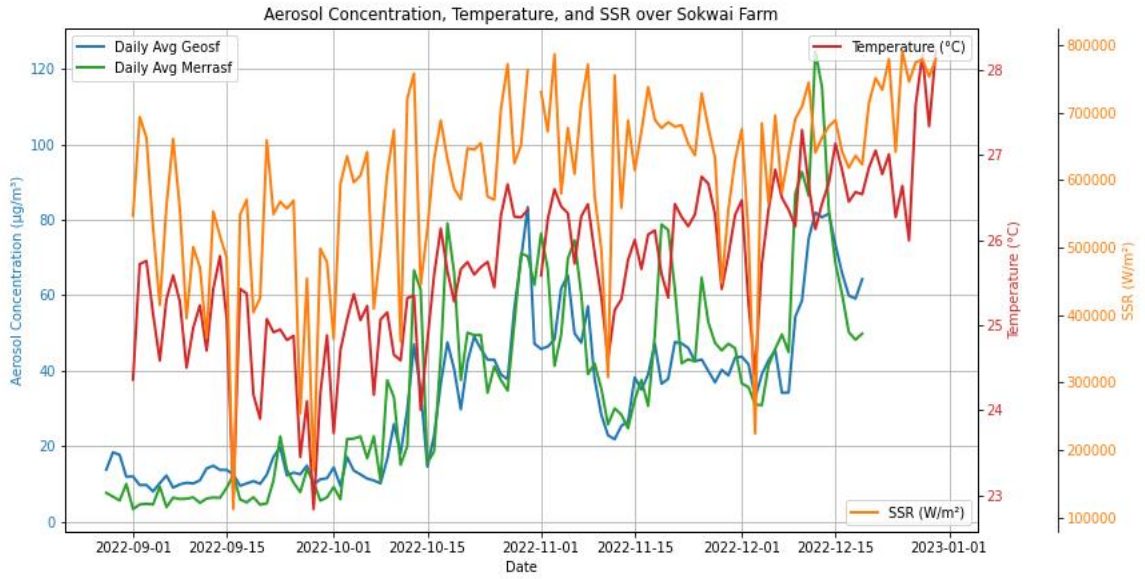

Figure 4.20: Daily average variations in aerosol concentration, temperature, and SSR over SF

4.5.2 Average weekly aerosol concentrations and the impact on solar radiation and temperature over all locations (FC, FF, SC, and SF).

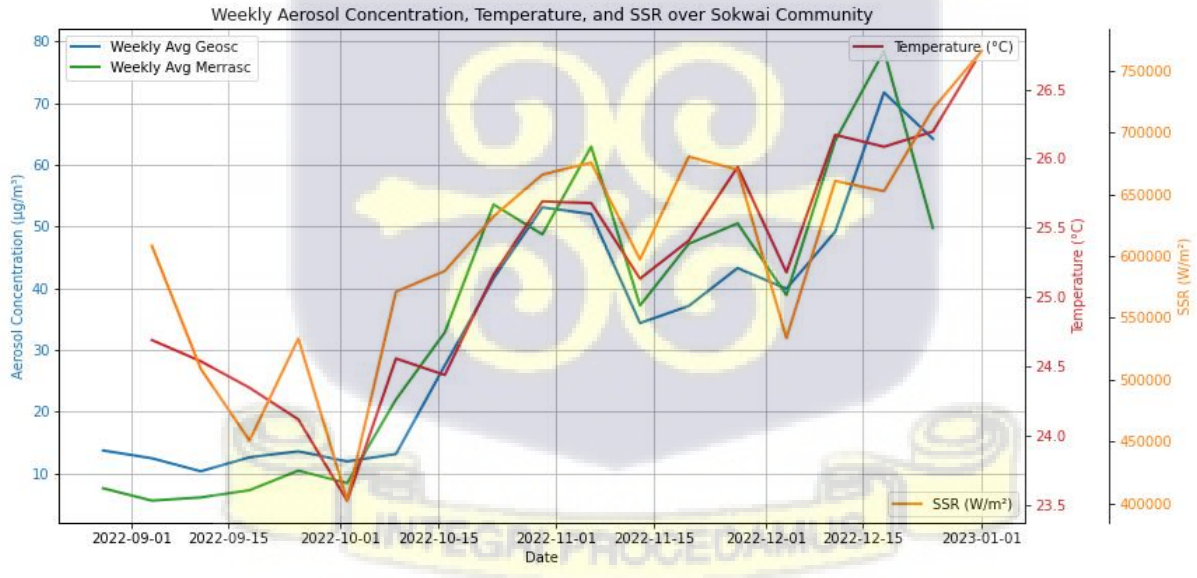

Figure 4.21: Average weekly aerosol concentrations and the impact on SSR and temperature, SC.

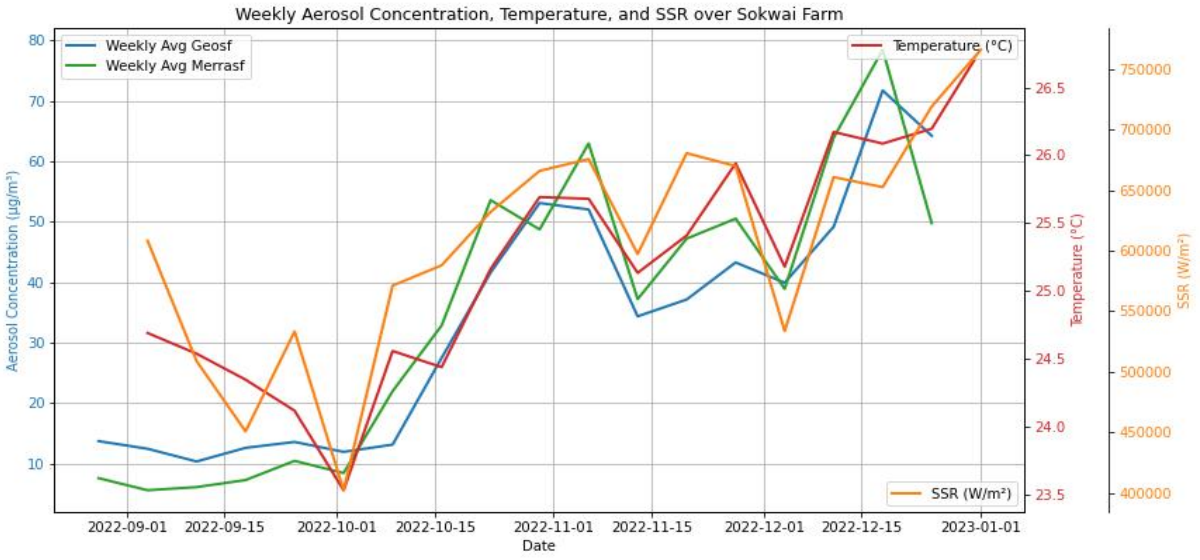

Figure 4.22: Average weekly aerosol concentrations and the impact on SSR and temperature, SF.

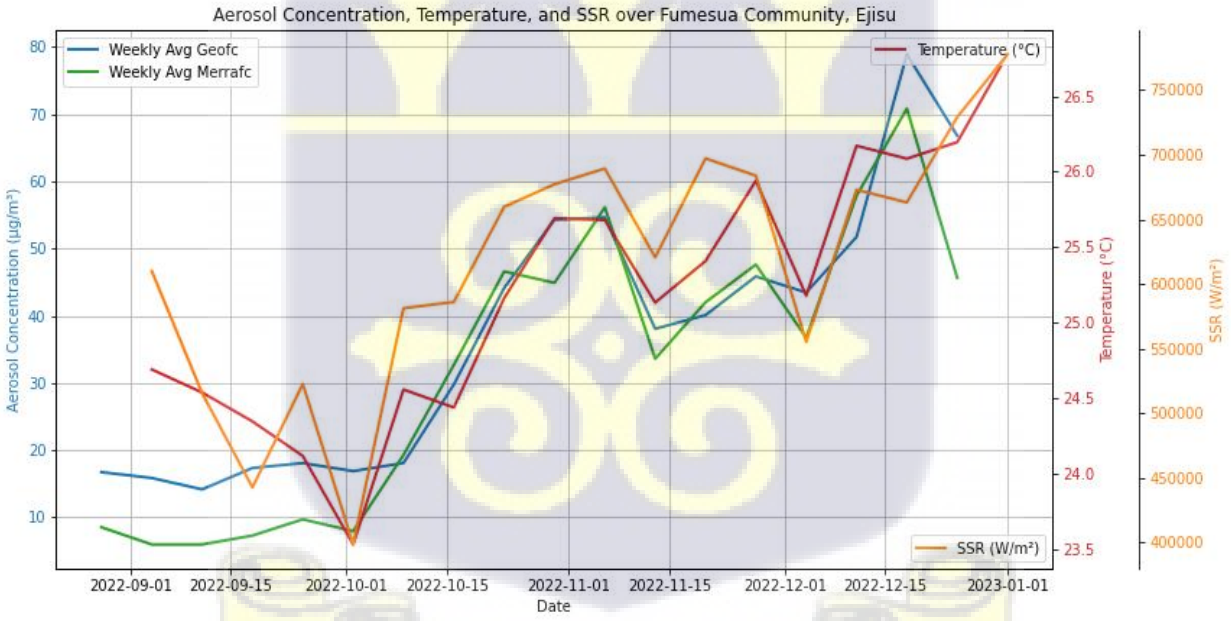

Figure 4.23: Average weekly aerosol concentrations and the impact on SSR and temperature, FC.

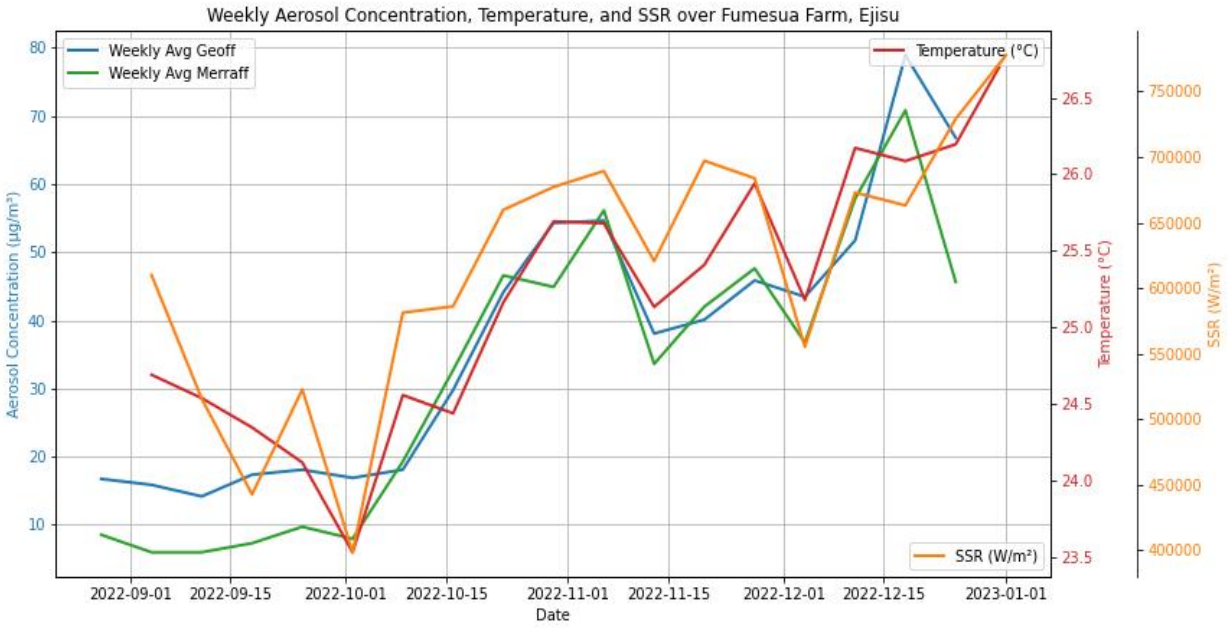

Figure 4.*24*: Average weekly aerosol concentrations and the impact on SSR and temperature, FF.

4.5.3 Mean monthly aerosol concentrations and the impact on solar radiation and temperature over all locations (FC, FF, SC and SF).

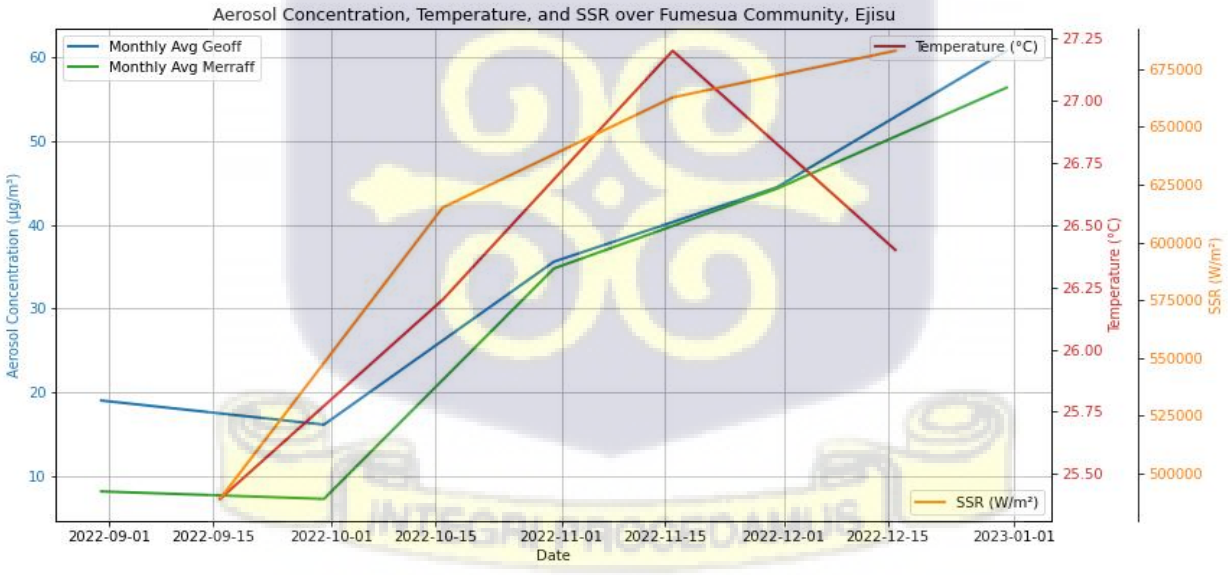

Figure 4.25: Mean monthly aerosol concentrations and the impact on solar radiation and temperature, FC.

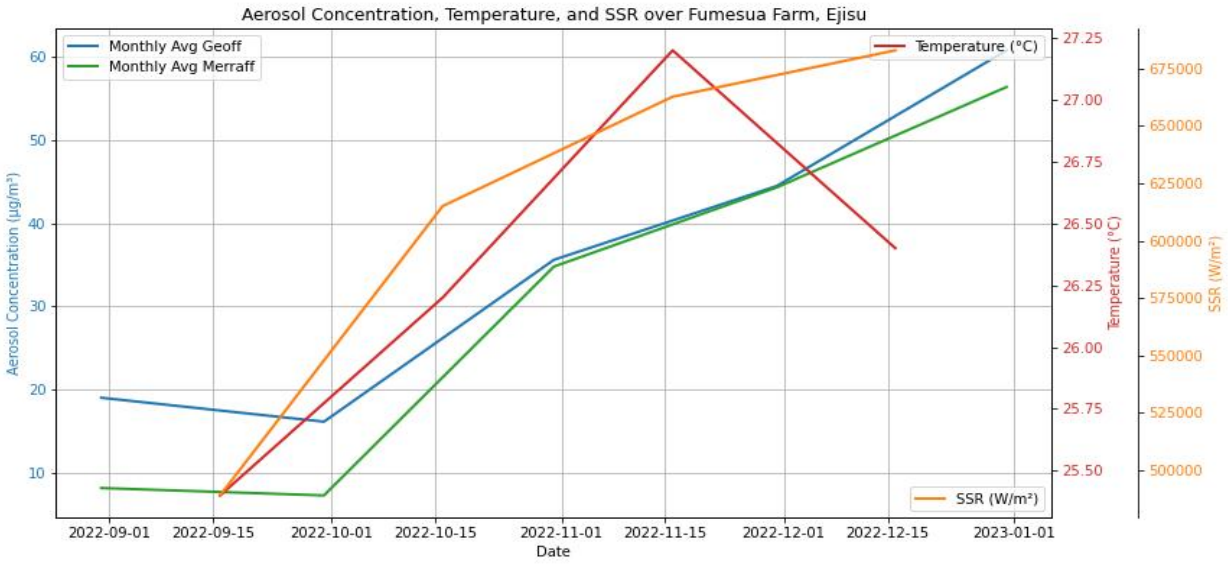

Figure 4.26: Mean monthly aerosol concentrations and the impact on solar radiation and temperature, FF.

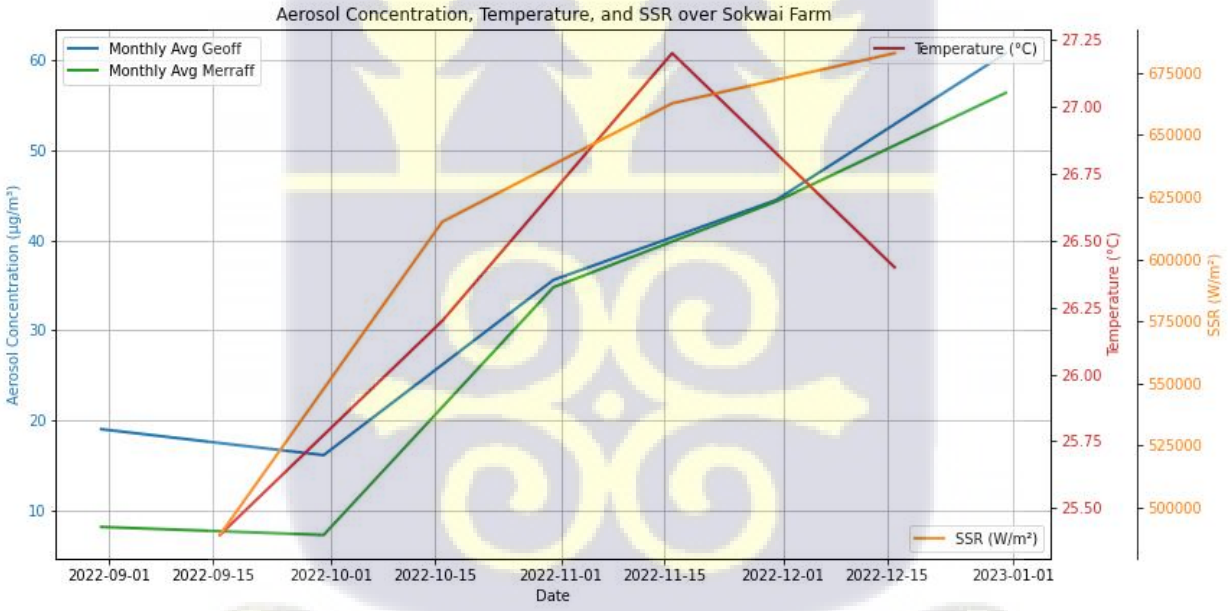

Figure 4.27: Mean monthly aerosol concentrations and the impact on solar radiation and temperature, SC.

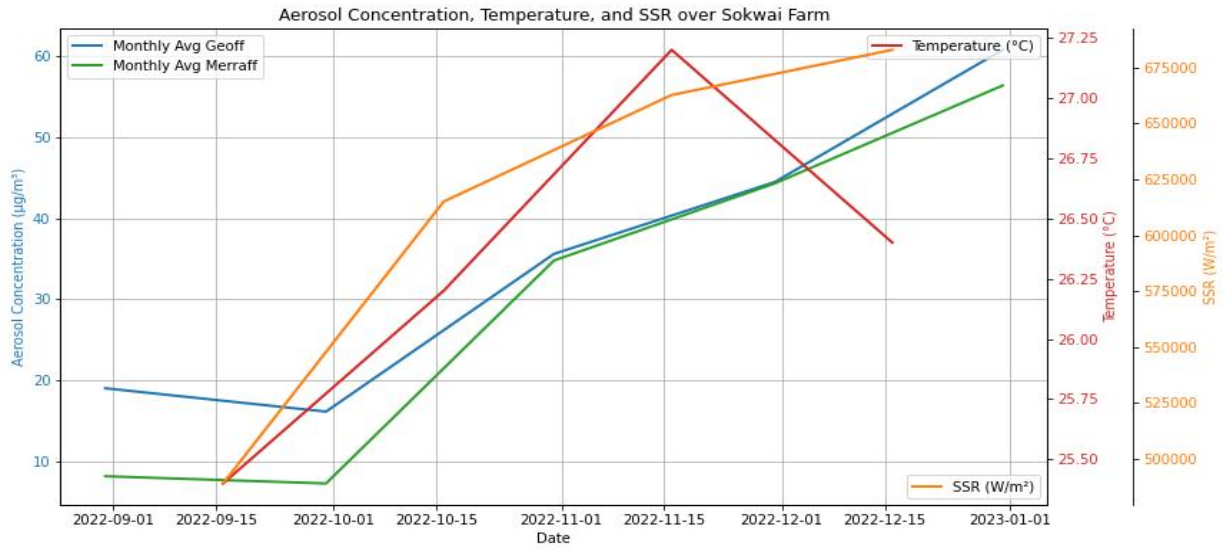

Figure 4.28: Mean monthly aerosol concentrations and the impact on solar radiation and temperature, SF.

4.5.4 Inverse Aerosol-SSR Relationship

An inverse relationship between aerosol loading and SSR is evident across all temporal scales and locations, consistent with fundamental aerosol-radiation physics (Ramanathan et al., 2001; Wild et al., 2005). At the daily scale (Figures 4.17-4.20), high aerosol episodes (greater than 80 $\mu g/m^3$) typically coincide with SSR reductions of $100{,}000 - 200{,}000\ W/m^2$ (approximately 15-25%) relative to low-aerosol periods. Weekly aggregation (Figures 4.21-4.24) reveals smoother inverse coupling, with correlation coefficients ranging from r = -0.45 to -0.60 across sites. Monthly patterns (Figures 4.25-4.28) show the clearest inverse trend during high aerosol periods.

The physical mechanisms underlying aerosol-SSR attenuation include direct scattering and absorption of incoming solar radiation. Scattering by sulfate and dust particles redirects radiation away from the surface, while absorption by black carbon converts radiation to atmospheric heating rather than surface illumination (Charlson et al., 1992; Haywood & Boucher, 2000). The observed approximately 20% SSR reduction during peak aerosol loading aligns with theoretical estimates for aerosol optical depths (AOD approximately 0.3-0.5) typical of Harmattan conditions (Boucher,

2015). However, the inverse relationship is not strictly linear, particularly at monthly scales, suggesting confounding seasonal factors discussed earlier.

4.5.5 Complex Aerosol-Temperature Interactions

The aerosol-temperature relationship exhibits greater complexity than the aerosol-SSR interaction, with scale-dependent patterns. At daily scales, temperature shows a weak positive correlation with aerosol concentration (r approximately $0.2 - 0.3$) during October-November, when rising aerosols and rising temperatures co-occur. However, this association reverses in December (r approximately $-0.1\ to\ -0.2$), when peak aerosol loading coincides with temperature stabilization or modest declines. Weekly data reveal clearer patterns: temperature increases progressively from September (approximately 24.5 °C) through mid-November (approximately 26.5 °C) alongside rising aerosols, then plateaus or decreases slightly in late December (approximately 26.0 °C) despite continued high aerosol loading.

Monthly aggregation (Figures $4.25 - 4.28$) demonstrates a non-monotonic aerosol-temperature relationship: temperature rises from September to mid-November with increasing aerosols, peaks at intermediate aerosol concentrations (approximately $40 - 50\mu g/m^3$), then declines at the highest aerosol loadings in December. This pattern suggests competing aerosol effects: absorption by black carbon warms the lower atmosphere at moderate loadings (Hansen et al., 2005; Ramanathan et al., 2001), while extreme aerosol concentrations suppress surface heating through enhanced SSR attenuation and potential semi-direct cloud effects (Ackerman et al., 2000; Koch & Del Genio, 2010).

The temperature response to aerosol loading also reflects seasonal confounding. The September-to-December temperature increase (approximately $1.5 - 2.0\ oC$) coincides with the dry season progression, when reduced cloud cover and evapotranspiration would elevate temperatures

independently of aerosol changes (Nicholson, 2013). Disentangling aerosol-driven temperature effects from these seasonal meteorological shifts requires multivariate analysis beyond this scope, highlighting a key limitation addressed in Section 4.6.

4.5.6 SSR-Temperature Coupling

Surface solar radiation and temperature exhibit a strong positive correlation across all temporal scales (r = 0.70-0.85), reflecting the fundamental energy balance relationship where incoming solar radiation drives surface and near-surface air warming (Oke, 1987). This coupling is most evident in weekly and monthly data, where SSR increases from September (approximately 525,000 W/m^2) to December (approximately 650,000 W/m^2), parallel temperature rises from approximately 25 °C to 27 °C. The seasonal SSR increase primarily reflects decreasing solar zenith angles as the sub-solar point moves southward, along with reduced cloud cover during the dry season (Wild, 2009).

However, the SSR-temperature relationship is modulated by aerosol loading. During high-aerosol episodes, the typical SSR-temperature coupling weakens: despite elevated SSR (due to seasonal sun angle effects), temperature increases are suppressed relative to expectations, consistent with aerosol-induced atmospheric heating and surface cooling (the semi-direct effect; Johnson et al., 2004). This modulation is most apparent in December, when SSR reaches approximately 650,000 W/m^2, but temperature stabilizes near 26.5 °C rather than continuing to rise proportionally.

4.5.7 Temporal Scale Synthesis

Comparing across temporal scales reveals both consistent patterns and scale-dependent features: Daily data capture episodic aerosol events and short-term SSR-temperature variability but exhibit high noise (R^2 approximately 0.4-0.6 for most relationships), limiting interpretation of causal mechanisms.

Weekly aggregation smooths short-term variations, revealing clearer inverse aerosol-SSR trends (r approximately -0.5) and staged seasonal progression (gradual September-October, rapid October-November, plateau December).

Monthly means provide the strongest statistical relationships (R^2 approximately 0.7-0.9) but conflate aerosol effects with seasonal meteorological changes, complicating attribution.

All temporal scales consistently show aerosol-SSR inverse coupling, but the magnitude varies: strongest at daily scales (approximately 25% SSR reduction during dust events), weakest at monthly scales (approximately 10% apparent reduction offset by seasonal SSR increases).

Aerosol-temperature relationships are scale-dependent: positive at weekly scales (September-November), non-monotonic at monthly scales (peak at intermediate loading), and highly variable at daily scales, reflecting competition between absorption warming and scattering cooling.

The overall pattern emerging across scales indicates that aerosol-climate interactions in Kumasi are governed by: direct aerosol radiative effects (scattering and absorption) operating at all scales, semi-direct effects on atmospheric stability and cloud properties becoming important at weekly-to-monthly scales, and seasonal meteorological transitions (ITCZ migration, Harmattan onset) dominating monthly-scale signals and potentially obscuring aerosol-specific impacts. Quantitative regression analyses of these relationships are presented in Section 4.7.

4.6 Regression Analysis: Variable Relationships

Regression analyses quantify the statistical relationships between aerosol concentration, SSR, and temperature observed qualitatively in Section 4.4. Given spatial uniformity (Section 4.3), analyses focus on Sokwai data as representative of the broader study area, with similar results obtained for Fumesua sites.

4.6.1 Aerosol-SSR Relationship

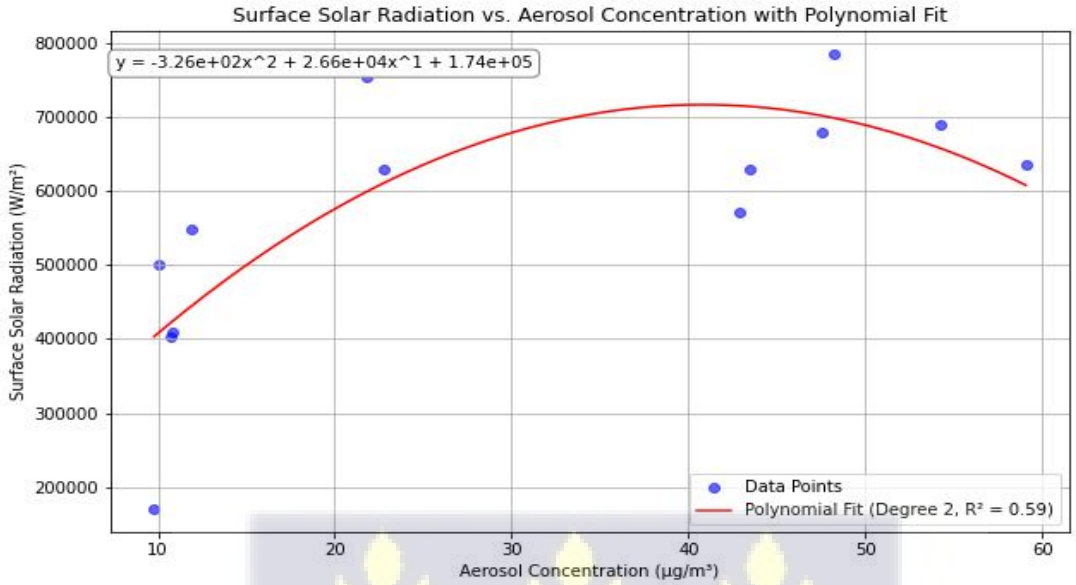

Figure 4.29: The correlation between aerosol concentration and SSR, Sokwai.

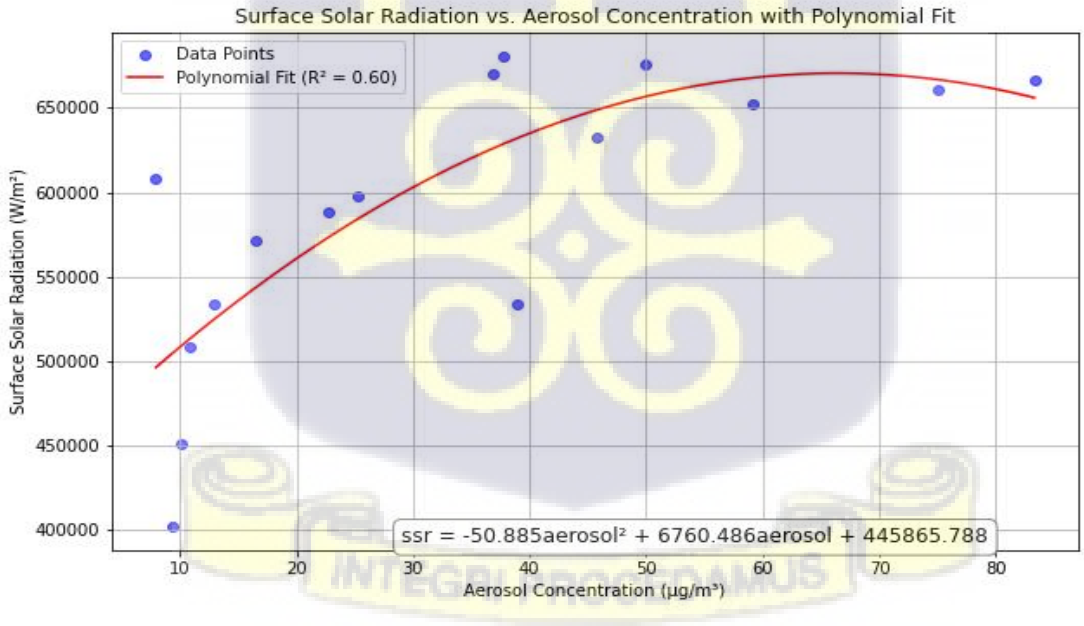

Figure 4.30: The correlation between aerosol concentration and SSR, Fumesua.

Analysis of the relationship between Aerosol Loading and Surface Solar Radiation (SSR) based on the graphs in Figures 4.29-4.30 shows a second-degree polynomial fit, expressed as:

Equation 4.1: regression equation between aerosol concentrations against SSR, Sokwai

$$y = -3.26e+02x^2 + 2.66e+04x + 1.74e+05$$

Equation 4.2: regression equation between aerosol concentration against SSR, Fumesua

$$y = -5.10e+01x^2 + 6.76e+04x + 4.46e+05$$

Where y represents Surface Solar Radiation (W/m²) and x represents Aerosol Concentration ($\mu g/m^3$).

The second-degree polynomial regression of SSR on aerosol concentration (Figures 4.29-4.30) yielded moderate fits: R-squared = 0.59 for Sokwai and R^2= 0.60 for Fumesua. The parabolic relationship exhibits initial SSR increases at low-to-moderate aerosol concentrations ($5-40\ \mu g/m^3$), followed by declines at higher loadings (greater than $40\ \mu g/m^3$). This non-monotonic pattern reflects competing mechanisms: at low concentrations, aerosol scattering enhances diffuse radiation without substantial absorption losses (Wild, 2009; Alpert & Kishcha, 2008), while at high concentrations, combined scattering and absorption produce net SSR attenuation (Ramanathan et al., 2001).

The moderate R^2 values (approximately 0.60) indicate that aerosol concentration explains only about 60%of SSR variability, with substantial unexplained variance (approximately 40%) attributable to factors not measured in this study: cloud cover, water vapor content, surface albedo changes, and solar zenith angle variations (Streets et al., 2009; Wang et al., 2012). The peak SSR

occurs at aerosol concentrations of $40 - 45\ \mu g/m^3$, suggesting an optimal aerosol loading for diffuse radiation enhancement before attenuation effects dominate. This finding aligns with observations from other tropical regions where moderate aerosol loadings (AOD approximately 0.2-0.3) maximize diffuse radiation and can enhance photosynthesis in forest canopies (Mercado et al., 2009).

The similar R^2 values across Sokwai (0.59) and Fumesua (0.60) sites reinforce the spatial uniformity finding (Section 4.3), suggesting consistent aerosol-SSR physics across the study area despite minor land use differences.

4.6.2 SSR-Temperature Relationship

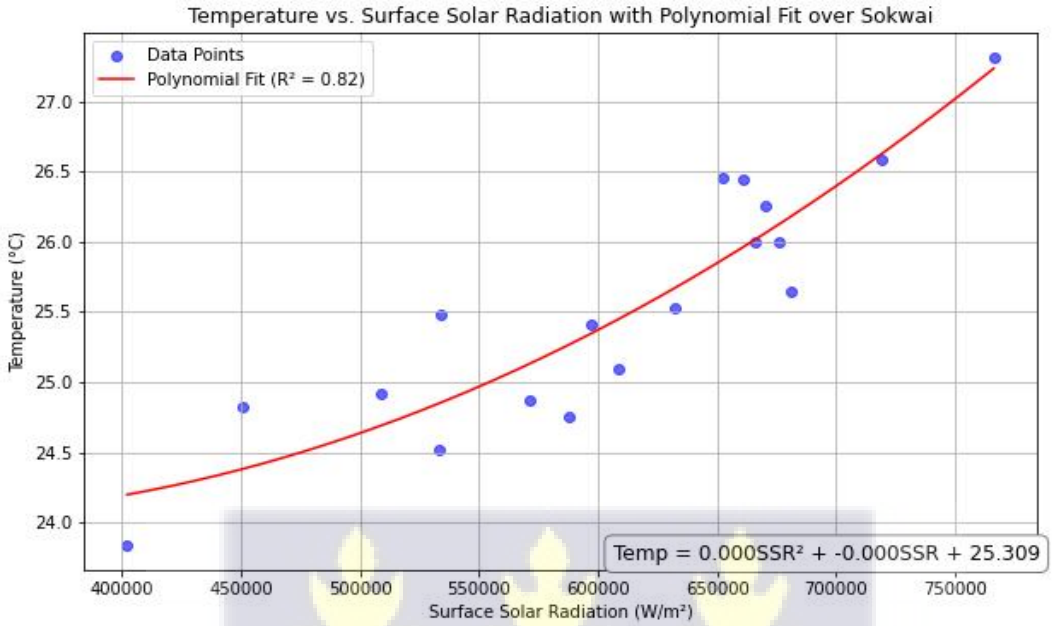

Figure *4*.31: The correlation between SSR and temperature, Sokwai.

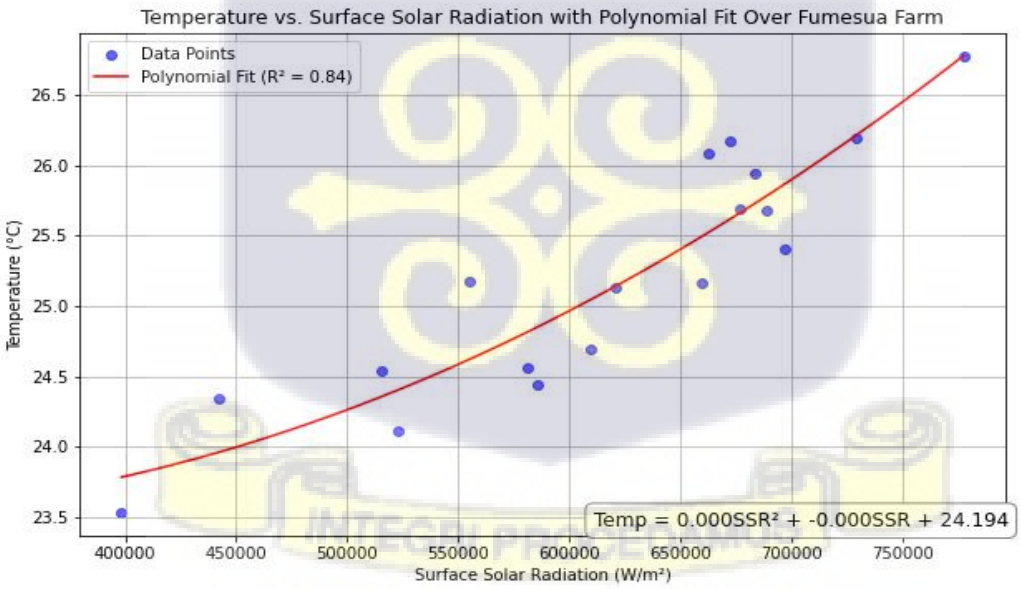

Figure 4.32: The correlation between SSR and temperature, Fumesua.

The graphs in Figures 4.31 and 4.32 illustrates a second-degree polynomial relationship between temperature (°C) and SSR (W/m²). The equations are:

Equation 4.1: SSR against temperature regression equation, Sokwai

$$\text{Temp} = 0.000\text{SSR}^2 - 0.000\text{SSR} + 0.24194\text{e} + 02,$$

Equation 4.2: SSR against temperature regression equation, Fumesua

$$\text{Temp} = 0.000\text{SSR}^2 - 0.000\text{SSR} + 0.24194\text{e} + 02,$$

Where, Temp. represents the temperature.

The second-degree polynomial regression of temperature on SSR (Figures 4.31-4.32) yielded strong fits: R-squared = 0.82 for Sokwai and R-squared = 0.84 for Fumesua. These high R^2 values indicate that SSR variations explain approximately $82 - 84\%$ of temperature variability, reflecting the fundamental energy balance relationship where solar heating drives near-surface air temperature (Oke, 1987). The positive quadratic coefficient indicates accelerating temperature response at higher SSR levels, consistent with non-linear feedbacks (e.g., reduced evapotranspiration at high temperatures) that amplify warming (Wang et al., 2020).

The high explanatory power (R^2 greater than 0.80) suggests that SSR is the dominant control on temperature at monthly time scales in this tropical region, with other factors (wind, humidity, cloud radiative effects) playing secondary roles totaling approximately 16-18% of variance. This finding aligns with energy balance studies in similar tropical environments showing SSR controls 75-90% of surface temperature variability during dry seasons (Wild, 2016). The similar R^2 values across sites (0.82 vs 0.84) again confirm spatial uniformity in fundamental energy balance processes.

4.6.3 Aerosol-Temperature Relationship

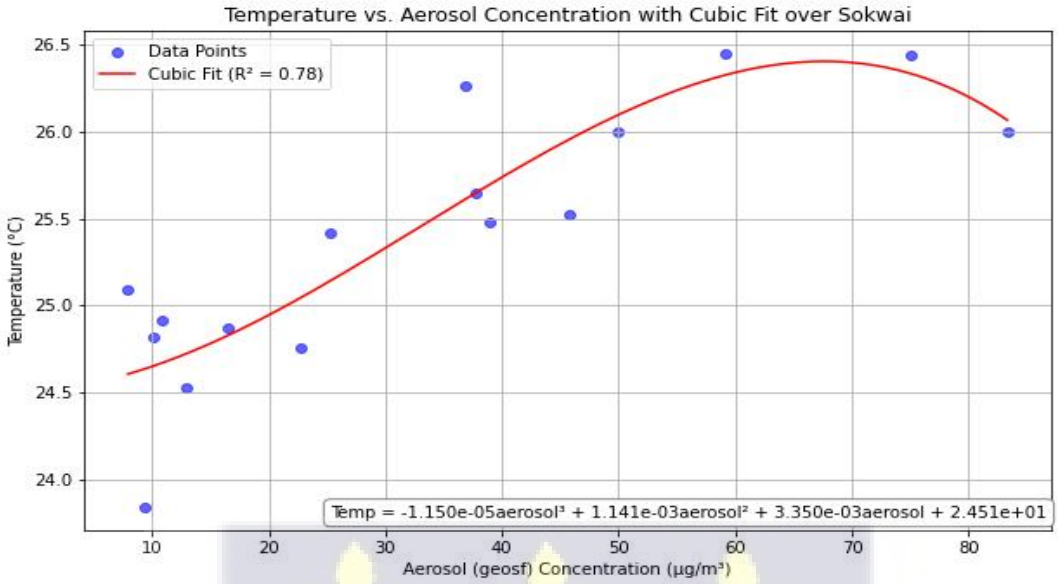

Figure 4.*33*: The correlation between aerosol concentration and temperature, Fumesua, Sokwai.

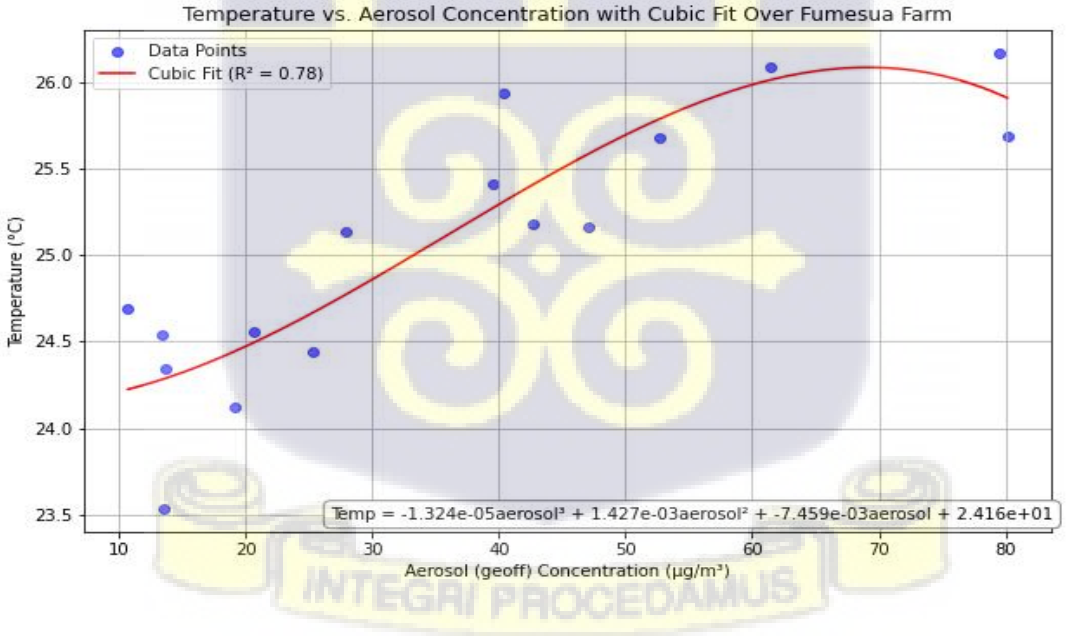

Figure 4.34: The correlation between aerosol concentration and temperature, Fumesua.

The graph in Figure 4.33-4.34 provides a detailed analysis of the relationship between aerosol concentration and temperature. The graphs show a cubic fit equation:

Equation 4.3: aerosol concentration against temperature regression equation, Sokwai

$$\text{Temp} = -1.324e-05(\text{aerosol}^3) + 1.427e-03(\text{aerosol}^2) - 7.459e-03(\text{aerosol}) + 2.416e+01$$

Where Temp represents Temperature (°C) and aerosol represents aerosol concentration ($\mu g/m^3$)

Third-degree polynomial regression of temperature on aerosol concentration (Figures 4.33-4.34) yielded moderate fits: R^2= 0.78 for both Sokwai and Fumesua. The cubic form captures the non-monotonic relationship observed in Section 4.4: temperature rises with aerosols from September through mid-November, peaks at intermediate concentrations (approximately 50-60 $\mu g/m^3$), then declines slightly at highest December loadings (greater than 80 micrograms per cubic meter). The negative linear term represents initial cooling through SSR attenuation, the positive quadratic term reflects atmospheric absorption warming at moderate loadings, and the negative cubic term indicates eventual dominance of cooling mechanisms (enhanced albedo, semi-direct effects) at extreme concentrations (Koch & Del Genio, 2010).

The moderate R^2 (0.78) is lower than the SSR-temperature relationship (R^2 approximately 0.83), indicating that aerosol effects on temperature are partially mediated through SSR changes but also involve direct atmospheric processes. The unexplained variance (approximately 22%) likely reflects: seasonal meteorological confounding (temperature would increase from September to December even without aerosol changes due to ITCZ migration), unmeasured factors like humidity and cloud cover that modulate temperature independently of aerosols, and complex non-linear feedbacks not captured by cubic polynomials (Ramanathan et al., 2001; Tost, 2017).

Other urban studies results, such as those of Zhao et al. (2017) in China, are in line with the reported R^2 value of 0.73.

Several regional studies, such as the one conducted by Baró et al. (2017), have documented the dual-effect link between aerosols and temperature.

The results of this research support the notion of the urban heat island effect and the role aerosols play in controlling local temperatures. Seasonal and diurnal patterns may influence the observed relationships between aerosol and temperature (Tost, 2017; Hu et al., 2021).

Long-term patterns might not be reflected in the graph's short-term associations. The non-linear relationship emphasizes the complex relationship between temperature and aerosols in urban areas. (Tost, 2017; Ramanathan et al., 2001; Shimadera et al., 2009).

Aerosols have a considerable and predictable impact on local temperature, as indicated by the overall analysis, which reveals a strong correlation between temperature and aerosol concentration (R^2 = 0.73). Additionally, a complex interplay exists between these variables (aerosol concentration, SSR, and temperature), where aerosols appear to influence both temperature and SSR, with temperature exhibiting saturation effects with both aerosols and SSR, as suggested by Ackerman et al. (2000) and Koren et al. (2004). The relationships are mostly nonlinear.

4.6.4 Summary of Regression Results

R^2 values range from 0.59 (aerosol-SSR) to 0.84 (SSR-temperature), indicating variable explanatory power. SSR is the strongest temperature predictor, aerosol-temperature relationships are intermediate, and aerosol-SSR relationships are weakest.

All relationships require non-linear (polynomial) models, indicating threshold effects and competing mechanisms rather than simple linear causality.

Spatial consistency is high: R^2values differ by less than 0.02 between Sokwai and Fumesua for all three relationships, confirming uniform aerosol-climate physics across the study area.

Unexplained variance ($16 - 41\%$ depending on relationship) highlights the multivariate nature of climate processes. Single-variable regressions capture major trends but cannot account for synergistic effects of multiple factors (clouds, humidity, wind) operating simultaneously.

The moderate aerosol-SSR correlation (R^2 = 0.59-0.60) is consistent with other satellite-based studies in West Africa (Levy et al., 2013), where spatial averaging and retrieval uncertainties limit correlation strengths.

4.6.5 Limitations of Regression Analyses

Several limitations affect the regression results and their interpretation. First, all regressions treat variables as independent when they are actually coupled: aerosols affect SSR, SSR affects temperature, and temperature influences aerosol transport and lifetime through circulation changes. This circular causality violates regression assumptions and may inflate or deflate correlation strengths unpredictably. Structural equation modeling or path analysis would be needed to properly account for coupled feedbacks (Bring, 1994).

Second, the 4-month study period conflates aerosol effects with seasonal trends. The September-December progression involves simultaneous changes in multiple factors: aerosols increase, sun angle changes, cloud cover decreases, and atmospheric circulation shifts from maritime to continental regimes. Attributing temperature or SSR changes specifically to aerosols versus these other seasonal factors is problematic with observational data alone; controlled model experiments would be needed for definitive attribution (Takemura et al., 2005).

Third, satellite data uncertainties (approximately 30-50% for aerosols, approximately 10-15% for SSR) introduce substantial measurement error that attenuates correlation coefficients. True

physical relationships may be stronger than observed statistical correlations suggest. Ground-based measurements with higher precision (uncertainties less than 10%) would likely yield stronger correlations for the same physical processes (Hsu et al., 2013).

Fourth, spatial averaging over satellite grid cells (25-60 km) may mask sub-grid variability and non-linear relationships. If aerosol-SSR interactions vary spatially within grid cells (e.g., stronger effects near emission sources), grid-average relationships would appear weaker than true local relationships. This "aggregation bias" is a known issue in satellite-based climate studies (Levy et al., 2013).

Finally, the polynomial regression forms chosen (2nd and 3rd degree) impose specific functional shapes that may not accurately represent true physical relationships. Alternative approaches (splines, non-parametric regression) might reveal different patterns, though the moderate sample sizes (n = 4 months) limit statistical power for flexible model forms. The R^2 values should thus be interpreted as measures of explained variance within the chosen model structures, not as definitive quantifications of physical coupling strengths.

4.7 Unexpected Findings and Critical Analysis

This section addresses unexpected results, apparent contradictions, and methodological limitations that complicate straightforward interpretation of the aerosol-climate relationships.

4.7.1 The Paradoxical SSR Increase with Rising Aerosols

A striking paradox emerges in the monthly data (Figures 4.25-4.28): SSR increases from September (approximately 525,000 $W/m^2$to December (approximately 650,000 W/m^2) despite concurrent three-fold increases in aerosol concentrations. Standard aerosol-radiation theory predicts inverse relationships (higher aerosols should reduce SSR through scattering and

absorption), yet the opposite pattern appears at monthly scales. This apparent contradiction requires careful explanation.

The resolution lies in recognizing that seasonal astronomical and meteorological factors dominate over aerosol effects at monthly scales. Three mechanisms explain the paradoxical SSR increase:

Solar geometry: The solar declination shifts from approximately +2 degrees in September to -23 degrees in December, but Kumasi's latitude (6.7 °C North) means the sun remains relatively high (zenith angles 15-30 °C) year-round. More importantly, the decrease in solar znith angle from September to December actually increases potential SSR by approximately 5-8 percent (Wild, 2009), partially offsetting aerosol attenuation.

Cloud cover reduction: West Africa's wet-to-dry transition involves dramatic decreases in cloud cover (approximately 70 % in September to approximately 20 % in December), which dominates SSR changes. Clouds block approximately 50-70 percent of incoming radiation, while aerosols block only approximately 15-25% (Eck et al., 2010). The shift from cloudy-wet to clear-dry conditions thus increases SSR by approximately $150{,}000 - 200{,}000\ \mathrm{W}/m^2$, overwhelming the aerosol-induced reduction of approximately $50{,}000 - 100{,}000\ \mathrm{W}/m^2$ (Ramanathan et al., 2001).

Semi-direct effects: Absorbing aerosols (black carbon from biomass burning) heat the lower atmosphere, potentially reducing cloud formation through atmospheric stabilization (Ackerman et al., 2000; Koch & Del Genio, 2010). This "semi-direct effect" may paradoxically increase SSR by suppressing clouds even as aerosol direct effects decrease SSR through scattering. The net outcome depends on the balance between direct (cooling) and semi-direct (warming) effects, which varies with aerosol composition and vertical distribution (Hansen et al., 2005).

The paradox thus reflects the limitations of bivariate analysis: examining only aerosols and SSR ignores the confounding influence of clouds, which is the dominant SSR control in tropical regions

(Wang et al., 2012). Daily-scale data (Section 4.4.1) show clearer inverse aerosol-SSR relationships because clouds vary less from day to day within months, allowing aerosol effects to emerge more clearly. At monthly scales, the seasonal cloud transition overwhelms aerosol signals, necessitating multivariate approaches to isolate aerosol-specific impacts.

4.7.2 Site-Specific Anomalies and Spatial Uniformity

The ANOVA results (Section 4.3) indicate no statistically significant spatial differences across study sites, yet visual inspection of daily and weekly data reveals consistent patterns: Sokwai locations (SC and SF) exhibit $5 - 10\ \mu g/m^3$ higher aerosol concentrations during peak periods compared to Fumesua sites (FC and FF). This apparent discrepancy, observing spatial patterns not confirmed statistically, warrants examination.

Three interpretations merit consideration. First, the observed $5 - 10\ \mu g/m^3$difference represents only approximately $10 - 15\%$ of typical concentrations, which falls within satellite retrieval uncertainty ranges (approximately $30 - 50$ % for aerosols). The difference may be genuine but undetectable above measurement noise. Second, the $15 - 20\ km$ spatial separation between sites is comparable to satellite grid cell dimensions ($25 - 60\ km$ for MERRA-2 and GEOS-CF), potentially limiting the ability to resolve fine-scale gradients (Levy et al., 2013). Ground-based measurements at higher spatial resolution might reveal sharper urban-rural contrasts not captured by satellite data.

Third, the apparent Sokwai elevation may reflect land use differences rather than true aerosol concentration gradients. Sokwai's more rural character involves greater unpaved surfaces, agricultural activities, and biomass burning, sources that could generate locally elevated concentrations. However, the strong temporal coherence across all sites (correlation r greater than 0.85) suggests regional-scale processes (Harmattan dust transport) dominate over local sources.

The subtle Sokwai elevation may represent minor local contributions superimposed on a strong regional background, analogous to "urban excess" aerosol patterns documented in other African cities (Arku et al., 2008; Dionisio et al., 2010).

The spatial uniformity finding has pragmatic value: it validates treating all four sites as collectively representative of Kumasi aerosol conditions. However, it also highlights limitations of the study design. The anticipated urban-rural gradient proved too subtle to detect with satellite data, suggesting future studies should employ either wider spatial coverage (e.g., $50 - 100\ km$ transects) or ground-based monitoring with higher spatial resolution to characterize local source influences more definitively (Hsu et al., 2013).

4.7.3 Interpreting Moderate Correlation Strengths

The regression analyses (Section 4.6) yielded R^2 values ranging from 0.59 (aerosol-SSR) to 0.84 (SSR-temperature), leaving $16 - 4\%$ of variance unexplained. In physical sciences, R^2 values less than 0.90 are sometimes viewed as indicating weak relationships, yet in atmospheric sciences, where multiple factors interact non-linearly, even moderate R^2 values can reflect strong physical coupling obscured by system complexity and measurement uncertainty (Nakagawa & Cuthill, 2007).

The observed R^2 values align with typical ranges for satellite-based aerosol-climate studies. A meta-analysis by Levy et al. (2013) found aerosol-SSR correlations of R^2 = 0.40-0.70 across diverse global regions, with lower values in tropical areas where cloud variability adds noise. Our R^2 = 0.59-0.60 for aerosol-SSR thus represents moderate-to-good performance given data limitations. Similarly, SSR-temperature correlations of R^2 = 0.70-0.90 are typical for monthly time scales in tropical regions (Wild, 2016), making our R^2 = 0.82-0.84 consistent with established patterns.

The unexplained variance reflects multiple factors not measured or controlled in this observational study:

Cloud cover: Not quantified in this study, yet clouds exert the largest influence on SSR (approximately $50-70\%$ attenuation) and modulate temperature through longwave radiation. Cloud variability alone likely accounts for $20-30\%$ of unexplained SSR variance (Wang et al., 2012).

Water vapor and humidity: Affect both SSR (through absorption) and temperature (through latent heat fluxes and greenhouse warming). Humid air masses can reduce SSR by $10-15\%$ independently of aerosols or clouds (Wild, 2009).

Wind patterns: Control aerosol transport, dispersion, and residence times, as well as surface heat exchange. Shifts between maritime and continental air masses during the wet-dry transition introduce temperature and SSR variations not captured by aerosol loading alone (Nicholson, 2013).

Surface properties: Changes in vegetation greenness, soil moisture, and albedo during the dry season affect energy partitioning independently of atmospheric aerosol and radiation changes (Oke, 1987).

Measurement uncertainties: Satellite retrieval errors (approximately $30-50\%$ for aerosols, approximately $10-15\%$ for SSR) attenuate correlation coefficients through random noise. If measurement uncertainties could be eliminated, true physical correlations would likely be 10-20%t stronger than observed (Hsu et al., 2013).

The moderate R^2 values thus reflect the multivariate nature of atmospheric processes rather than weak physical coupling. The regressions successfully identify aerosol effects within a complex system but cannot capture all relevant processes with single-variable models. More sophisticated

approaches, multivariate regression, machine learning, or process-based modeling, would be needed to account for simultaneous influences of multiple factors and their interactions (Streets et al., 2009).

4.7.4 Broader Implications

The study findings have several broader implications for understanding aerosol-climate interactions in West African urban environments:

1. Regional vs. Local Controls: The spatial uniformity and strong temporal coherence indicate that regional-scale meteorological processes (Harmattan transport, ITCZ migration) dominate urban aerosol variability. Local emission sources contribute subtle spatial gradients but do not fundamentally alter seasonal patterns. This suggests regional air quality management strategies must address transboundary dust transport alongside local emissions.

2. Solar Energy Implications: The approximately $15-25\%$ SSR reductions during peak aerosol loading (December) represent significant impacts on solar energy potential. Photovoltaic system design and performance modeling in Kumasi should account for seasonal aerosol attenuation, particularly during the historically energy-intensive dry season when Harmattan conditions prevail.

3. Data Limitations and Future Needs: The moderate correlation strengths (R^2= 0.59-0.84) and substantial unexplained variance highlight the need for comprehensive ground-based monitoring. Establishing surface networks measuring aerosol properties, radiation, and meteorological variables would enable more definitive mechanistic understanding and validation of satellite retrievals (currently uncertain to approximately $30-50\%$).

4. Methodological Lessons: The paradoxical monthly-scale results demonstrate the importance of temporal scale selection in aerosol-climate studies. Daily data reveal clearer direct effects by

minimizing seasonal confounding, while monthly aggregation conflates aerosol impacts with meteorological transitions. Future studies should employ hierarchical temporal analyses to separate scales of variability.

5. Climate Change Context: The documented seasonal aerosol patterns provide a baseline against which future changes can be assessed. Climate projections suggest potential shifts in West African monsoon dynamics and Saharan dust transport, which would alter Kumasi aerosol loading patterns. The present findings enable detection of such changes through comparison with future observations.

CHAPTER FIVE

5.0 CONCLUSION

5.1 Introduction

This chapter synthesises the key findings of the study in relation to the three research objectives, outlines the limitations encountered, presents policy and research recommendations, and highlights the broader implications of the findings for air quality management and climate resilience in Ghana.

5.2 Summary of Key Findings

The study examined aerosol loading and its effects on surface temperature and solar radiation across selected locations in Kumasi using MERRA-2, GEOS-CF and ERA5 satellite datasets spanning September to December 2022. The findings demonstrated notable temporal variations in aerosol concentrations, with values increasing from $5 - 25\ \mu g/m^3$ during September to peaks of $80 - 125\ \mu g/m^3$ in December, reflecting the transition from the wet season to the Harmattan period. A distinct shift was observed in mid-October, corresponding with the onset of Harmattan and heightened biomass burning. Polynomial regression analysis produced strong predictive capabilities ($R^2 = 0.73 - 0.74$ for GEOS-CF and $R^2 = 0.63 - 0.66$ for MERRA-2).

Spatial differences in aerosol concentrations across the four locations were minimal and statistically insignificant ($F = 0.7027$; $p > 0.05$), indicating that regional atmospheric processes, particularly Saharan dust transport, exert a stronger influence on aerosol loading than local emission sources. Analysis of aerosol-climate interactions revealed an inverse relationship between aerosols and surface solar radiation ($R^2 = 0.59 - 0.60$), and a non-linear temperature

response characterised initially by warming at moderate aerosol levels, followed by cooling above 80 μg/m³ due to increased albedo and cloud formation ($R^2 = 0.78$). The relationship between solar radiation and temperature remained consistently strong ($R^2 = 0.82 - 0.84$).

This research provides the first location-specific aerosol dataset for Kumasi and establishes that regional-scale Saharan dust transport dominates aerosol loading during Harmattan. Consequently, effective mitigation requires coordinated regional policies rather than interventions limited to local emission control.

5.3 Study Limitations

The study is constrained by its four-month duration, representing only one annual cycle with potential inter-annual variability. Satellite retrieval uncertainties ($\pm 30 - 50\%$) and coarse spatial resolution may obscure finer-scale emissions. Additional limitations include the absence of ground-based validation, limited aerosol characterisation without compositional data, and the omission of key meteorological variables such as cloud cover, relative humidity, and wind.

5.4 Recommendations

5.4.1 Policy Recommendations

- Establish a national ground-based aerosol monitoring network through EPA Ghana and GMet, including PM sensors and AERONET stations, with real-time AQI communication.

- Implement seasonal Harmattan interventions led by NADMO and the Ministry of Health, including public advisories, restrictions on biomass burning, dust control measures at construction sites, and provision of respiratory protection for vulnerable groups.

- Integrate aerosols into national climate adaptation strategies and NDCs, and develop agricultural advisories to address seasonal dust impacts.

- Strengthen enforcement of biomass-burning regulations through the Forestry Commission and Energy Commission, while promoting clean energy alternatives such as LPG and improved cookstoves.

5.4.2 Research Recommendations

- Extend the monitoring period to 3–5 years to capture wet and dry season cycles and inter-annual variability.

- Expand spatial coverage across diverse climatic and land-use zones in Ghana including urban, industrial, agricultural, coastal and remote areas.

- Integrate satellite-based datasets with ground-based measurements for validation and calibration.

- Conduct public health studies assessing respiratory and cardiovascular outcomes, personal exposure, and cost-benefit analyses of mitigation measures.

5.5 Concluding Statement

This study has provided the first comprehensive, site-specific characterization of aerosol-climate interactions in Kumasi, Ghana, filling a critical knowledge gap in the Sub-Saharan African context where systematic aerosol monitoring remains severely limited. The findings demonstrate that aerosol concentrations in the region undergo dramatic seasonal variations, increasing three-fold from the wet to dry season and reaching levels that substantially exceed World Health Organization air quality guidelines during the Harmattan period. These elevated aerosol levels, driven primarily by regional Saharan dust transport and local biomass burning, exert significant

and complex influences on surface solar radiation and temperature through competing direct and indirect radiative mechanisms.

The observed spatial uniformity across urban and rural sites underscores the dominance of regional-scale atmospheric processes over local emission sources in determining aerosol concentrations, with important implications for air quality management strategies. Rather than focusing solely on local emission controls, effective mitigation must address the broader regional drivers, including transboundary dust transport and widespread biomass burning practices. The complex, non-linear aerosol-temperature relationship identified in this study—characterized by an initial warming phase followed by cooling at high aerosol concentrations—highlights the need for sophisticated modeling approaches and long-term monitoring to fully understand and predict aerosol impacts on local and regional climate.

In the broader context of climate change and sustainable development in Sub-Saharan Africa, this research provides essential baseline data and methodological frameworks that can inform both national air quality management policies and regional climate adaptation strategies. The findings are particularly timely given Ghana's commitments under the Paris Agreement and the Sustainable Development Goals, specifically SDG 3 (Good Health and Well-being), SDG 11 (Sustainable Cities and Communities), and SDG 13 (Climate Action). The establishment of continuous aerosol monitoring networks, implementation of seasonal air quality interventions, and integration of aerosol considerations into climate policy frameworks represent critical next steps toward protecting public health and building climate resilience in Ghana and the wider West African region.

Ultimately, this study demonstrates that aerosols represent a crucial but often overlooked component of the West African climate system and air quality landscape. As the region continues to experience rapid urbanization, agricultural intensification, and climate change, understanding and managing aerosol impacts will become increasingly important for ensuring environmental sustainability, protecting public health, and achieving equitable development. The methodologies and findings presented here provide a foundation upon which future research, policy development, and practical interventions can be built, contributing to the growing body of African-generated scientific evidence needed to address the continent's unique environmental challenges.

REFERENCES

Ackerman, A. S., Toon, O. B., Stevens, D. E., Heymsfield, A. J., Ramanathan, V., & Welton, E. J. (2000). Reduction of tropical cloudiness by soot. Science, 288(5468), 1042-1047. https://doi.org/10.1126/science.288.5468.1042

Adebiyi, A., Kok, J. F., Murray, B. J., Ryder, C. L., Stuut, J. W., Kahn, R. A., Knippertz, P., Formenti, P., Mahowald, N. M., García-Pando, C. P., Klose, M., Ansmann, A., Samset, B. H., Ito, A., Balkanski, Y., Di Biagio, C., Romanias, M. N., Huang, Y., & Meng, J. (2022). A review of coarse mineral dust in the Earth system. Aeolian Research, 60, 100849. https://doi.org/10.1016/j.aeolia.2022.100849

Aerosols and their relation to global climate and climate sensitivity. (n.d.). Nature Education Knowledge, 4, 7, 2013.

Afeti, G., & Resch, F. (2000). Physical characteristics of Saharan dust near the Gulf of Guinea. Atmospheric Environment, 34(8), 1273--1279.

Ahrens, C. D. (2009). Meteorology today: An Introduction to Weather, Climate, and the Environment. Cengage Learning.

Al-Timimi, Y. K., & Khraibet, A. C. (2017). Impact of aerosol on air temperature in Baghdad. Journal of Applied and Advanced Research, 317-323.

Albrecht, B. A. (1989). Aerosols, cloud microphysics, and fractional cloudiness. Science, 245(4923), 1227--1230. https://doi.org/10.1126/science.245.4923.1227

Almeida, S., Manousakas, M., Diapouli, E., Kertesz, Z., Samek, L., Hristova, E., Šega, K., Alvarez, R. P., Belis, C., & Eleftheriadis, K. (2020). Ambient particulate matter source apportionment using receptor modelling in European and Central Asia urban areas. Environmental Pollution, 266, 115199. https://doi.org/10.1016/j.envpol.2020.115199

Alpert, P., & Kishcha, P. (2008). Quantification of the effect of urbanization on solar dimming. Geophysical Research Letters, 35(8). https://doi.org/10.1029/2007gl033012

Andre, M., Sartelet, K., Moukhtar, S., Andre, J., & Redaelli, M. (2020). Diesel, petrol, or electric vehicles: What choices to improve urban air quality in the Ile-de-France region? A simulation platform and case study. Atmospheric Environment, 241, 117752. https://doi.org/10.1016/j. atmosenv.2020.117752

Andreae, M. O., & Crutzen, P. J. (1997). Atmospheric aerosols: Biogeochemical sources and role in atmospheric chemistry. Science, 276(5315), 1052-1058.

Andreae, M. O., Jones, C. D., & Cox, P. M. (2005). Strong present-day aerosol cooling implies a hot future. Nature, 435(7046), 1187-1190. https://doi.org/10.1038/nature03671

Arku, F. S. (2013). The modelled solar radiation pattern of Ghana: Its prospects for alternative energy source. Journal of African Studies, 3(3), 45-64.

Arku, R. E., Vallarino, J., Dionisio, K. L., Willis, R., Choi, H., Wilson, J. G., Hemphill, C., Agyei-Mensah, S., Spengler, J. D., & Ezzati, M. (2008). Characterizing air pollution in two low-income neighborhoods in Accra, Ghana. The Science of the Total Environment, 402(2-3), 217--231. https://doi.org/10.1016/j.scitotenv.2008.04.042

Atmospheric chemistry and physics: from air pollution to climate change. (1998). Choice Reviews Online, 35(10), 35--5721. https://doi.org/10.5860/choice.35–5721

BMKG. (2022). Kapan awal musim hujan 2022? Ini prakiraan lengkap BMKG. (n.d.). BMKG. (2022). Kapan Awal Musim Hujan 2022? Ini Prakiraan Lengkap BMKG.

Balarabe, M., Abdullah, K., & Nawawi, M. (2015). Long-Term trend and seasonal variability of horizontal visibility in Nigerian troposphere. Atmosphere, 6(10), 1462-1486. https://doi.org/10.3390/atmos6101462

Balarabe, M., Abdullah, K., & Nawawi, M. (2016). Seasonal Variations of Aerosol Optical Properties and Identification of Different Aerosol Types Based on AERONET Data over Sub-Sahara West-Africa. Atmospheric and Climate Sciences, 06(01), 13-28. https://doi.org/10.4236/acs. 2016.61002

Barbosa, P. M., Stroppiana, D., Grégoire, J., & Pereira, J. M. C. (1999). An assessment of vegetation fire in Africa (1981-1991): Burned areas, burned biomass, and atmospheric emissions. Global Biogeochemical Cycles, 13(4), 933-950. https://doi.org/10.1029/1999gb900042

Bardouki, H., Liakakou, H., Economou, C., Sciare, J., Smolík, J., Ždímal, V., Eleftheriadis, K., Lazaridis, M., Dye, C., & Mihalopoulos, N. (2003). Chemical composition of size-resolved atmospheric aerosols in the eastern Mediterranean during summer and winter. Atmospheric Environment, 37(2), 195-208. https://doi.org/10.1016/s1352-2310(02)00859–2

Baró, R., Palacios-Peña, L., Baklanov, A., Balzarini, A., Brunner, D., Forkel, R., Hirtl, M., Honzak, L., Pérez, J. L., Pirovano, G., José, R. S., Schröder, W., Werhahn, J., Wolke, R., Žabkar, R., & Jiménez-Guerrero, P. (2017). Regional effects of atmospheric aerosols on temperature: an evaluation of an ensemble of online coupled models. Atmospheric Chemistry and Physics, 17(15), 9677-9696. https://doi.org/10.5194/acp-17–9677-2017

Bates T.S. (1999). Preface to Special Section: First Aerosol Characterisation Experiment (ACE-1) part-2. Journal of Geophysical Research: Atmospheres, 104(D17), 21645-21647.

Bates, T. S., Quinn, P. K., Covert, D. S., Coffman, D. J., Johnson, J. E., & Wiedensohler, A. (2000). Aerosol physical properties and processes in the lower marine boundary layer: a comparison of shipboard sub-micron data from ACE-1 and ACE-2. Tellus B, 52(2), 258. https://doi.org/10.3402/tellusb.v52i2.16104

Bauer, S. E., Im, U., Mezuman, K., & Gao, C. Y. (2019). Desert dust, Industrialization, and Agricultural fires: Health impacts of Outdoor air pollution in Africa. Journal of Geophysical Research Atmospheres, 124(7), 4104-4120. https://doi.org/10.1029/2018jd029336

Bellouin, N., Quaas, J., Gryspeerdt, E., Kinne, S., Stier, P., Watson-Parris, D., Bouche, O., Carslaw, K. S., Christensen, M., Daniau, A.-L., Dufresne, J.-L., Feingold, G., Fiedler, S., Forster, P., Gettelman, A., Haywood, J. M., Lohmann, U., Malavelle, F., Mauritsen, T., . . . Stevens, B. (2019). Bounding global aerosol radiative forcing of climate change. Reviews of Geophysics, 58(1). https://doi.org/10.1029/2019RG000660

Bertrand, J. (1976). Visibilite et brume se \` che en Afrique. La Meteorologie 6,. La Meteorologie 6, 201-211.

Bond, T. C., Streets, D. G., Yarber, K. F., Nelson, S. M., Woo, J., & Klimont, Z. (2004). A technology-based global inventory of black and organic carbon emissions from combustion. Journal of Geophysical Research Atmospheres, 109(D14). https://doi.org/10.1029/2003jd003697

Bortey-Sam, N., Ikenaka, Y., Akoto, O., Nakayama, S. M. M., Yohannes, Y. B., Baidoo, E., Mizukawa, H., & Ishizuka, M. (2015). Levels, potential sources and human health risk of polycyclic aromatic hydrocarbons (PAHs) in particulate matter (PM10) in Kumasi, Ghana. Environmental Science and Pollution Research, 22(13), 9658-9667. https://doi.org/10.1007/s11356-014-4022-1

Boucher, O. (2015). Atmospheric aerosols: Properties and Climate Impacts. Springer.

Boulon, J., Sellegri, K., Hervo, M., & Laj, P. (2011). Observations of nucleation of new particles in a volcanic plume. Proceedings of the National Academy of Sciences of the United States of America, 108(30), 12223--12226. https://doi.org/10.1073/pnas.1104923108

Bowman, D. M. J. S., Balch, J., Artaxo, P., Bond, W. J., Cochrane, M. A., D'Antonio, C. M., DeFries, R., Johnston, F. H., Keeley, J. E., Krawchuk, M. A., Kull, C. A., Mack, M., Moritz, M. A., Pyne, S., Roos, C. I., Scott, A. C., Sodhi, N. S., & Swetnam, T. W. (2011). The human dimension of fire regimes on Earth. Journal of Biogeography, 38(12), 2223-2236. https://doi.org/10.1111/j.1365-2699.2011.02595.x

Buchard, V., Randles, C. A., Da Silva, A. M., Darmenov, A., Colarco, P. R., Govindaraju, R., Ferrare, R., Hair, J., Beyersdorf, A. J., Ziemba, L. D., & Yu, H. (2017). The MERRA-2 Aerosol Reanalysis, 1980 onward. Part II: Evaluation and case studies. Journal of Climate, 30(17), 6851-6872. https://doi.org/10.1175/jcli-d-16-0613.1

Buchwitz, M., Reuter, M., Schneising, O., Bovensmann, H., Burrows, J. P., Boesch, H., Anand, J., Parker, R., Detmers, R. G., Aben, I., Hasekamp, O. P., Crevoisier, C., Armante, R., Zehner, C., & Schepers, D. (2018). Copernicus Climate Change Service (C3S) global satellite observations of atmospheric carbon dioxide and methane. Advances in Astronautics Science and Technology, 1(1), 57-60. https://doi.org/10.1007/s42423–018-0004-6

Carlson, T. N., & Prospero, J. M. (1972). The Large-Scale Movement of Saharan Air Outbreaks over the Northern Equatorial Atlantic. Journal of Applied Meteorology, 11(2), 283-297. https://doi.org/10.1175/1520–0450(1972)011

Carslaw, K. S. (2022a). Introduction. In Elsevier eBooks (pp. 1-8). https://doi.org/10.1016/b978–0-12–819766-0.00013-4

Carslaw, K. S. (2022b). Introduction. In Elsevier eBooks (pp. 1-8). https://doi.org/10.1016/b978–0-12–819766-0.00013-4

Charlson, R. J., Ackerman, A. S., Bender, F. A., Anderson, T. L., & Liu, Z. (2007). On the climate forcing consequences of the albedo continuum between cloudy and clear air. Tellus B, 59(4), 715. https://doi.org/10.1111/j.1600-0889.2007.00297.x

Charlson, R. J., Langner, J., Rodhe, H., Leovy, C. B., & Warren, S. G. (1991). Perturbation of the northern hemisphere radiative balance by backscattering from anthropogenic sulfate aerosols\. Tellus a Dynamic Meteorology and Oceanography, 43(4), 152-163.https://doi.org/10.1034/j. 1600–0870.1991.00013.x

Charlson, R. J., Schwartz, S. E., Hales, J. M., Cess, R. D., Coakley, J. A., Hansen, J. E., & Hofmann, D. J. (1992a). Climate forcing by anthropogenic aerosols. Science, 255(5043), 423-430. https://doi.org/10.1126/science.255.5043.423

Charlson, R. J., Schwartz, S. E., Hales, J. M., Cess, R. D., Coakley, J. A., Hansen, J. E., & Hofmann, D. J. (1992b). Climate forcing by anthropogenic aerosols. Science, 255(5043), 423-430. https://doi.org/10.1126/science.255.5043.423

Charlson, R. J., Schwartz, S. E., Hales, J. M., Cess, R. D., Coakley, J. A., Hansen, J. E., & Hofmann, D. J. (1992c). Climate forcing by anthropogenic aerosols. Science, 255(5043), 423-430. https://doi.org/10.1126/science.255.5043.423

Chen, J., Lu, J., Avise, J. C., DaMassa, J. A., Kleeman, M. J., & Kaduwela, A. P. (2014). Seasonal modeling of PM2.5 in California's San Joaquin Valley. Atmospheric Environment, 92, 182-190. https://doi.org/10.1016/j.atmosenv.2014.04.030

Chen, P., Bi, X., Zhang, J., Wu, J., & Feng, Y. (2014). Assessment of heavy metal pollution characteristics and human health risk of exposure to ambient PM2.5 in Tianjin, China. Particuology, 20, 104-109. https://doi.org/10.1016/j.partic.2014.04.020

Chin, M., Diehl, T., Dubovik, O., Eck, T. F., Holben, B. N., Sinyuk, A., & Streets, D. G. (2009). Light absorption by pollution, dust, and biomass burning aerosols: a global model study and evaluation with AERONET measurements. Annales Geophysicae, 27(9), 3439--3464. https://doi.org/10.5194/angeo-27-3439-2009.

Chin, M., Schwartz, S. E., & Kahn, R. A. (2009). Atmospheric aerosol properties and climate impacts. In U.S. Climate Change Science Program eBooks. https://digital.library.unt.edu/ark:/67531/metadc12022/m2/1/highresd/sap2–3-final-report-all.pdf

Chylek, P., & Wong, J. (1995). Effect of absorbing aerosols on global radiation budget. Geophysical Research Letters, 22(8), 929-931. https://doi.org/10.1029/95gl00800

Clarke, A. D. (1993). Atmospheric nuclei in the Pacific midtroposphere: Their nature, concentration, and evolution. Journal of Geophysical Research Atmospheres, 98(D11), 20633-20647. https://doi.org/10.1029/93jd00797

Clarke, A. D., Varner, J. L., Eisele, F., Mauldin, R. L., Tanner, D., & Litchy, M. (1998). Particle production in the remote marine atmosphere: Cloud outflow and subsidence during ACE 1. Journal of Geophysical Research, 103(D13), 16397-16409.

Climate change, 1994: radiative forcing of climate change and an evaluation of the IPCC IS92 emission scenarios. (1996). Choice/Choice Reviews, 33(07), 33-3969. https://doi.org/10.5860/choice. 33-3969

Coakley, J. A., & Cess, R. D. (1985). Response of the NCAR Community Climate Model to the radiative forcing by the naturally occurring tropospheric aerosol. Journal of the Atmospheric Sciences, 42(16), 1677-1692. https://doi.org/10.1175/1520–0469(1985)042

Coakley, J. A., Cess, R. D., & Yurevich, F. B. (1983). The effect of tropospheric aerosols on the Earth's radiation budget: A parameterization for climate models. Journal of the Atmospheric Sciences, 40(1), 116--138. https://doi.org/10.1175/1520-0469(1983)040

Cooke, W. F., Jennings, S. G., & Spain, T. G. (1997). Black carbon measurements at Mace Head, 1989-1996. Journal of Geophysical Research Atmospheres, 102(D21), 25339--25346. https://doi.org/10.1029/97jd01430

Council, N. R. (1996). A plan for a research program on aerosol radiative forcing and climate change. In National Academies Press eBooks. https://doi.org/10.17226/5107

Cox, R. E., Mazurek, M. A., & Simoneit, B. R. T. (1982). Lipids in Harmattan aerosols of Nigeria. Nature, 296(5860), 848-849. https://doi.org/10.1038/296848a0

Crutzen, P. J., & Andreae, M. O. (1990). Biomass burning in the Tropics: Impact on atmospheric chemistry and biogeochemical cycles. Science, 250(4988), 1669-1678. https://doi.org/10.1126/science.250.4988.1669

D'Almeida, G. A. (1986). A model for Saharan dust transport. Journal of Climate and Applied Meteorology, 25(7), 903--916. https://doi.org/10.1175/1520–0450(1986)025

Dey, S., Di Girolamo, L., Van Donkelaar, A., Tripathi, S., Gupta, T., & Mohan, M. (2012). Variability of outdoor fine particulate (PM2.5) concentration in the Indian Subcontinent: A remote sensing approach. Remote Sensing of Environment, 127, 153-161. https://doi.org/10.1016/j.rse. 2012. 08.021

Dionisio, K. L., Arku, R. E., Hughes, A. F., Vallarino, J., Carmichael, H., Spengler, J. D., Agyei-Mensah, S., & Ezzati, M. (2010). Air pollution in Accra neighborhoods: spatial, socioeconomic, and temporal patterns. Environmental Science & Technology, 44(7), 2270-2276. https://doi.org/10.1021/es903276s

Dionisio, K. L., Rooney, M. S., Arku, R. E., Friedman, A. B., Hughes, A. F., Vallarino, J., Agyei-Mensah, S., Spengler, J. D., & Ezzati, M. (2010). Within-Neighborhood Patterns and Sources of particle pollution: mobile monitoring and Geographic Information System analysis in four communities in Accra, Ghana. Environmental Health Perspectives, 118(5), 607-613. https://doi.org/10.1289/ehp.0901365

Engel-Cox, J. A., Holloman, C. H., Coutant, B. W., & Hoff, R. M. (2004). Qualitative and quantitative evaluation of MODIS satellite sensor data for regional and urban-scale air quality. Atmospheric Environment, 38(16), 2495-2509. https://doi.org/10.1016/j.atmosenv.2004.01.039

Engelstaedter, S., Tegen, I., & Washington, R. (2006). North African dust emissions and transport. Earth-Science Reviews, 79(1-2), 73-100.

Etyemezian, V., Kuhns, H., Gillies, J., Green, M., Pitchford, M., & Watson, J. (2003). Vehicle-based road dust emission measurement: I-methods and calibration. Atmospheric Environment, 37(32), 4559-4571. https://doi.org/10.1016/s1352-2310(03)00528-4

Feng, J., Li, Y., Qiu, Y., & Zhu, F. (2023). Capturing synoptic-scale variations in surface aerosol pollution using deep learning with meteorological data. Atmospheric Chemistry and Physics, 23(1), 375-388. https://doi.org/10.5194/acp-23-375-2023

Fosu-Amankwah, K., Bessardon, G. E., Quansah, E., Amekudzi, L. K., Brooks, B. J., & Damoah, R. (2021). Assessment of aerosol burden over Ghana. Scientific African, 14, e00971. https://doi.org/10.1016/j.sciaf.2021.e00971

Funk, R., Reuter, H. I., Hoffmann, C., Engel, W., & Öttl, D. (2008). Effect of moisture on fine dust emission from tillage operations on agricultural soils. Earth Surface Processes and Landforms, 33(12), 1851-1863. https://doi.org/10.1002/esp.1737

Gelaro, R., McCarty, W., Suárez, M. J., Todling, R., Molod, A., Takacs, L., Randles, C. A., Darmenov, A., Bosilovich, M. G., Reichle, R., Wargan, K., Coy, L., Cullather, R., Draper, C., Akella, S., Buchard, V., Conaty, A., Da Silva, A. M., Gu, W., . . . Zhao, B. (2017). The Modern-Era Retrospective Analysis for Research and Applications, Version 2 (MERRA-2). Journal of Climate, 30(14), 5419-5454. https://doi.org/10.1175/jcli-d-16–0758.1

Ghana - Weather and climate. (n.d.). https://safarideal.com/safari-destination/ghana/weather-and-climate/.

Gillett, N. P., Stone, D. A., Stott, P. A., Nozawa, T., Karpechko, A. Y., Hegerl, G. C., Wehner, M. F., & Jones, P. D. (2008). Attribution of polar warming to human influence. Nature Geoscience, 1(11), 750--754. https://doi.org/10.1038/ngeo338

Ginoux, P., Chin, M., Tegen, I., Prospero, J. M., Holben, B., Dubovik, O., & Lin, S. (2001). Sources and distributions of dust aerosols simulated with the GOCART model. Journal of Geophysical Research, 106(D17), 20255-20273. https://doi.org/10.1029/2000jd000053

Ginoux, P., Prospero, J., Torres, O., & Chin, M. (2004). Long-term simulation of global dust distribution with the GOCART model: correlation with North Atlantic Oscillation. Environmental Modelling & Software, 19(2), 113-128. https://doi.org/10.1016/s1364-8152(03)00114-2

Giorgi, F., Bi, X., & Qian, Y. (2002). Direct radiative forcing and regional climatic effects of anthropogenic aerosols over East Asia: A regional coupled climate-chemistry/aerosol model study. Journal of Geophysical Research Atmospheres, 107(D20). https://doi.org/10.1029/2001 jd001066

Giorgi, F., Bi, X., & Qian, Y. (2003). Indirect vs. direct effects of anthropogenic sulfate on the climate of East Asia as simulated with a regional coupled climate-chemistry/aerosol model. Climatic Change, 58(3), 345-376. https://doi.org/10.1023/a:1023946010350

Gong, D., Ho, C., Chen, D., Qian, Y., Choi, Y., & Kim, J. (2007). Weekly cycle of aerosol-meteorology interaction over China. Journal of Geophysical Research Atmospheres, 112(D22). https://doi.org/10.1029/2007jd008888

Graham, R. M., Hudson, S. R., & Maturilli, M. (2019). Improved performance of ERA5 in Arctic Gateway relative to four global atmospheric reanalyses. Geophysical Research Letters, 46(11), 6138-6147. https://doi.org/10.1029/2019gl082781

Han, W., Li, Z., Wu, F., Zhang, Y., Guo, J., Su, T., Cribb, M., Fan, J., Chen, T., Wei, J., & Lee, S. (2020). The mechanisms and seasonal differences of the impact of aerosols on daytime surface urban heat island effect. Atmospheric Chemistry and Physics, 20(11), 6479-6493. https://doi.org/10.5194/acp-20-6479-2020

Hansen, J. E., Sato, M., Lacis, A., Ruedy, R., Tegen, I., & Matthews, E. (1998). Climate forcings in the Industrial era. Proceedings of the National Academy of Sciences of the United States of America, 95(22), 12753-12758. https://doi.org/10.1073/pnas.95.22.12753

Hansen, J., & Nazarenko, L. (2003). Soot climate forcing via snow and ice albedos. Proceedings of the National Academy of Sciences of the United States of America, 101(2), 423-428. https://doi.org/10.1073/pnas.2237157100

Hansen, J., Sato, M., & Ruedy, R. (1997). Radiative forcing and climate response. Journal of Geophysical Research, 102(D6), 6831-6864. https://doi.org/10.1029/96jd03436

Hansen, J., Sato, M., Ruedy, R., Lacis, A., & Oinas, V. (2000). Global warming in the twenty-first century: An alternative scenario. Proceedings of the National Academy of Sciences, 97(18), 9875--9880. https://doi.org/10.1073/pnas.170278997

Hansen, J., Sato, M., Ruedy, R., Nazarenko, L., Lacis, A., Schmidt, G. A., Russell, G., Aleinov, I., Bauer, M., Bauer, S., Bell, N., Cairns, B., Canuto, V., Chandler, M., Cheng, Y., Del Genio, A., Faluvegi,

G., Fleming, E., Friend, A., . . . Zhang, S. (2005a). Efficacy of climate forcings. Journal of Geophysical Research Atmospheres, 110(D18). https://doi.org/10.1029/2005j d005776

Hansen, J., Sato, M., Ruedy, R., Nazarenko, L., Lacis, A., Schmidt, G. A., Russell, G., Aleinov, I., Bauer, M., Bauer, S., Bell, N., Cairns, B., Canuto, V., Chandler, M., Cheng, Y., Del Genio, A., Faluvegi, G., Fleming, E., Friend, A., . . . Zhang, S. (2005b). Efficacy of climate forcings. Journal of Geophysical Research Atmospheres, 110(D18). https://doi.org/10.1029/2005jd005 776

Hao, W. M., & Liu, M. (1994). Spatial and temporal distribution of tropical biomass burning. Global Biogeochemical Cycles, 8(4), 495-503. https://doi.org/10.1029/94gb02086

Harte, J. (1989). Consider a spherical cow: a course in environmental problem solving. Choice Reviews Online, 26(09), 26-5054. https://doi.org/10.5860/choice.26-5054

Haywood, J. M., & Ramaswamy, V. (1998). Global sensitivity studies of the direct radiative forcing due to anthropogenic sulfate and black carbon aerosols. Journal of Geophysical Research Atmospheres, 103(D6), 6043-6058. https://doi.org/10.1029/97jd03426

Haywood, J., & Boucher, O. (2000). Estimates of the direct and indirect radiative forcing due to tropospheric aerosol: a review. Rev Geophys 38, 513-543.

Haywood, J., Francis, P., Osborne, S., Glew, M., Loeb, N., Highwood, E., Tanré, D., Myhre, G., Formenti, P., & Hirst, E. (2003). Radiative properties and direct radiative effect of Saharan dust measured by the C-130 aircraft during SHADE: 1. Solar spectrum. Journal of Geophysical Research Atmospheres, 108(D18). https://doi.org/10.1029/2002jd002687

Heintzenberg, J. (1989). Fine particles in the global troposphere A review. Tellus. Series B, Chemical and Physical Meteorology, 41B(2), 149-160. https://doi.org/10.1111/j.1600-0889.1989.tb0013 2.x

Hersbach, H., Bell, B., Berrisford, P., Hirahara, S., Horányi, A., Muñoz-Sabater, J., Nicolas, J., Peubey, C., Radu, R., Schepers, D., Simmons, A., Soci, C., Abdalla, S., Abellan, X., Balsamo, G., Bechtold, P., Biavati, G., Bidlot, J., Bonavita, M., . . . Thépaut, J. (2020). The ERA5 global reanalysis. Quarterly Journal of the Royal Meteorological Society, 146(730), 1999-2049. https://doi.org/10.1002/qj.3803

Hinds, W. C. (1999). Aerosol technology : properties, behavior, and measurement of airborne particles. https://lib.ugent.be/en/catalog/rug01:000658373

Hodzic, A., Jimenez, J. L., Madronich, S., Canagaratna, M. R., DeCarlo, P. F., Kleinman, L. I., & Fast, J. D. (2010). Modeling organic aerosols in a megacity: potential contribution of semi-volatile and intermediate volatility primary organic compounds to secondary organic aerosol formation. Atmospheric Chemistry and Physics, 10(12), 5491-5514. https://doi.org/10.5194/ acp-10-5491-2010

Hofmann, D. J. (1987). Perturbations to the global atmosphere associated with the El Chichon volcanic eruption of 1982. Reviews of Geophysics, 25(4), 743-759. https://doi.org/10.1029/rg025i004p00743

Hopke, P. K., Dai, Q., Li, L., & Feng, Y. (2020). Global review of recent source apportionments for airborne particulate matter. The Science of the Total Environment, 740, 140091. https://doi.org/10.1016/j.scitotenv.2020.140091

Houghton, J. T., Ding, Y., Griggs, D. J., Noguer, M., Van Der Linden, P., & Xiaosu, D. (2001). Climate change 2001: the scientific basis. Contribution of Working Group I to the Third Assessment Report of the Intergovernmental Panel on Climate Change (IPCC). Cambridge University Press. https://www.osti.gov/etdeweb/biblio/20207706

Hu, S., Wang, D., Wu, J., Zhou, L., Feng, X., Fu, T., Yang, X., Ziegler, A. D., & Zeng, Z. (2021). Aerosol presence reduces the diurnal temperature range: an interval when the COVID-19 pandemic reduced aerosols revealing the effect on climate. Environmental Science Atmospheres, 1(5), 208-213. https://doi.org/10.1039/d1ea00021g

Huang, C., Li, J., Sun, W., Chen, Q., Mao, Q., & Yuan, Y. (2021). Long-Term Variation Assessment of Aerosol Load and Dominant Types over Asia for Air Quality Studies Using Multi-Sources Aerosol Datasets. Remote Sensing, 13(16), 3116. https://doi.org/10.3390/rs13163116

Huang, R., Zhang, Y., Bozzetti, C., Ho, K., Cao, J., Han, Y., Daellenbach, K. R., Slowik, J. G., Platt, S. M., Canonaco, F., Zotter, P., Wolf, R., Pieber, S. M., Bruns, E. A., Crippa, M., Ciarelli, G., Piazzalunga, A., Schwikowski, M., Abbaszade, G., . . . Prévôt, A. S. H. (2014). High secondary aerosol contribution to particulate pollution during haze events in China. Nature, 514(7521), 218-222. https://doi.org/10.1038/nature13774

IPCC. Climate Change 2007: Synthesis Report. In contribution of Working Group I, II, and III to the Fourth Assessment Report of the Intergovernmental Panel on Climate Change. (2007). Cambridge University Press: Cambridge, UK; New York, NY, USA, 2007; pp. 1-103.

IPCC. Climate Change 2014: Synthesis Report. In contribution of Working Group I, II, and III to the Fifth Assessment Report of the Intergovernmental Panel on Climate Change. (2014). Cambridge University Press: Cambridge, UK; New York, NY, USA, 2014; pp. 1-151.

Intergovernmental Panel on Climate Change, 2001. Climate Change 1994: Radiative Forcing of Climate. Report to IPCC from the Scientific Assessment Group (WGI). (n.d.). Cambridge University Press, NewYork.

Ives, A. R. (2018). R\$\^{2}\$s for Correlated Data: Phylogenetic Models, LMMs, and GLMMs. Systematic Biology, 68(2), 234--251. https://doi.org/10.1093/sysbio/syy060

Jacob, D. J. (2000). Introduction to Atmospheric Chemistry.

Ji, Z., Wang, G., Pal, J. S., & Yu, M. (2015). Potential climate effect of mineral aerosols over West Africa. Part I: model validation and contemporary climate evaluation. Climate Dynamics, 46(3--4), 1223-1239. https://doi.org/10.1007/s00382–015-2641-y

Johnson, B. T., Shine, K. P., & Forster, P. M. (2004). The semi-direct aerosol effect: Impact of absorbing aerosols on marine stratocumulus. Quarterly Journal of the Royal Meteorological Society, 130(599), 1407-1422. https://doi.org/10.1256/qj.03.61

Kai, Z., Hui-Wang, G., Ren-Jian, Z., Yan-Jun, Z., & Yue-Si, W. (2005). sources and movement routes of sand-dust aerosols and their impact probabilities on china seas in 2000–2002. Advance in Earth Sciences. https://en.cnki.com.cn/Article_en/CJFDTOTAL-DXJZ200506005.htm

Kaiser, J. (2005). Mounting evidence indicts Fine-Particle pollution. Science, 307(5717), 1858-1861. https://doi.org/10.1126/science.307.5717.1858a

Kasoar, M., Voulgarakis, A., Lamarque, J., Shindell, D., Bellouin, N., Collins, W., Faluvegi, G., & Tsigaridis, K. (2016). Regional and global temperature response to anthropogenic SO₂ emissions from China in three climate models. Atmospheric Chemistry and Physics, 16(15), 9785-9804. https://doi.org/10.5194/acp-16–9785-2016

Kaufman, Y. J., & Fraser, R. S. (1997). The effect of smoke particles on clouds and climate forcing. Science, 277(5332), 1636-1639. https://doi.org/10.1126/science.277.5332.1636

Kaufman, Y. J., Koren, I., Remer, L. A., Tanré, D., Ginoux, P., & Fan, S. (2005). Dust transport and deposition observed from the Terra-Moderate Resolution Imaging Spectroradiometer (MODIS) spacecraft over the Atlantic Ocean. Journal of Geophysical Research Atmospheres, 110(D10). https://doi.org/10.1029/2003jd004436

Kaufman, Y. J., Tanré, D., Gordon, H. R., Nakajima, T., Lenoble, J., Frouin, R., Grassl, H., Herman, B. M., King, M. D., & Teillet, P. M. (1997). Passive remote sensing of tropospheric aerosol and atmospheric correction for the aerosol effect. Journal of Geophysical Research Atmospheres, 102(D14), 16815-16830.

Kaufman, Y. J., Tanré, D., Remer, L. A., Vermote, E. F., Chu, A., & Holben, B. N. (1997). Operational remote sensing of tropospheric aerosol over land from EOS moderate resolution imaging spectroradiometer. Journal of Geophysical Research, 102(D14), 17051-17067. https://doi.org/10.1029/96jd03988

Kedia, S., Ramachandran, S., Holben, B., & Tripathi, S. (2014). Quantification of aerosol type, and sources of aerosols over the Indo-Gangetic Plain. Atmospheric Environment, 98, 607-619. https://doi.org/10.1016/j.atmosenv.2014.09.022

Keita, S., Liousse, C., Assamoi, E., Doumbia, T., N'Datchoh, E. T., Gnamien, S., Elguindi, N., Granier, C., & Yoboué, V. (2021). African anthropogenic emissions inventory for gases and particles from 1990 to 2015. Earth System Science Data, 13(7), 3691-3705. https://doi.org /10.5194/essd-13–3691-2021

Kholif, A., Elghandour, M., Rodríguez, G., Olafadehan, O., & Salem, A. (2016). Anaerobic ensiling of raw agricultural waste with a fibrolytic enzyme cocktail as a cleaner and sustainable biological product. Journal of Cleaner Production, 142, 2649-2655. https://doi.org/ 10.1016/j.jclepro.2016.11.012

Knippertz, P., Ansmann, A., Althausen, D., Müller, D., Tesche, M., Bierwirth, E., Dinter, T., Müller, T., Von Hoyningen-Huene, W., Schepanski, K., Wendisch, M., Heinold, B., Kandler, K., Petzold, A., Schütz, L., & Tegen, I. (2009). Dust mobilization and transport in the northern Sahara during SAMUM 2006 - a meteorological overview. Tellus B, 61(1).

https://doi.org/10.3402/tellusb.v61i1.16794

Knippertz, P., Evans, M. J., Field, P. R., Fink, A. H., Liousse, C., & Marsham, J. H. (2015). The possible role of local air pollution in climate change in West Africa. Nature Climate Change, 5(9), 815--822. https://doi.org/10.1038/nclimate2727

Koch, D., & Del Genio, A. D. (2010). Black carbon semi-direct effects on cloud cover: review and synthesis. Atmospheric Chemistry and Physics, 10(16), 7685-7696. https://doi.org/10. 5194/acp-10–7685-2010

Kommalapati, R. R., & Valsaraj, K. T. (2009). Atmospheric aerosols and their importance. In ACS symposium series (pp. 1-10). https://doi.org/10.1021/bk-2009–1005.ch001

Koren, I., Kaufman, Y. J., Remer, L. A., & Martins, J. V. (2004a). Measurement of the effect of Amazon smoke on inhibition of cloud formation. Science, 303(5662), 1342-1345. https://doi.org/10.1126/science.1089424

Koren, I., Kaufman, Y. J., Remer, L. A., & Martins, J. V. (2004b). Measurement of the effect of Amazon smoke on inhibition of cloud formation. Science, 303(5662), 1342-1345. https://doi.org/10.1126/science.1089424

Koren, I., Martins, J. V., Remer, L. A., & Afargan, H. (2008). Smoke Invigoration Versus Inhibition of Clouds over the Amazon. Science, 321(5891), 946-949. https://doi.org/10.1126/ science. 1159185

Kumar, A., Saxena, D., & Yadav, R. (2011). Measurements of atmospheric aerosol concentration of various sizes during monsoon season at Roorkee, India. Atmospheric Science Letters, 12(4), 345--350. https://doi.org/10.1002/asl.347

Kurniawati, S., Santoso, M., Nurhaini, F. F., Da, D. P., Lestiani, D. D., Ramadhani, M. F., Kusmartini, I., Syahfitri, W. Y. N., & Damastuti, E. (2023). Evaluation of Low-Cost sensors for PM2.5

monitoring: performance, reliability, and implications for air quality assessment. Research Square (Research Square). https://doi.org/10.21203/rs.3.rs-3047338/v1

Lelieveld, J., Evans, J. S., Fnais, M., Giannadaki, D., & Pozzer, A. (2015). The contribution of outdoor air pollution sources to premature mortality on a global scale. Nature, 525(7569), 367-371. https://doi.org/10.1038/nature15371

Lepeule, J., Laden, F., Dockery, D., & Schwartz, J. (2012). Chronic Exposure to Fine Particles and Mortality: An Extended Follow-up of the Harvard Six Cities Study from 1974 to 2009. Environmental Health Perspectives, 120(7), 965-970. https://doi.org/10.1289/ehp.1104660

Levine, J. S., Cofer, I. W. R., Cahoon, J. D. R., & Winstead, E. L. (1995). Biomass burning: a driver for global change! Environmental Science & Technology, 29(3). https://agris.fao.org/agris-search/search.do?recordID=US9633078

Levy, H., Horowitz, L. W., Schwarzkopf, M. D., Ming, Y., Golaz, J., Naik, V., & Ramaswamy, V. (2013). The roles of aerosol direct and indirect effects in past and future climate change. Journal of Geophysical Research Atmospheres, 118(10), 4521-4532. https://doi.org/10.1002/jgrd.50 192

Li, C., Zhao, T., & Ying, K. (2015). Effects of anthropogenic aerosols on temperature changes in China during the twentieth century based on CMIP5 models. Theoretical and Applied Climatology, 125(3--4), 529--540. https://doi.org/10.1007/s00704–015-1527–6

Li, J., Ge, X., He, Q., & Abbas, A. (2021). Aerosol optical depth (AOD): spatial and temporal variations and association with meteorological covariates in Taklimakan desert, China. PeerJ, 9, e10542. https://doi.org/10.7717/peerj.10542

Li, X., Jiang, L., Bai, Y., Yang, Y., Liu, S., Chen, X., Xu, J., Liu, Y., Wang, Y., Guo, X., Wang, Y., & Wang, G. (2018). Wintertime aerosol chemistry in Beijing during haze period: Significant

contribution from secondary formation and biomass burning emission. Atmospheric Research, 218, 25--33. https://doi.org/10.1016/j.atmosres.2018.10.010

Li, X., Wagner, F., Peng, W., Yang, J., & Mauzerall, D. L. (2017). Reduction of solar photovoltaic resources due to air pollution in China. Proceedings of the National Academy of Sciences, 114(45), 11867--11872. https://doi.org/10.1073/pnas.1711462114

Liao, H., & Seinfeld, J. H. (1998). Radiative forcing by mineral dust aerosols: Sensitivity to key variables. Journal of Geophysical Research, 103(D24), 31637-31645. https://doi.org/10.1029/ 1998jd200036

Liou, K. N., & Bohren, C. (1981). An introduction to atmospheric radiation. Physics Today, 34(7), 66-67. https://doi.org/10.1063/1.2914664

Liousse, C., Assamoi, E., Criqui, P., Granier, C., & Rosset, R. (2014). Explosive growth in African combustion emissions from 2005 to 2030. Environmental Research Letters, 9(3), 035003. https://doi.org/10.1088/1748–9326/9/3/035003

Liu, L., Shawki, D., Voulgarakis, A., Kasoar, M., Samset, B. H., Myhre, G., Forster, P. M., Hodnebrog, Ø., Sillmann, J., Aalbergsjø, S. G., Boucher, O., Faluvegi, G., Iversen, T., Kirkevåg, A., Lamarque, J., Olivié, D., Richardson, T., Shindell, D., & Takemura, T. (2018). A PDRMIP multimodel study on the impacts of regional aerosol forcings on global and regional precipitation. Journal of Climate, 31(11), 4429-4447. https://doi.org/10.1175/jcli-d-17–0439.1

Luo, C., Mahowald, N. M., & Del Corral, J. (2003). Sensitivity study of meteorological parameters on mineral aerosol mobilization, transport, and distribution. Journal of Geophysical Research, 108(D15). https://doi.org/10.1029/2003jd003483

Léon, J., Akpo, A. B., Bedou, M., Djossou, J., Bodjrenou, M., Yoboué, V., & Liousse, C. (2021). PM_{2.5} surface concentrations in southern West

African urban areas based on sun photometer and satellite observations. Atmospheric Chemistry and Physics, 21(3), 1815--1834. https://doi.org/10.5194/acp-21–1815-2021

Mbow, C., Nielsen, T., & Rasmussen, K. (2000). Savanna Fires in East-Central Senegal: Distribution Patterns, Resource Management and Perceptions. Human Ecology, 28(4), 561-583. https://doi.org/10.1023/a:1026487730947

McKnight, T. L., & Hess, D. (2000). Physical geography: A Landscape Appreciation.

McTainsh, G. (1980). Harmattan dust deposition in northern Nigeria. Nature, 286(5773), 587-588. https://doi.org/10.1038/286587a0

McTainsh, G. H., & Walker, P. H. (1982). Nature and distribution of Harmattan dust. Zeitschrift Für Geomorphologie, 26(4), 417--435. https://doi.org/10.1127/zfg/26/1982/417

Meehl, G. A., Washington, W. M., Erickson, D. J., Briegleb, B. P., & Jaumann, P. J. (1996). Climate change from increased CO2 and direct and indirect effects of sulfate aerosols. Geophysical Research Letters, 23(25), 3755-3758. https://doi.org/10.1029/96gl03478

Mensah, C. A. (2014). Destruction of urban green spaces: A problem beyond urbanization in Kumasi City (Ghana). American Journal of Environmental Protection, 3(1), 1. https://doi.org/10. 11648/j.ajep.20140301.11

Mercado, L. M., Bellouin, N., Sitch, S., Boucher, O., Huntingford, C., Wild, M., & Cox, P. M. (2009). Impact of changes in diffuse radiation on the global land carbon sink. Nature, 458(7241), 1014--1017. https://doi.org/10.1038/nature07949

Mitchell, J. F. B., Johns, T. C., Gregory, J. M., & Tett, S. F. B. (1995). Climate response to increasing levels of greenhouse gases and sulphate aerosols. Nature, 376(6540), 501-504. https://doi.org/10.1038/376501a0

Mitchell, J. M. (1971). The Effect of Atmospheric Aerosols on Climate with Special Reference to Temperature near the Earth's Surface. Journal of Applied Meteorology, 10(4), 703-714. https://doi.org/10.1175/1520-0450(1971)010

Moorthy, K. K., Nair, P. R., Murthy, B. K., & Satheesh, S. (1996). Time evolution of the optical effects and aerosol characteristics of Mt. Pinatubo origin from ground-based observations. Journal of Atmospheric and Terrestrial Physics, 58(10), 1101-1116. https://doi.org/10.1016/0021-9169(95)00079-8

Murthy, K. (1988). Aerosols and radiation budget in the middle atmosphere. Indian Journal of Radio and Space Physics, 17, 203–219., 17, 203--219.

Myhre, G., Highwood, E. J., Shine, K. P., & Stordal, F. (1998). New estimates of radiative forcing due to well mixed greenhouse gases. Geophysical Research Letters, 25(14), 2715-2718. https://doi.org/10.1029/98gl01908

NASA Earth Observatory. (n.d.). Aerosols: tiny particles, big impact.

Niamien, A. F., Léon, J., Adon, M., Rajot, J., Feron, A., & Yoboué, V. (2024). Variability of Aerosol Optical Depth and Altitude for Key Aerosol Types over Southern West Africa via CALIPSO/CALIOP Observations. Atmosphere, 15(4), 396.

Niyogi, D., Kishtawal, C., Tripathi, S., & Govindaraju, R. S. (2010). Observational evidence that agricultural intensification and land use change may be reducing the Indian summer monsoon rainfall. Water Resources Research, 46(3).

Nordling, K., Korhonen, H., Räisänen, P., Alper, M. E., Uotila, P., O'Donnell, D., & Merikanto, J. (2019). Role of climate model dynamics in estimated climate responses to anthropogenic aerosols. Atmospheric Chemistry and Physics, 19(15), 9969-9987. https://doi.org/10.5194/acp-19-9969-2019

Norris, J. R., & Wild, M. (2009). Trends in aerosol radiative effects over China and Japan inferred from observed cloud cover, solar "dimming," and solar "brightening." Journal of Geophysical Research Atmospheres, 114(D10). https://doi.org/10.1029/2008jd011378

Nwofor, O., Chineke, T. C., & Pinker, R. (2007). Seasonal characteristics of spectral aerosol optical properties at a sub-Saharan site. Atmospheric Research, 85(1), 38-51. https://doi.org/10.1016/ j.atmosres.2006.11.002

Ochei, M. C., Oluleye, A., Wolke, R., Pratt, D. A., & Njie, T. (2023). Aerosols' variability and their relationship with climatic parameters over West Africa. Environmental Monitoring and Assessment, 195(6). https://doi.org/10.1007/s10661-023-11204-x

Ochei, M., Oluleye, A., Wolke, R., Pratt, D., & Njie, T. (2023). Aerosols' variability and their relationship with climatic parameters over West Africa. Environmental Monitoring and Assessment, 195(6). https://doi.org/10.1007/s10661–023-11204-x

Ofosu, F. G., Hopke, P. K., Aboh, I. J. K., & Bamford, S. A. (2013a). Biomass burning contribution to ambient air particulate levels at Navrongo in the Savannah zone of Ghana. Journal of the Air & Waste Management Association, 63(9), 1036-1045. https://doi.org/10.1080/10962247. 2013.783888

Ofosu, F. G., Hopke, P. K., Aboh, I. J. K., & Bamford, S. A. (2013b). Biomass burning contribution to ambient air particulate levels at Navrongo in the Savannah zone of Ghana. Journal of the Air & Waste Management Association, 63(9), 1036-1045. https://doi.org/10.1080/10962247.20 13 .783888

Ogunjobi, K., Ajayi, V., Balogun, I., Omotosho, J., & He, Z. (2007). The synoptic and optical characteristics of the harmattan dust spells over Nigeria. Theoretical and Applied Climatology, 93(1-2), 91-105. https://doi.org/10.1007/s00704-007-0332–2

Onyeuwaoma, N. D., Nwofor, O. K., Chineke, T. C., Eguaroje, E. O., & Dike, V. N. (2015). Implications of MODIS impression of aerosol loading over urban and rural settlements in Nigeria: Possible links to energy consumption patterns in the country. Atmospheric Pollution Research, 6(3), 484-494. https://doi.org/10.5094/apr.2015.054

Palacios-Peña, L., Montávez, J. P., López-Romero, J. M., Jerez, S., Gómez-Navarro, J. J., Lorente-Plazas, R., Ruiz, J., & Jiménez-Guerrero, P. (2020). Added Value of Aerosol-Cloud Interactions for Representing Aerosol Optical Depth in an Online Coupled Climate-Chemistry Model over Europe. Atmosphere, 11(4), 360. https://doi.org/10.3390/atmos11040360

Park, C., Jeong, S., Ho, C., & Kim, J. (2015). Regional variations in potential plant habitat changes in response to multiple global warming scenarios*. Journal of Climate, 28(7), 2884-2899. https://doi.org/10.1175/jcli-d-13-00753.1

Penner, J. E., Quaas, J., Storelvmo, T., Takemura, T., Boucher, O., Guo, H., Kirkevåg, A., Kristjánsson, J. E., & Seland, Ø. (2006). Model intercomparison of indirect aerosol effects. Atmospheric Chemistry and Physics, 6(11), 3391-3405.

Persad, G., & Caldeira, K. (2018). Divergent global-scale temperature effects from identical aerosols emitted in different regions. Nature Communications, 9(1).

Perumpully, S. J., & Gautam, S. (2024). Impact of aerosols on atmospheric processes and climate variability: A synthesis of recent research findings. Geosystems and Geoenvironment, 100317. https://doi.org/10.1016/j.geogeo.2024.100317

Pilinis, C., Pandis, S. N., & Seinfeld, J. H. (1995). Sensitivity of direct climate forcing by atmospheric aerosols to aerosol size and composition. Journal of Geophysical Research Atmospheres, 100(D9), 18739-18754. https://doi.org/10.1029/95jd02119

Pope, C. A., & Dockery, D. W. (2006). Health Effects of Fine Particulate Air Pollution: Lines that Connect. Journal of the Air & Waste Management Association, 56(6), 709-742. https://doi.org/10.1080/10473289.2006.10464485

Prospero, J. M., & Carlson, T. N. (1980). Saharan air outbreaks over the tropical North Atlantic. Pure and Applied Geophysics, 119(3), 677--691. https://doi.org/10.1007/bf00878167

Prospero, J. M., & Lamb, P. J. (2003). African droughts and dust transport to the Caribbean: climate change implications. Science, 302(5647), 1024-1027.

Prospero, J. M., Ginoux, P., Torres, O., Nicholson, S. E., & Gill, T. E. (2002). Environmental characterization of global sources of atmospheric soil dust identified with the nimbus 7 total ozone mapping spectrometer (toms) absorbing aerosol product. Reviews of Geophysics, 40(1). https://doi.org/10.1029/2000rg000095

Pruppacher, H. R., Klett, J. D., & Wang, P. K. (1998). Microphysics of clouds and precipitation. Aerosol Science and Technology, 28(4), 381-382.

Pöschl, U. (2005). Atmospheric aerosols: composition, transformation, climate and health effects. Angewandte Chemie, 44(46), 7520-7540.

Qian, Y., Leung, L. R., Ghan, S. J., & Giorgi, F. (2003). Regional climate effects of aerosols over China: modeling and observation. Tellus B, 55(4), 914-934. https://doi.org/10.1046/j.1435-6935.2003.00070.x

Raes, F., Van Dingenen, R., Vignati, E., Wilson, J., Putaud, J., Seinfeld, J. H., & Adams, P. (2000). Formation and cycling of aerosols in the global troposphere. Atmospheric Environment, 34(25), 4215-4240. https://doi.org/10.1016/s1352-2310(00)00239-9

Ramachandran, S., & Kedia, S. (2010). Black carbon aerosols over an urban region: Radiative forcing and climate impact. Journal of Geophysical Research Atmospheres, 115(D10).

https://doi.org/10.1029/2009jd013560

Raman, A., Arellano, A., & Sorooshian, A. (2016). Decreasing aerosol loading in the North American monsoon region. Atmosphere, 7(2), 24. https://doi.org/10.3390/atmos7020024

Ramanathan, V. (1975). Greenhouse effect due to chlorofluorocarbons: Climatic implications. Science, 190(4209), 50--52. https://doi.org/10.1126/science.190.4209.50

Ramanathan, V., & Feng, Y. (2008). Air pollution, greenhouse gases, and climate change: Global and regional perspectives. Atmospheric Environment, 43(1), 37-50. https://doi.org/10.1016/j. atmosenv.2008.09.063

Ramanathan, V., Cess, R. D., Harrison, E. F., Minnis, P., Barkstrom, B. R., Ahmad, E., & Hartmann, D. (1989). Cloud-Radiative Forcing and Climate: Results from the Earth Radiation Budget Experiment. Science, 243(4887), 57--63.

Ramanathan, V., Chung, C., Kim, D., Bettge, T., Buja, L., Kiehl, J. T., Washington, W. M., Fu, Q., Sikka, D. R., & Wild, M. (2005). Atmospheric brown clouds: Impacts on South Asian climate and hydrological cycle. Proceedings of the National Academy of Sciences, 102(15), 5326--5333. https://doi.org/10.1073/pnas.0500656102

Ramanathan, V., Crutzen, P. J., Kiehl, J. T., & Rosenfeld, D. (2001). Aerosols, climate, and the hydrological cycle. Science, 294(5549), 2119-2124.

Ramanathan, V., Crutzen, P., Lelieveld, J., Mitra, A., Althausen, D., Anderson, J., Andreae, M., Cantrell, W., Cass, G., Chung, C., Clarke, A., Coakley, J., Collins, W., Conant, W., Dulac, F., Heintzenberg, J., Heymsfield, A., Holben, B., Howell, S., . . . Valero, F. (2001). Indian Ocean Experiment: An integrated analysis of the climate forcing and effects of the great Indo-Asian haze. Journal of Geophysical Research, 106(D22), 28371-28398. https://doi.org/10.1029/2001j d900133

Robock, A. (2000). Volcanic eruptions and climate. Reviews of Geophysics, 38(2), 191--219.

https://doi.org/10.1029/1998rg000054

Rodhe, H. (2000). The second Aerosol Characterization Experiment (ACE-2). Tellus B, 52(2), 109. https://doi.org/10.3402/tellusb.v52i2.16087

Rooney, M. S., Arku, R. E., Dionisio, K. L., Paciorek, C., Friedman, A. B., Carmichael, H., Zhou, Z., Hughes, A. F., Vallarino, J., Agyei-Mensah, S., Spengler, J. D., & Ezzati, M. (2012). Spatial and temporal patterns of particulate matter sources and pollution in four communities in Accra, Ghana. The Science of the Total Environment, 435-436, 107-114. https://doi.org/10.1016/j. scitotenv.2012.06.077

Rosenfeld, D., Sherwood, S., Wood, R., & Donner, L. (2014). Climate effects of Aerosol-Cloud interactions. Science, 343(6169), 379-380. https://doi.org/10.1126/science.1247490

Russell, P. B., Hobbs, P. V., & Stowe, L. L. (1999). Aerosol properties and radiative effects in the United States East Coast haze plume: An overview of the Tropospheric Aerosol Radiative Forcing Observational Experiment (TARFOX). Journal of Geophysical Research, 104(D2), 2213--2222. https://doi.org/10.1029/1998jd200028

Saliba, N., Jam, F. E., Tayar, G. E., Obeid, W., & Roumie, M. (2010). Origin and variability of particulate matter (PM10 and PM2.5) mass concentrations over an Eastern Mediterranean city. Atmospheric Research, 97(1-2), 106-114.

Samset, B. H., Sand, M., Smith, C. J., Bauer, S. E., Forster, P. M., Fuglestvedt, J. S., Osprey, S., & Schleussner, C. (2018). Climate impacts from a removal of anthropogenic aerosol emissions. Geophysical Research Letters, 45(2), 1020-1029. https://doi.org/10.1002/2017gl076079

Santer, B. D., Taylor, K. E., Wigley, T. M. L., Penner, J. E., Jones, P. D., & Cubasch, U. (1995). Towards the detection and attribution of an anthropogenic effect on climate. Climate Dynamics, 12(2), 77-100. https://doi.org/10.1007/bf00223722

Satheesh, S., & Krishnamoorthy, K. (2005). Radiative effects of natural aerosols: A review. Atmospheric Environment, 39(11), 2089-2110.

Schepanski, K., Tegen, I., & Macke, A. (2009). Saharan dust transport and deposition towards the tropical northern Atlantic. Atmospheric Chemistry and Physics, 9(4), 1173-1189. https://doi.org/10.5194/acp-9-1173-2009

Schütz, L. (1980). LONG-RANGE TRANSPORT OF DESERT DUST WITH SPECIAL EMPHASIS ON THE SAHARA\. Annals of the New York Academy of Sciences, 338(1), 515-532. https://doi.org/10.1111/j.1749-6632.1980.tb17144.x

Seinfeld, J. H., & Pandis, S. N. (2006). Atmospheric Chemistry and Physics: From Air Pollution to Climate Change, 2nd Ed. John Wiley and Sons: Hoboken, NJ, USA.

Seinfeld, J. H., & Pandis, S. N. (2016). Atmospheric Chemistry and Physics: From Air Pollution to Climate Change. John Wiley & Sons.

Seinfeld, J. H., Carmichael, G. R., Arimoto, R., Conant, W. C., Brechtel, F. J., Bates, T. S., Cahill, T. A., Clarke, A. D., Doherty, S. J., Flatau, P. J., Huebert, B. J., Kim, J., Markowicz, K. M., Quinn, P. K., Russell, L. M., Russell, P. B., Shimizu, A., Shinozuka, Y., Song, C. H., . . . Zhang, X. Y. (2004). ACE-ASIA: regional climatic and atmospheric chemical effects of Asian dust and pollution. Bulletin of the American Meteorological Society, 85(3), 367-380. https://doi.org/10.1175/bams-85–3-367

Seinfeld, J. H., Pandis, S. N., & Noone, K. (1998). Atmospheric Chemistry and Physics: From air pollution to climate change. Physics Today, 51(10), 88-90.

Setiawan, B. I. (2020). A simple method to determine patterns of wet and dry seasons. IOP Conference Series Earth and Environmental Science, 542(1), 012055. https://doi.org/10.1088/1755-1315/542/1/012055

Shaw, G. E. (1990). Bio-controlled thermostasis involving the sulfur cycle. Climatic Change, 5(3), 297-303. https://doi.org/10.1007/bf00140186

Shimadera, H., Kondo, A., Kaga, A., Shrestha, K. L., & Inoue, Y. (2009). Contribution of transboundary air pollution to ionic concentrations in fog in the Kinki Region of Japan. Atmospheric Environment, 43(37), 5894-5907.

Shindell, D., Schulz, M., Ming, Y., Takemura, T., Faluvegi, G., & Ramaswamy, V. (2010). Spatial scales of climate response to inhomogeneous radiative forcing. Journal of Geophysical Research Atmospheres, 115(D19). https://doi.org/10.1029/2010jd014108

Singh, A. K., Rai, J., & Niwas, S. (2000). Variation of aerosols in relation to some meteorological parameters during different weather conditions. Atmósfera, 13(3), 177-184. http://www.scielo.org.mx/pdf/atm/v13n3/v13n3a4.pdf

Soden, B. J., Wetherald, R. T., Stenchikov, G. L., & Robock, A. (2002). Global cooling after the eruption of Mount Pinatubo: A test of climate feedback by water vapor. Science, 296(5568), 727--730. https://doi.org/10.1126/science.296.5568.727

Sokolik, I. N., & Toon, O. B. (1996). Direct radiative forcing by anthropogenic airborne mineral aerosols. Nature, 381(6584), 681-683. https://doi.org/10.1038/381681a0

Solar radiation energy (fundamentals). (n.d.).

Srivastava, A. K., Yadav, V., Pathak, V., Singh, S., Tiwari, S., Bisht, D. S., & Goloub, P. (2014). Variability in radiative properties of major aerosol types: A year-long study over Delhi-An urban station in Indo-Gangetic Basin. The Science of the Total Environment, 473-474, 659-666. https://doi.org/10.1016/j.scitotenv.2013.12.064

Stier, P., Seinfeld, J. H., Kinne, S., & Boucher, O. (2007). Aerosol absorption and radiative forcing. Atmospheric Chemistry and Physics, 7(19), 5237-5261.

Stocker, T. (2013). Climate change 2013 : the physical science basis : Working Group I contribution to the Fifth Assessment Report of the Intergovernmental Panel on Climate Change. In the Intergovernmental Panel on Climate Change eBooks.

Stowe, L. L., Jacobowitz, H., Ohring, G., Knapp, K. R., & Nalli, N. R. (2002). The Advanced Very High Resolution Radiometer (AVHRR) Pathfinder Atmosphere (PATMOS) Climate Dataset: Initial analyses and evaluations. Journal of Climate, 15(11), 1243--1260. https://doi.org/ 10.1175/1520–0442(2002)015

Streets, D. G., Wu, Y., & Chin, M. (2006). Two-decadal aerosol trends as a likely explanation of the global dimming/brightening transition. Geophysical Research Letters, 33(15). https://doi.org/10.1029/2006gl026471

Sultan, B., & Janicot, S. (2003). The West African Monsoon Dynamics. Part II: The "Preonset" and "Onset" of the summer Monsoon. Journal of Climate, 16(21), 3407--3427. https://doi.org/10.1175/1520–0442(2003)016

Sunnu, A., Afeti, G., & Resch, F. (2007). A long-term experimental study of the Saharan dust presence in West Africa. Atmospheric Research, 87(1), 13--26.

Swap, R., Garstang, M., Greco, S., Talbot, R., & Kållberg, P. (1992). Saharan dust in the Amazon Basin. Tellus B, 44(2), 133. https://doi.org/10.3402/tellusb.v44i2.15434

Tao, J., Gao, J., Zhang, L., Zhang, R., Che, H., Zhang, Z., Lin, Z., Jing, J., Cao, J., & Hsu, S. (2014). PM_{2.5} pollution in a megacity of southwest China: source apportionment and implication. Atmospheric Chemistry and Physics, 14(16), 8679--8699. https://doi.org/10.5194/acp-14–8679-2014

Tella, A. A., & Danjibo, N. D. N. D. (2024). The environmental impact of mining activities in the local community: A structural equation modelling approach. International Journal of Social Work, 11(1), 44. https://doi.org/10.5296/ijsw.v11i1.21747

Thangavel, P., Park, D., & Lee, Y. (2022). Recent Insights into Particulate Matter (PM2.5)-Mediated Toxicity in Humans: An Overview. International Journal of Environmental Research and Public Health, 19(12), 7511. https://doi.org/10.3390/ijerph19127511

Tie, X., Huang, R., Cao, J., Zhang, Q., Cheng, Y., Su, H., Chang, D., Pöschl, U., Hoffmann, T., Dusek, U., Li, G., Worsnop, D. R., & O'Dowd, C. D. (2017). Severe pollution in China amplified by atmospheric moisture. Scientific Reports, 7(1).

Tost, H. (2017a). Chemistry--climate interactions of aerosol nitrate from lightning. Atmospheric Chemistry and Physics, 17(2), 1125--1142. https://doi.org/10.5194/acp-17–1125-2017

Tost, H. (2017b). Chemistry--climate interactions of aerosol nitrate from lightning. Atmospheric Chemistry and Physics, 17(2), 1125--1142. https://doi.org/10.5194/acp-17–1125-2017

Treut, H. L., Forichon, M., Boucher, O., & Li, Z. (1998). Sulfate aerosol indirect effect and CO2Greenhouse forcing: EquilibriumResponse of the LMD GCM and Associated Cloud Feedbacks. Journal of Climate, 11(7), 1673--1684.

Twomey, S. (1977). The influence of pollution on the shortwave albedo of clouds. Journal of the Atmospheric Sciences, 34(7), 1149--1152. https://doi.org/10.1175/1520–0469(1977)034

United Nations. (2015). Transforming Our World: The 2030 Agenda for Sustainable Development. United Nations General Assembly.

Veefkind, J., Van Der Hage, J., & Brink, H. T. (1996). Nephelometer derived and directly measured aerosol optical depth of the atmospheric boundary layer. Atmospheric Research, 41(3--4), 217--228. https://doi.org/10.1016/0169–8095(96)00011–7

Vijayakumar, K., Safai, P., Devara, P., Rao, S. V. B., & Jayasankar, C. (2016). Effects of agriculture crop residue burning on aerosol properties and long-range transport over northern India: A study using satellite data and model simulations. Atmospheric Research, 178--179, 155--163. https://doi.org/10.1016/j.atmosres.2016.04.003

Voiland, A. (2010). Aerosols: Tiny Particles, Big Impact : Feature Articles. Nasa Earth Observatory. http://earthobservatory.nasa.gov/Features/Aerosols/

Wang, A., Xie, X., Liu, X., & Yin, Z. (2022). Direct radiative effect (DRE) of dust aerosols on West African and East Asian Monsoon: The role of Ocean-Atmosphere Interactions. Journal of Geophysical Research Atmospheres, 127(6).

Wang, J., Wang, S., Jiang, J., Ding, A., Zheng, M., Zhao, B., Wong, D. C., Zhou, W., Zheng, G., Wang, L., Pleim, J. E., & Hao, J. (2014). Impact of aerosol--meteorology interactions on fine particle pollution during China's severe haze episode in January 2013. Environmental Research Letters, 9(9), 094002.

Wang, J., Xing, J., Wang, S., Mathur, R., Wang, J., Zhang, Y., Liu, C., Pleim, J., Ding, D., Chang, X., Jiang, J., Zhao, P., Sahu, S. K., Jin, Y., Wong, D. C., & Hao, J. (2022). The pathway of impacts of aerosol direct effects on secondary inorganic aerosol formation. Atmospheric Chemistry and Physics, 22(8), 5147-5156. https://doi.org/10.5194/acp-22–5147-2022

Wang, L., Li, Z., Tian, Q., Ma, Y., Zhang, F., Zhang, Y., Li, D., Li, K., & Li, L. (2013). Estimate of aerosol absorbing components of black carbon, brown carbon, and dust from ground-based remote sensing data of sun-sky radiometers. Journal of Geophysical Research Atmospheres, 118(12), 6534--6543. https://doi.org/10.1002/jgrd.50356

Wang, X., Li, Y., Wang, M., Li, Y., Gong, X., Chen, Y., Chen, Y., & Cao, W. (2020). Changes in daily extreme temperature and precipitation events in mainland China from 1960 to 2016 under global warming. International Journal of Climatology, 41(2), 1465--1483. https://doi.org/10.1002/joc.6865

Watson, R. T. (1990). Greenhouse gases and aerosols. Climate Change: The IPCC Scientific Assessment, 1, 17., 1-40. https://ci.nii.ac.jp/naid/10003749001

Wei, J., Peng, Y., Mahmood, R., Sun, L., & Guo, J. (2019). Intercomparison in spatial distributions and temporal trends derived from multi-source satellite aerosol products. Atmospheric Chemistry and Physics, 19(10), 7183-7207. https://doi.org/10.5194/acp-19–7183-2019

Wells, C., Kasoar, M., Bellouin, N., & Voulgarakis, A. (2023). Local and remote climate impacts of future African aerosol emissions. Atmospheric Chemistry and Physics, 23(6), 3575--3593. https://doi.org/10.5194/acp-23-3575-2023

Westervelt, D. M., Mascioli, N. R., Fiore, A. M., Conley, A., Lamarque, J., Shindell, D., Faluvegi, G., Previdi, M., Correa, G., & Horowitz, L. W. (2020). Local and remote mean and extreme temperature response to regional aerosol emissions reductions. Atmospheric Chemistry and Physics, 20(5), 3009--3027. https://doi.org/10.5194/acp-20–3009-2020

Wikipedia contributors. (2023, January 29). Fumesua. Wikipedia.

Wilcox, L., Liu, Z., Samset, B. H., Hawkins, E., Lund, M. T., Nordling, K., Undorf, S., Bollasina, M., Ekman, A. M. L., Krishnan, S., Merikanto, J., & Turner, A. (2020). Accelerated increases in global and Asian summer monsoon precipitation from future aerosol reductions. Atmospheric Chemistry and Physics, 20(20), 11955-11977. https://doi.org/10.5194/acp-20–11955-2020

Wild, M. (2009). Global dimming and brightening: A review. Journal of Geophysical Research Atmospheres, 114(D10). https://doi.org/10.1029/2008jd011470

Wild, M., Gilgen, H., Roesch, A., Ohmura, A., Long, C. N., Dutton, E. G., Forgan, B., Kallis, A., Russak, V., & Tsvetkov, A. (2005). From dimming to brightening: decadal changes in solar radiation at Earth's surface. Science, 308(5723), 847-850.

Wong, C. W. Y., Lai, K., Shang, K., Lu, C., & Leung, T. K. P. (2012). Green operations and the moderating role of environmental management capability of suppliers on manufacturing firm performance. International Journal of Production Economics, 140, 283-294. . https://dissem.in/p/22014081/green-operations-and-the-moderating-role-of-environmental-management-capability-of-suppliers-on-manufacturing-firm-performance-international-journal-of-production-economics-140-283-294

Xian, P., Zhang, J., O'Neill, N. T., Reid, J. S., Toth, T. D., Sorenson, B., Hyer, E. J., Campbell, J. R., & Ranjbar, K. (2022a). Arctic spring and summertime aerosol optical depth baseline from long-term observations and model reanalyses - Part 2: Statistics of extreme AOD events, and implications for the impact of regional biomass burning processes. Atmospheric Chemistry and Physics, 22(15), 9949-9967. https://doi.org/10.5194/acp-22–9949-2022

Xian, P., Zhang, J., O'Neill, N. T., Reid, J. S., Toth, T. D., Sorenson, B., Hyer, E. J., Campbell, J. R., & Ranjbar, K. (2022b). Arctic spring and summertime aerosol optical depth baseline from long-term observations and model reanalyses - Part 2: Statistics of extreme AOD events, and implications for the impact of regional biomass burning processes. Atmospheric Chemistry and Physics, 22(15), 9949--9967. https://doi.org/10.5194/acp-22–9949-2022

Xie, P., Janowiak, J. E., Arkin, P. A., Adler, R., Gruber, A., Ferraro, R., Huffman, G. J., & Curtis, S. (2003). GPCP Pentad Precipitation Analyses: an experimental dataset based on gauge observations and satellite estimates. Journal of Climate, 16(13), 2197-2214. https://doi.org/ 10. 1175/2769.1

Xing, J., Wang, J., Mathur, R., Wang, S., Sarwar, G., Pleim, J., Hogrefe, C., Zhang, Y., Jiang, J., Wong, D. C., & Hao, J. (2017). Impacts of aerosol direct effects on tropospheric ozone through changes in atmospheric dynamics and photolysis rates. Atmospheric Chemistry and Physics, 17(16), 9869-9883. https://doi.org/10.5194/acp-17-9869-2017

Yu, H., Chin, M., Yuan, T., Bian, H., Remer, L. A., Prospero, J. M., Omar, A., Winker, D., Yang, Y., Zhang, Y., Zhang, Z., & Zhao, C. (2015). The fertilizing role of African dust in the Amazon rainforest: A first multiyear assessment based on data from Cloud-Aerosol Lidar and Infrared Pathfinder Satellite Observations. Geophysical Research Letters, 42(6), 1984-1991. https://doi.org/10.1002/2015gl063040

Zeng, S., Riedi, J., Trepte, C. R., Winker, D. M., & Hu, Y. (2014). Study of global cloud droplet number concentration with A-Train satellites. Atmospheric Chemistry and Physics, 14(14), 7125--7134. https://doi.org/10.5194/acp-140-7125-2014

Zhang, F., Wang, Z., Cheng, H., Lv, X., Gong, W., Wang, X., & Zhang, G. (2015). Seasonal variations and chemical characteristics of PM2.5 in Wuhan, central China. The Science of the Total Environment, 518--519, 97-105.

Zhang, J., Ding, J., Zhang, J., Yuan, M., Li, P., Xiao, Z., Peng, C., Chen, H., Wang, M., & Zhu, Q. (2019). Effects of increasing aerosol optical depth on the gross primary productivity in China during 2000-2014. Ecological Indicators, 108, 105761.

Zhang, R., Khalizov, A. F., Pagels, J., Zhang, D., Xue, H., & McMurry, P. H. (2008). Variability in morphology, hygroscopicity, and optical properties of soot aerosols during atmospheric processing. Proceedings of the National Academy of Sciences of the United States of America, 105(30), 10291--10296. https://doi.org/10.1073/pnas.0804860105

Zhang, Y., Wen, X., & Jang, C. (2010). Simulating chemistry-aerosol-cloud-radiation-climate feedbacks over the continental U.S. using the online-coupled Weather Research Forecasting Model with chemistry (WRF/Chem). Atmospheric Environment, 44(29), 3568-3582. https://doi.org/10.1016/j.atmosenv.2010.05.056

Zhao, X., Xu, Z., Li, P., Dong, Z., Fu, P., Liu, C., & Pavuluri, C. M. (2022). Characteristics and seasonality of trace elements in fine aerosols from Tianjin, North China during 2018–2019. Environmental Advances, 9, 100263. https://doi.org/10.1016/j.envadv.2022.100263

Zhu, Y., Hinds, W. C., Shen, S., & Sioutas, C. (2004). Seasonal Trends of Concentration and Size Distribution of Ultrafine Particles Near Major Highways in Los Angeles Special Issue ofAerosol Science and Technologyon Findings from the Fine Particulate Matter Supersites Program. Aerosol Science and Technology, 38(sup1), 5-13.

APPENDICES

APPENDIX A: SATELLITE DATA PRODUCTS SPECIFICATIONS

A.1 MERRA-2 (Modern-Era Retrospective analysis for Research and Applications, Version 2)

Provider: NASA Global Modeling and Assimilation Office (GMAO)

Spatial Resolution: 0.5° × 0.625° (latitude × longitude), approximately 50 km × 65 km at equator

Temporal Resolution: Hourly

Variables Used: $PM_{2.5}$ surface mass concentration ($\mu g/m^3$), PM_{10} total column mass density, 2-meter air temperature (K), surface incident shortwave radiation flux (W/m^2)

Data Assimilation System: GEOS-5 Data Assimilation System with 3D-Var aerosol analysis

Aerosol Components: Black carbon, organic carbon, sulfate, dust (5 size bins), sea salt (5 size bins)

Quality Control: Bias correction using MODIS AOD, AERONET sun photometer data

Uncertainty: ±30-40% for $PM_{2.5}$, ±20-30% for temperature, ±10-15% for radiation

A.2 GEOS-CF (Goddard Earth Observing System Composition Forecast)

Provider: NASA GMAO

Spatial Resolution: 0.25° × 0.25°, approximately 25 km × 25 km at equator

Temporal Resolution: Hourly forecasts

Variables Used: $PM_{2.5}$ surface concentration ($\mu g/m^3$), Aerosol Optical Depth at 550 nm

Chemistry Mechanism: GOCART aerosol module coupled with GEOS-Chem tropospheric chemistry

Emission Inventories: EDGAR anthropogenic emissions, GFED biomass burning, MEGAN biogenic emissions

Uncertainty: ±40-50% for $PM_{2.5}$ in West Africa due to limited emission data validation

A.3 ERA5 (ECMWF Reanalysis v5)

Provider: European Centre for Medium-Range Weather Forecasts (ECMWF)

Spatial Resolution: 0.25° × 0.25°, approximately 31 km × 31 km

Temporal Resolution: Hourly

Variables Used: 2-meter temperature (K), surface solar radiation downwards (J/m^2), total column water vapor, total cloud cover

Data Assimilation: 4D-Var assimilation with hourly coupling of atmosphere and land surface

Observational Input: Satellite data, radiosondes, aircraft, surface stations, ocean buoys

Uncertainty: ±1-2°C for temperature, ±10-15% for surface solar radiation

APPENDIX B: STUDY SITE COORDINATES AND CHARACTERISTICS

Table B.1: Geographic Coordinates and Site Descriptions

Site Name	Latitude	Longitude	Elevation (m)	Classification	Dominant Land Use
Fumesua Community (FC)	6.70°N	1.52°W	287	Urban	Residential, commercial

Fumesua Farm (FF)	6.72°N	1.50°W	295	Peri-urban	Agriculture, scattered settlement
Sokwai Community (SC)	6.68°N	1.64°W	278	Rural	Small settlement, farming
Sokwai Farm (SF)	6.66°N	1.66°W	271	Rural	Active farmland, minimal development

Note: Sites span approximately 15-20 km east-west. All elevations are above mean sea level. Classifications based on population density, infrastructure development, and land use patterns observed via Google Earth imagery.

APPENDIX C: DATA PROCESSING WORKFLOW AND PYTHON CODE

C.1 Data Acquisition and Pre-processing

Python libraries used: NumPy (1.23.5), Pandas (1.5.3), xarray (2023.1.0), netCDF4 (1.6.2), scipy (1.10.0), matplotlib (3.7.0), seaborn (0.12.2)

Sample code for MERRA-2 data extraction:

```
import xarray as xr
import numpy as np
import pandas as pd

# Load MERRA-2 NetCDF file
ds = xr.open_dataset('MERRA2_tavg1_2d_aer_Nx.20220901.nc4')

# Define site coordinates
sites = {'FC': (6.70, -1.52), 'FF': (6.72, -1.50),
    'SC': (6.68, -1.64), 'SF': (6.66, -1.66)}
```

```
# Bilinear interpolation to site locations
pm25 = ds['PM25_SFC'].interp(lat=6.70, lon=-1.52, method='linear')
```

C.2 Quality Control Implementation

Modified Z-score outlier detection:

```
def modified_zscore(data):
    median = np.median(data)
    mad = np.median(np.abs(data - median))
    modified_z = 0.6745 * (data - median) / mad
    return modified_z

# Flag outliers
outliers = np.abs(modified_zscore(pm25_data)) > 3.5
```

APPENDIX D: AEROSOL DATA (DAILY AVERAGE)

Date	geoff	geofc	geosf	geosc	merraff	merrafc	merrasf	merrasc
28/08/22	16.72155	16.72155	13.68704	13.68704	8.521007	8.521007	7.558748	7.558748
29/08/22	22.1421	22.1421	18.31983	18.31983	8.368061	8.368061	6.553477	6.553477
30/08/22	22.0435	22.0435	17.64669	17.64669	5.609297	5.609297	5.541406	5.541406
31/08/22	15.21815	15.21815	11.82492	11.82492	10.24366	10.24366	9.912844	9.912844
01/09/22	14.87323	14.87323	11.91392	11.91392	4.187863	4.187863	3.245945	3.245945
02/09/22	12.98049	12.98049	9.640319	9.640319	4.83524	4.83524	4.473227	4.473227
03/09/22	12.99404	12.99404	9.649964	9.649964	4.546372	4.546372	4.668101	4.668101
04/09/22	10.72317	10.72317	7.937038	7.937038	3.952802	3.952802	4.490093	4.490093

05/09/22	14.50575	14.50575	10.13107	10.13107	5.137508	5.137508	9.22424	9.22424
06/09/22	15.48552	15.48552	12.15544	12.15544	3.552218	3.552218	3.78994	3.78994
07/09/22	13.55522	13.55522	8.936407	8.936407	7.464921	7.464921	6.292033	6.292033
08/09/22	14.74683	14.74683	9.816167	9.816167	6.361114	6.361114	5.927584	5.927584
09/09/22	14.36765	14.36765	10.23679	10.23679	6.859424	6.859424	6.007306	6.007306
10/09/22	13.04125	13.04125	10.03735	10.03735	6.941652	6.941652	6.379052	6.379052
11/09/22	13.42765	13.42765	10.88598	10.88598	5.426543	5.426543	4.903177	4.903177
12/09/22	19.90675	19.90675	14.03631	14.03631	6.553103	6.553103	6.059358	6.059358
13/09/22	20.3951	20.3951	14.76424	14.76424	6.076039	6.076039	6.333271	6.333271
14/09/22	17.40666	17.40666	13.6495	13.6495	6.648545	6.648545	6.249865	6.249865
15/09/22	18.65713	18.65713	13.66397	13.66397	8.835227	8.835227	8.912372	8.912372
16/09/22	18.23749	18.23749	12.41588	12.41588	10.22291	10.22291	12.28996	12.28996
17/09/22	13.16221	13.16221	9.453873	9.453873	7.375557	7.375557	5.840663	5.840663
18/09/22	13.64604	13.64604	10.04415	10.04415	5.301065	5.301065	5.023516	5.023516
19/09/22	14.85109	14.85109	10.6854	10.6854	6.209772	6.209772	6.404629	6.404629
20/09/22	13.788	13.788	9.957918	9.957918	4.145956	4.145956	4.430966	4.430966
21/09/22	16.1101	16.1101	12.37801	12.37801	5.805186	5.805186	4.759852	4.759852
22/09/22	23.87448	23.87448	17.11472	17.11472	9.873689	9.873689	10.87107	10.87107
23/09/22	23.16921	23.16921	19.64316	19.64316	19.82149	19.82149	22.50455	22.50455
24/09/22	15.55798	15.55798	12.15368	12.15368	12.37189	12.37189	13.68871	13.68871
25/09/22	19.16275	19.16275	12.92642	12.92642	9.700864	9.700864	10.27144	10.27144
26/09/22	18.18557	18.18557	12.48146	12.48146	8.188989	8.188989	7.749318	7.749318
27/09/22	20.17815	20.17815	14.79403	14.79403	12.09032	12.09032	13.78475	13.78475
28/09/22	15.06237	15.06237	9.791858	9.791858	8.493718	8.493718	10.40059	10.40059
29/09/22	16.72533	16.72533	11.15339	11.15339	5.798405	5.798405	5.497594	5.497594
30/09/22	15.9544	15.9544	11.44757	11.44757	6.162817	6.162817	6.365736	6.365736
01/10/22	18.45633	18.45633	14.29682	14.29682	9.034563	9.034563	9.13845	9.13845
02/10/22	13.57647	13.57647	9.419896	9.419896	5.799422	5.799422	5.854913	5.854913

03/10/22	25.28694	25.28694	17.02457	17.02457	17.71995	17.71995	21.81436	21.81436
04/10/22	17.77591	17.77591	13.46015	13.46015	15.88309	15.88309	21.94634	21.94634
05/10/22	17.15961	17.15961	12.44314	12.44314	18.92315	18.92315	22.52015	22.52015
06/10/22	16.3024	16.3024	11.35448	11.35448	15.90818	15.90818	16.71889	16.71889
07/10/22	14.92681	14.92681	10.84055	10.84055	22.06807	22.06807	22.57201	22.57201
08/10/22	14.45015	14.45015	10.10152	10.10152	9.989405	9.989405	10.67793	10.67793
09/10/22	20.6734	20.6734	16.5191	16.5191	34.42095	34.42095	37.4548	37.4548
10/10/22	25.16203	25.16203	25.80135	25.80135	32.48308	32.48308	32.92841	32.92841
11/10/22	18.77682	18.77682	18.03333	18.03333	16.15381	16.15381	14.98551	14.98551
12/10/22	34.19556	34.19556	29.63696	29.63696	21.13607	21.13607	19.92539	19.92539
13/10/22	48.94773	48.94773	46.89304	46.89304	67.62791	67.62791	66.58016	66.58016
14/10/22	36.99469	36.99469	34.63271	34.63271	55.30882	55.30882	61.37284	61.37284
15/10/22	18.98077	18.98077	14.5003	14.5003	16.14136	16.14136	15.5081	15.5081
16/10/22	25.27498	25.27498	22.72681	22.72681	19.93566	19.93566	18.52274	18.52274
17/10/22	37.56428	37.56428	36.52392	36.52392	41.37425	41.37425	43.80065	43.80065
18/10/22	49.14515	49.14515	47.47067	47.47067	60.77031	60.77031	79.00473	79.00473
19/10/22	45.54318	45.54318	40.38042	40.38042	45.82828	45.82828	65.94735	65.94735
20/10/22	34.45897	34.45897	29.71939	29.71939	34.48425	34.48425	37.46565	37.46565
21/10/22	45.36977	45.36977	42.41404	42.41404	47.8963	47.8963	50.04091	50.04091
22/10/22	49.78336	49.78336	48.96825	48.96825	48.8938	48.8938	49.37462	49.37462
23/10/22	47.07243	47.07243	45.71306	45.71306	46.85024	46.85024	49.41708	49.41708
24/10/22	44.36518	44.36518	42.90164	42.90164	33.4821	33.4821	34.08855	34.08855
25/10/22	43.57126	43.57126	42.87334	42.87334	43.39462	43.39462	41.08305	41.08305
26/10/22	39.48305	39.48305	38.93618	38.93618	31.77226	31.77226	37.45897	37.45897
27/10/22	39.00809	39.00809	37.68518	37.68518	33.04161	33.04161	34.68458	34.68458
28/10/22	60.37119	60.37119	56.48187	56.48187	47.30192	47.30192	52.47888	52.47888
29/10/22	73.07318	73.07318	69.53672	69.53672	64.45061	64.45061	70.97755	70.97755
30/10/22	80.13274	80.13274	83.30201	83.30201	60.8337	60.8337	70.34078	70.34078

31/10/22	47.75147	47.75147	47.10043	47.10043	59.58259	59.58259	62.72302	62.72302
01/11/22	46.56656	46.56656	45.72802	45.72802	68.98788	68.98788	76.31842	76.31842
02/11/22	49.30101	49.30101	46.34268	46.34268	53.8956	53.8956	66.87791	66.87791
03/11/22	50.42125	50.42125	48.21292	48.21292	41.36492	41.36492	41.17491	41.17491
04/11/22	65.7993	65.7993	61.7394	61.7394	45.22591	45.22591	49.50721	49.50721
05/11/22	69.93666	69.93666	65.24916	65.24916	63.98316	63.98316	69.65543	69.65543
06/11/22	52.65804	52.65804	49.86637	49.86637	59.92663	59.92663	74.53101	74.53101
07/11/22	48.34481	48.34481	47.38648	47.38648	43.64886	43.64886	60.2249	60.2249
08/11/22	62.04606	62.04606	57.03825	57.03825	38.03599	38.03599	39.03483	39.03483
09/11/22	41.91124	41.91124	37.72374	37.72374	43.75781	43.75781	41.84858	41.84858
10/11/22	32.74173	32.74173	28.31595	28.31595	34.41015	34.41015	35.22306	35.22306
11/11/22	27.16531	27.16531	22.81895	22.81895	24.90539	24.90539	25.71141	25.71141
12/11/22	26.25624	26.25624	21.794	21.794	26.94543	26.94543	29.95553	29.95553
13/11/22	27.903	27.903	25.32618	25.32618	23.48058	23.48058	28.30394	28.30394
14/11/22	27.28667	27.28667	26.4937	26.4937	21.65551	21.65551	24.69726	24.69726
15/11/22	40.26027	40.26027	38.17954	38.17954	27.92652	27.92652	32.23111	32.23111
16/11/22	42.39743	42.39743	34.92608	34.92608	33.26994	33.26994	37.54	37.54
17/11/22	43.75633	43.75633	38.9256	38.9256	31.69628	31.69628	30.60837	30.60837
18/11/22	49.25633	49.25633	47.10269	47.10269	48.11485	48.11485	49.40682	49.40682
19/11/22	38.08984	38.08984	36.48568	36.48568	63.99303	63.99303	78.74384	78.74384
20/11/22	39.57677	39.57677	37.79943	37.79943	67.35796	67.35796	77.24038	77.24038
21/11/22	48.97257	48.97257	47.56632	47.56632	49.59554	49.59554	61.57628	61.57628
22/11/22	48.98988	48.98988	47.18259	47.18259	39.08061	39.08061	41.91461	41.91461
23/11/22	46.04896	46.04896	45.96303	45.96303	40.12917	40.12917	42.98092	42.98092
24/11/22	42.09513	42.09513	42.4545	42.4545	49.16797	49.16797	42.42041	42.42041
25/11/22	47.79067	47.79067	42.94692	42.94692	61.82384	61.82384	64.64502	64.64502
26/11/22	46.66963	46.66963	39.88317	39.88317	50.2647	50.2647	52.76019	52.76019
27/11/22	40.38642	40.38642	36.8734	36.8734	43.23735	43.23735	47.33361	47.33361

28/11/22	45.04564	45.04564	40.17975	40.17975	41.42023	41.42023	45.32229	45.32229
29/11/22	41.20259	41.20259	38.70389	38.70389	44.7414	44.7414	47.11734	47.11734
30/11/22	44.73473	44.73473	43.42744	43.42744	46.51429	46.51429	45.8924	45.8924
01/12/22	46.4542	46.4542	43.68337	43.68337	33.28011	33.28011	36.57859	36.57859
02/12/22	46.56445	46.56445	41.67512	41.67512	29.45082	29.45082	35.60503	35.60503
03/12/22	37.52392	37.52392	32.68278	32.68278	30.48249	30.48249	30.97088	30.97088
04/12/22	42.65273	42.65273	38.99908	38.99908	31.24754	31.24754	30.80416	30.80416
05/12/22	46.06518	46.06518	42.74486	42.74486	38.2718	38.2718	41.30638	41.30638
06/12/22	51.29945	51.29945	45.41403	45.41403	41.5199	41.5199	45.78536	45.78536
07/12/22	36.86809	36.86809	34.10246	34.10246	38.98683	38.98683	49.56649	49.56649
08/12/22	35.1507	35.1507	34.18065	34.18065	45.53807	45.53807	44.87672	44.87672
09/12/22	54.21633	54.21633	54.27883	54.27883	85.62369	85.62369	86.98098	86.98098
10/12/22	58.98701	58.98701	58.52868	58.52868	71.635	71.635	92.68586	92.68586
11/12/22	79.48989	79.48989	75.02634	75.02634	83.46477	83.46477	86.32545	86.32545
12/12/22	91.72405	91.72405	81.85947	81.85947	104.4728	104.4728	124.7061	124.7061
13/12/22	84.87321	84.87321	80.64405	80.64405	101.2363	101.2363	114.9805	114.9805
14/12/22	88.06224	88.06224	81.59349	81.59349	75.84027	75.84027	82.79353	82.79353
15/12/22	85.79978	85.79978	73.34666	73.34666	61.60633	61.60633	68.41408	68.41408
16/12/22	76.82489	76.82489	65.77541	65.77541	54.97933	54.97933	60.13898	60.13898
17/12/22	63.65688	63.65688	59.86521	59.86521	52.27517	52.27517	50.14051	50.14051
18/12/22	61.41419	61.41419	59.06784	59.06784	45.27582	45.27582	48.1701	48.1701
19/12/22	66.79139	66.79139	64.23409	64.23409	45.6408	45.6408	49.77259	49.77259

A. 1 Temperature data (daily average)

valid_time	Daily
01/09/2022	297.023253
02/09/2022	298.284395
03/09/2022	298.361055
04/09/2022	297.6928
05/09/2022	297.226013
06/09/2022	297.90095
07/09/2022	298.135072
08/09/2022	297.963255
09/09/2022	297.267832
10/09/2022	297.61252
11/09/2022	297.708424
12/09/2022	297.013285
13/09/2022	297.924153
14/09/2022	298.346628
15/09/2022	297.503672
16/09/2022	295.698993
17/09/2022	298.05425
18/09/2022	297.932628
19/09/2022	296.700716
20/09/2022	296.351694
21/09/2022	297.592864

22/09/2022	297.415628
23/09/2022	297.51525
24/09/2022	297.617076
25/09/2022	297.678751
26/09/2022	295.959341
27/09/2022	296.866658
28/09/2022	295.61681
29/09/2022	297.123343
30/09/2022	297.441231
01/10/2022	296.367728
02/10/2022	297.394533
03/10/2022	297.777617
04/10/2022	298.043877
05/10/2022	297.898458
06/10/2022	297.807375
07/10/2022	296.84725
08/10/2022	297.669871
09/10/2022	297.908346
10/10/2022	297.21635
11/10/2022	297.282836
12/10/2022	298.120299
13/10/2022	298.053019
14/10/2022	296.738342
15/10/2022	297.483176
16/10/2022	298.22531
17/10/2022	298.549682
18/10/2022	298.321127

19/10/2022	298.036927
20/10/2022	298.314514
21/10/2022	298.27525
22/10/2022	298.248038
23/10/2022	298.443715
24/10/2022	298.60201
25/10/2022	298.165395
26/10/2022	298.962982
27/10/2022	299.180848
28/10/2022	299.082773
29/10/2022	298.921652
30/10/2022	298.978202
01/11/2022	298.386994
02/11/2022	298.795523
03/11/2022	299.129763
04/11/2022	299.09986
05/11/2022	298.998588
06/11/2022	298.566345
07/11/2022	299.057171
08/11/2022	299.15152
09/11/2022	298.483571
10/11/2022	298.04601
11/11/2022	297.414998
12/11/2022	297.923926
13/11/2022	297.906931
14/11/2022	298.489765
15/11/2022	298.832245

16/11/2022	298.518483
17/11/2022	298.755139
18/11/2022	298.82787
19/11/2022	298.337982
20/11/2022	298.148662
21/11/2022	299.044617
22/11/2022	298.939727
23/11/2022	298.860372
24/11/2022	299.003459
25/11/2022	299.471052
26/11/2022	299.405091
27/11/2022	298.907042
28/11/2022	298.067098
29/11/2022	298.375039
30/11/2022	298.982333
01/12/2022	299.1592
02/12/2022	297.929678
03/12/2022	297.195506
04/12/2022	298.595201
05/12/2022	299.165598
06/12/2022	299.541953
07/12/2022	299.222594
08/12/2022	299.038289
09/12/2022	298.886533
10/12/2022	299.980429
11/12/2022	299.416706
12/12/2022	298.957265

13/12/2022	299.085917
14/12/2022	299.391216
15/12/2022	299.736164
16/12/2022	299.453195
17/12/2022	299.02528
18/12/2022	299.005138
19/12/2022	298.923106
20/12/2022	299.473339
21/12/2022	299.641114
22/12/2022	299.344248
23/12/2022	299.506459
24/12/2022	299.114268
25/12/2022	299.416658
26/12/2022	298.6928
27/12/2022	300.006968
28/12/2022	300.415863
29/12/2022	299.79951
30/12/2022	300.723755

APPENDIX E: ANOVA

E 3: Single Factor For Merra2 Data Over All Locations

Result

Groups	*Count*	*Sum*	*Average*	*Variance*
merraff	114	3729.559	32.71543	550.2736
merrafc	114	3729.559	32.71543	550.2736
merrasf	114	4075.213	35.74748	715.9541
merrasc	114	4075.213	35.74748	715.9541

ANOVA

Source of Variation	*SS*	*df*	*MS*	*F*	*P-value*	*F crit*
Between Groups	1048.042	3	349.3472	0.551792	0.647169	2.624636
Within Groups	286167.4	452	633.1138			

Total	287215.5	455

E 2: F-Test Two-Sample for Variances for the merrasf and merraff date

Result

	merrasf	*merraff*
Mean	35.74748234	32.71542893
Variance	715.9540532	550.273576
Observations	114	114
df	113	113
F	1.301087467	
P(F<=f) one-tail	0.08168361	
F Critical one-tail	1.364483001	

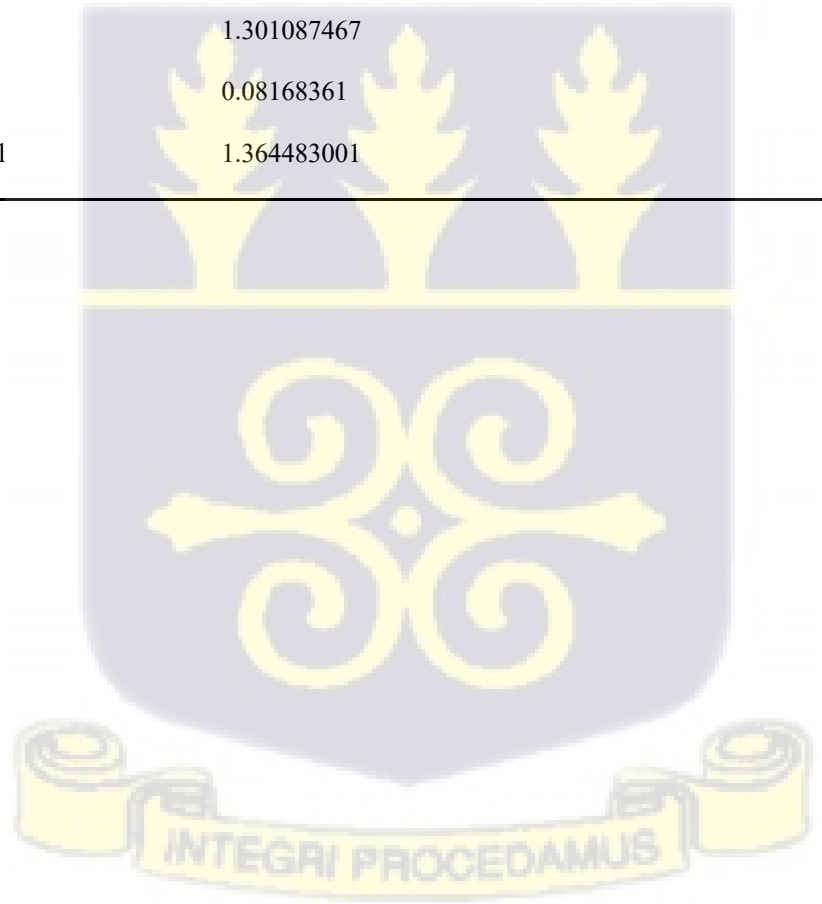

E 4: Single Factor for the GeosCF data over all locations

Result

Groups	*Count*	*Sum*	*Average*	*Variance*
geoff	114	4152.52	36.42561778	403.47418
geofc	114	4152.52	36.42561778	403.47418
geosf	114	3743.405	32.83688194	406.24743
geosc	114	3743.405	32.83688194	406.24743

ANOVA

Source of Variation	*SS*	*df*	*MS*	*F*	*P-value*	*F crit*
Between Groups	1468.208843	3	489.4029475	1.2088178	0.306029	2.624636
Within Groups	182997.0832	452	404.8608036			
Total	184465.2921	455				

F: F-Test

F 1: Two-Sample for Variances for the GeoSF and GeoFF data sets

Result

	geosf	*geoff*

Mean	32.83688194	36.42561778
Variance	406.2474298	403.4741774
Observations	114	114
df	113	113
F	1.006873432	
P(F<=f) one-tail	0.485510684	

APPENDIX G: PYTHON CODES

G 1: PYTHON CODE FOR CORRELATION GRAPHS

```
import netCDF4 as nc

import numpy as np

import xarray as xr

import matplotlib.pyplot as plt

import pandas as pd

# Load the datasets

data = pd.read_excel("/home/josh/Downloads/temperature.xlsx")

data1 = pd.read_csv("/home/josh/Downloads/mydatav1.csv")

dataa = xr.open_dataset("/home/josh/fa0d521b23e11a821cb66e403d6d190.nc")

# The latitude and longitude for Fumesua, Ejisu
```

```
lat_fumesua = 6.712377

lon_fumesua = -1.516972

# Extract temperature ('Daily') and time ('valid_time') data

temp_kelvin1 = data['temp']  # Temperature data

time_points = pd.to_datetime(data['valid_time'])  # Corresponding dates

# Convert temperature from Kelvin to Celsius

temp_kelvin = temp_kelvin1 - 273.15

# Extract SSR (surface solar radiation) data for the selected point

nearest_point_ssr = dataa.sel(latitude=lat_fumesua, longitude=lon_fumesua, method='nearest')

ssr = nearest_point_ssr['ssr']

# Check if 'date' exists in data1

if 'date' in data1.columns:

    data1['date'] = pd.to_datetime(data1['date'])

    data1.set_index('date', inplace=True)

else:

    data1.index = pd.to_datetime(data1.index)

# Calculate weekly averages for 'geosf' and 'merrasf'
```

```
monthly_avg = data1[['geoff', 'merraff']].resample('W').mean()

# Resample SSR data to weekly averages

ssr_weekly = ssr.resample(valid_time='W').mean()

# Resample temperature data to weekly averages

temp_kelvin_series = pd.Series(temp_kelvin.values, index=time_points)

temp_kelvin_weekly = temp_kelvin_series.resample('W').mean()

# Plotting geosf and merrasf against weekly averages with temperature and SSR on secondary axes

fig, ax1 = plt.subplots(figsize=(12, 6))

# Plot geosf and merrasf

ax1.plot(monthly_avg.index, monthly_avg['geoff'], label='Weekly Avg Geoff', color='tab:blue',
linewidth=2)

ax1.plot(monthly_avg.index, monthly_avg['merraff'], label='Weekly Avg Merraff',
color='tab:green', linewidth=2)

# Customize the primary y-axis

ax1.set_xlabel('Date')

ax1.set_ylabel('Aerosol Concentration (µg/m³)', color='tab:blue')

ax1.tick_params(axis='y', labelcolor='tab:blue')

# Create a secondary y-axis for temperature
```

```
ax2 = ax1.twinx()

ax2.plot(temp_kelvin_weekly.index, temp_kelvin_weekly, label='Temperature (°C)',
color='tab:red', linewidth=2)

ax2.set_ylabel('Temperature (°C)', color='tab:red')

ax2.tick_params(axis='y', labelcolor='tab:red')

# Create a third y-axis for SSR

ax3 = ax1.twinx()

ax3.spines['right'].set_position(('outward', 60))

ax3.plot(ssr_weekly['valid_time'], ssr_weekly, label='SSR (W/m²)', color='tab:orange',
linewidth=2)

ax3.set_ylabel('SSR (W/m²)', color='tab:orange')

ax3.tick_params(axis='y', labelcolor='tab:orange')

# Title and grid

plt.title('Weekly Aerosol Concentration, Temperature, and SSR over Fumesua Farm, Ejisu')

ax1.grid(True)

# Legends

ax1.legend(loc='upper left')

ax2.legend(loc='upper right')
```

```
ax3.legend(loc='lower right')

# Final layout

plt.tight_layout()

plt.savefig('/home/josh/Downloads/ff_weekly_with_ssr.jpeg')

plt.show()
```

G 2: PYTHON CODE FOR WEEKLY TIMESERIES GRAPHS

```
import netCDF4 as nc

import numpy as np

import xarray as xr

import matplotlib.pyplot as plt

import pandas as pd


# Load the datasets

data = pd.read_excel("/home/josh/Downloads/temperature.xlsx")

data1 = pd.read_csv("/home/josh/Downloads/mydatav1.csv")

dataa = xr.open_dataset("/home/josh/fa0d521b23e11a821cb66e403d6d190.nc")


# The latitude and longitude for Fumesua, Ejisu

lat_fumesua = 6.712377

lon_fumesua = -1.516972


# Extract temperature ('Daily') and time ('valid_time') data
```

```
temp_kelvin1 = data['temp']  # Temperature data
time_points = pd.to_datetime(data['valid_time'])  # Corresponding dates

# Convert temperature from Kelvin to Celsius
temp_kelvin = temp_kelvin1 - 273.15

# Extract SSR (surface solar radiation) data for the selected point
nearest_point_ssr = dataa.sel(latitude=lat_fumesua, longitude=lon_fumesua, method='nearest')
ssr = nearest_point_ssr['ssr']

# Check if 'date' exists in data1
if 'date' in data1.columns:
    data1['date'] = pd.to_datetime(data1['date'])
    data1.set_index('date', inplace=True)
else:
    data1.index = pd.to_datetime(data1.index)

# Calculate weekly averages for 'geosf' and 'merrasf'
monthly_avg = data1[['geoff', 'merraff']].resample('W').mean()

# Resample SSR data to weekly averages
ssr_weekly = ssr.resample(valid_time='W').mean()
```

```
# Resample temperature data to weekly averages
temp_kelvin_series = pd.Series(temp_kelvin.values, index=time_points)
temp_kelvin_weekly = temp_kelvin_series.resample('W').mean()

# Plotting geosf and merrasf against weekly averages with temperature and SSR on secondary axes
fig, ax1 = plt.subplots(figsize=(12, 6))

# Plot geosf and merrasf
ax1.plot(monthly_avg.index, monthly_avg['geoff'], label='Weekly Avg Geoff', color='tab:blue', linewidth=2)
ax1.plot(monthly_avg.index, monthly_avg['merraff'], label='Weekly Avg Merraff', color='tab:green', linewidth=2)

# Customize the primary y-axis
ax1.set_xlabel('Date')
ax1.set_ylabel('Aerosol Concentration (µg/m³)', color='tab:blue')
ax1.tick_params(axis='y', labelcolor='tab:blue')

# Create a secondary y-axis for temperature
ax2 = ax1.twinx()
ax2.plot(temp_kelvin_weekly.index, temp_kelvin_weekly, label='Temperature (°C)', color='tab:red', linewidth=2)
ax2.set_ylabel('Temperature (°C)', color='tab:red')
```

```
ax2.tick_params(axis='y', labelcolor='tab:red')

# Create a third y-axis for SSR
ax3 = ax1.twinx()
ax3.spines['right'].set_position(('outward', 60))
ax3.plot(ssr_weekly['valid_time'], ssr_weekly, label='SSR (W/m²)', color='tab:orange',
linewidth=2)
ax3.set_ylabel('SSR (W/m²)', color='tab:orange')
ax3.tick_params(axis='y', labelcolor='tab:orange')

# Title and grid
plt.title('Weekly Aerosol Concentration, Temperature, and SSR over Fumesua Farm, Ejisu')
ax1.grid(True)

# Legends
ax1.legend(loc='upper left')
ax2.legend(loc='upper right')
ax3.legend(loc='lower right')

# Final layout
plt.tight_layout()
plt.savefig('/home/josh/Downloads/ff_weekly_with_ssr.jpeg')
plt.show()
```

APPENDIX H: ABBREVIATIONS AND ACRONYMS

Abbreviation	Full Form
ANOVA	Analysis of Variance
AOD	Aerosol Optical Depth
BC	Black Carbon
ECMWF	European Centre for Medium-Range Weather Forecasts

EPA	Environmental Protection Agency
ERA5	ECMWF Reanalysis v5
GEOS-CF	Goddard Earth Observing System Composition Forecast
GMAO	Global Modeling and Assimilation Office
GMet	Ghana Meteorological Agency
IPCC	Intergovernmental Panel on Climate Change
KMA	Kumasi Metropolitan Assembly
KNUST	Kwame Nkrumah University of Science and Technology
MAD	Median Absolute Deviation
MERRA-2	Modern-Era Retrospective analysis for Research and Applications, Version 2
MESTI	Ministry of Environment, Science, Technology and Innovation
NADMO	National Disaster Management Organisation
NASA	National Aeronautics and Space Administration
NDC	Nationally Determined Contributions
OC	Organic Carbon
PM	Particulate Matter
$PM_{2.5}$	Particulate Matter with diameter $\leq$ 2.5 micrometers
PM_{10}	Particulate Matter with diameter $\leq$ 10 micrometers
SDG	Sustainable Development Goals
SSR	Surface Solar Radiation
UTC	Coordinated Universal Time
WASCAL	West African Science Service Centre on Climate Change and Adapted Land Use
WHO	World Health Organization

APPENDIX I: ETHICAL CONSIDERATIONS

This study utilized publicly available satellite data products and did not involve human subjects, animal subjects, or collection of primary data requiring ethical approval. All data sources are openly accessible through NASA Earthdata, ECMWF Climate Data Store, and related repositories. No ethical clearance was required for this research as per University of Ghana School of Graduate Studies guidelines for satellite-based environmental studies.

Data access and usage complied with the terms and conditions specified by respective data providers:

- MERRA-2: NASA Earthdata Login required; data freely available for research and educational purposes
- GEOS-CF: Publicly available through NASA GMAO without restrictions
- ERA5: Available under Copernicus License; free for academic and research use

Acknowledgment: Appropriate citations provided for all data products used in this research as required by data providers' usage policies.